Titre: Title:	Poly (3,4-ethylenedioxythiophene) (PEDOT) Coatings for High Quality Electromyography Recording
Auteur: Author:	Nicolo Rossetti
Date:	2019
Type:	Mémoire ou thèse / Dissertation or Thesis
Référence: Citation:	Rossetti, N. (2019). Poly (3,4-ethylenedioxythiophene) (PEDOT) Coatings for High Quality Electromyography Recording [Mémoire de maîtrise, Polytechnique Montréal]. PolyPublie. https://publications.polymtl.ca/3931/

POLYTECHNIQUE MONTRÉAL

affiliée à l'Université de Montréal

Poly (3,4-ethylenedioxythiophene) (PEDOT) Coatings for High Quality Electromyography Recording

NICOLO ROSSETTI

Institut de génie biomédical

Mémoire présenté en vue de l'obtention du diplôme de *Maîtrise ès sciences appliquées*

Génie biomédical

Juin 2019

POLYTECHNIQUE MONTRÉAL

affiliée à l'Université de Montréal

Ce mémoire intitulé :

Poly (3,4-ethylenedioxythiophene) (PEDOT) Coatings for High Quality Electromyography Recording

présenté par **Nicolo ROSSETTI**

en vue de l'obtention du diplôme de *Maîtrise ès sciences appliquées*

a été dûment accepté par le jury d'examen constitué de :

Jean-François MASSON, président
Fabio CICOIRA, membre et directeur de recherche
Frédéric BRETZNER, membre et codirecteur de recherche
Joshua BYERS, membre

DEDICATION

To my family, my girlfriend, my colleagues and friends.

"Because limits, like fears, are often just an illusion" M.J. Jordan

ACKNOWLEDGEMENTS

This work would not have been possible without my colleagues and friends who helped me throughout this amazing journey.

First, I would like to sincerely thank my research supervisor Professor Fabio Cicoira for giving me the great opportunity to work in his lab and pursue my studies in Canada. His work ethics, passion for science and friendship put me in the best conditions to give my best and accomplish my goals. Grazie.

I want also to thank Professor Clara Santato for her great commitment and all the fruitful discussions that helped the realization of this work.

I would like to thank Professor Bénédicte Amilhon and Dr. Guillaume Ducharme for welcoming me in their lab and for giving me the opportunity to learn and perform in vivo experiments.

A special thanks to Ada, Prabhjot, Côme and Jo'Elen who helped me to complete this work and for all the great moments we had together.

I would like to thank Professor Francesca Soavi for her help and advices on this project, and for teaching me so much about electrochemistry.

I am also thankful to Professor Frédéric Bretzner for all the inputs that led to the realization of this project, and to Professor Florin Amzica for his help during the deep brain stimulation project.

I would like to thank all the technicians that helped me during the project: Christophe Clément, Yves Drolet, Chi-Yuan Chang and Daniel Pilon.

I am thankful to the TransMedTech Institute for funding this project through a 2 years Master scholarship and to allow me to participate to national and international conferences.

I would like to thank all my colleagues at Polytechnique that helped me to grow, complete this work, and whose hard work was always an inspiration: Yang, Arun, Ben, Tom, Sunny, Xinda, Michel, Michael, Shiming, Mona, Natalie, Eduardo, Julien, Manuel, Zhaojing, Abdel, Xu, Xin, Chen, KyoungOh, Nitin, Sam (both of them), Tim, Floriane, Leslie, Michelle, Yasmine.

I would like to thank all my friends from Montréal who made these 2 years so great: Filippo, Ilaria, Lucas, Gauthier, Benjamin, Alessandra, Marion, Marina, Vlad, Kristina, Asif, Raj, Chiara.

I would also like to thank my friends from Italy who helped me to go through these university years: Davide, Alberto, Luca, Martina, Stefano, Michel, Gianfi, Giulia, Lisa, Ornella, Ylenia, Alessandro, Lorenzo, Gabriele, Luca.

A special thanks to my girlfriend Francesca whose unconditional love made these university years so special and helped me to overcome all the difficulties that I encountered.

Last (but not least), a big thanks to my parents for all that they have done for me and my brother and to allow us to pursue our dreams. A special thanks to my brother, friend and Milan roommate Andrea, for being an inspiring figure in my life and for helping me during all these years.

RÉSUMÉ

Les revêtements en polymère conducteur sur les électrodes métalliques constituent une solution efficace pour améliorer l'enregistrement et la stimulation des signaux neuronaux en raison de leurs conductivités électronique et ionique ainsi que de leur biocompatibilité.

Cependant, très peu d'études ont été réalisées sur les revêtements de polymères conducteurs sur des fils métalliques pour l'enregistrement du signal musculaire. Ces travaux traitent surtout les électrodes pour l'enregistrement chronique sous anesthésie. L'enregistrement chronique du signal musculaire chez les animaux en mouvement pose un de défis pour les revêtements d'électrode, en raison des déplacements musculaires qui peuvent provoquer un délaminage du revêtement et une défaillance du dispositif. De plus, la faible adhérence des polymères conducteurs à certains substrats inorganiques et la dégradation de leurs propriétés électrochimiques après des traitements sévères tels que la stérilisation ou pendant l'implantation, limitent davantage leur utilisation pour les applications biomédicales.

Dans ce travail, nous avons développé des électrodes invasives électrochimiquement stables pour l'enregistrement de signaux musculaires chez les petits animaux à base de fils multibrins en acier inoxydable revêtus du polymère conducteur poly(3,4-ethylenedioxythiophene) (PEDOT). La stabilité électrochimique et mécanique a été obtenue en ajustant les conditions d'électropolymérisation. Le PEDOT, dopé par des anions ClO_4^- , a été électropolymérisé de manière galvanostatique sur des fils d'acier inoxydable en utilisant trois solvants différents: le carbonate de propylène (organique), l'acétonitrile (organique) et l'eau (inorganique). L'adhérence du revêtement au substrat métallique a été testée par ultrasonication et la stabilité électrochimique a été évaluée par vieillissement accéléré dans une solution tampon de phosphate salin et par stérilisation à l'autoclave.

Le solvant a joué un rôle clé dans l'adhérence du revêtement PEDOT. Les solvants organiques offraient la meilleure stabilité mécanique. Les électrodes préparées avec ces solvants possédaient une excellente stabilité électrochimique et survivaient à la stérilisation et au trempage prolongé sans changement majeur des propriétés électrochimiques.

Des électrodes en acier inoxydable sans revêtements de polymères conducteurs et d'autres revêtues de PEDOT ont été implantées dans le muscle acromiotrapezius de cinq souris pour l'enregistrement

du signal musculaire durant une période de 6 semaines. Le revêtement PEDOT a amélioré les propriétés électrochimiques des électrodes en acier inoxydable, abaissant l'impédance, ce qui a permis d'améliorer le rapport signal / bruit lors de l'enregistrement du signal musculaire in vivo par rapport aux électrodes sans polymère.

ABSTRACT

Conductive polymer coatings on metal electrodes are an efficient solution to improve neural signal recording and stimulation due to their mixed electronic-ionic conduction and biocompatibility.

To date only a few studies have been reported on conductive polymer coatings on metallic wire electrodes for muscle signal recording. These studies mainly deal with testing of electrodes for acute recording during anaesthesia. Chronic muscle signal recording in free-walking animals offers more challenges for the electrode coatings, due to the muscle displacements which may cause coating delamination and device failure. The poor adhesion of conductive polymers to some inorganic substrates and the possible degradation of their electrochemical properties after harsh treatments, such as sterilization, or during implantation still limit their use for biomedical applications.

In this work, we developed mechanically and electrochemically stable invasive electrodes for muscle signal recording in small animals based on stainless steel multi-stranded wires coated with the conductive polymer poly(3,4-ethylenedioxythiophene) (PEDOT). The electrochemical and mechanical stability was achieved by tuning the electropolymerization conditions. PEDOT doped with ClO_4^- anions was galvanostatically electropolymerized using three different solvents: propylene carbonate (organic), acetonitrile (organic) and water (inorganic). The coating's adhesion to the metallic substrate was tested through ultrasonication and the electrochemical stability was evaluated through accelerated ageing in phosphate buffer solution and autoclave sterilization.

The solvent played a key role in the adhesion of the PEDOT coating, with organic solvents giving the best mechanical stability. Electrodes prepared with these solvents possessed excellent electrochemical stability, and survived sterilization and prolonged soaking without major changes in electrochemical properties.

PEDOT-coated and bare electrodes were implanted in the acromiotrapezius muscle of five mice for muscle signal recording during a period of 6 weeks. The PEDOT coating improved the electrochemical properties of the stainless steel electrodes, lowering the impedance, which resulted in enhanced signal to noise ratio during in vivo muscle signal recording compared to bare electrodes.

TABLE OF CONTENTS

LIST OF TABLES

LIST OF FIGURES

LIST OF SYMBOLS AND ABBREVIATIONS

Ag/AgCl	Silver/silver-chloride
AP	Action potential
$BF4^-$	Tetrafluoroborate
CB	Conduction band
CE	Counter electrode
$ClO4^-$	Perchlorate
CNT	Carbon nanotubes
CP	Conducting polymer
CSC	Charge storage capacity
CV	Cyclic voltammetry
DIW	Deionized water
DBS	Deep brain stimulation
EDOT	Ethylenedioxithiophene
EEG	Electroencephalography
EIS	Electrochemical impedance spectroscopy
EMG	Electromyography
FBR	Foreign body reaction
Ir	Iridium
IrOx	Iridium oxide
$LiClO_4$	Lithium perchlorate
MU	Motor unit
MUAP	Motor unit action potential
OECT	Organic electrochemical transistor

OLED	Organic light emitting diode
PANI	Polyaniline
PBS	Phosphate buffer solution
PC	Propylene carbonate
PEDOT	Poly(3,4-ethylenedioxithiophene)
PFA	Perfluoroalkoxy
PPY	Polypyrrole
PSS	Poly(styrenesulfonate)
Pt	Platinum
PtIr	Platinum-iridium
pTS	p-toluene sulfonate
RE	Reference electrode
SEM	Scanning electron microscopy
sEMG	Surface electromyography
SNR	Signal to noise ratio
TEABF4	Tetraethylammonium tetrafluoroborate
VB	Valence band
VPP	Vapour Phase Polymerization
WE	Working electrode

CHAPTER 1 INTRODUCTION

1.1 Implantable electrodes

The advancements in healthcare and biomedical sciences in the past decades have led to a widespread use of electrodes for electrostimulation and recording. The range of applications for such electrodes encompasses neural disease treatments such as Deep Brain Stimulation (DBS) for Parkinson's disease, cochlear and retinal implants, advanced prosthesis limb control, and even depression treatment [1]. All these applications call for highly performant electrodes able to satisfy the electrical and medical requirements for safe and efficient healthcare.

1.1.1 Biopotential recording

Biopotential recording involves the placement of recording electrodes in contact with the body in order to record the electrical activity of a particular physiological system of interest. Biopotentials generally differ in frequency content, amplitude and duration, and specific standards have been developed for their acquisition. The type of electrode, together with the signal acquisition and processing methods, depends on the type of recorded signal and the locations of electrodes in the body. Biopotentials are of paramount importance as they are a direct window into our body and can be used to assess its condition and predict potentially harmful complications. They are also relevant for body-machine interfaces, in which a biopotential, such as the brain or muscles electrical signal, can be used to control a machine such as a robotic arm.

1.1.1.1 Electromyography

The electromyography (EMG) is one of the most studied electrophysiological signals, and it consists of recording muscle electrical activity by means of electrodes in direct contact with the body. The spectrum of applications is quite broad, and some examples are neuromuscular disease detection, the study of body movement (kinesiology) or the control of artificial limbs.

There are two main types of EMG signals that can be acquired: surface EMG (sEMG) or invasive EMG. The two techniques differ substantially in regard to the type of electrodes used to acquire the signal, specifically, sEMG employs external surface electrodes, while implanted needles are used for invasive EMG. Even though sEMG represents a valid and non-invasive tool to obtain

information on muscle activity, its resolution is limited to several muscle fibers. Higher resolution is required for diagnostic purposes, thus invasive needle electrodes are normally used [2].

1.2 Problematics

A variety of electrode designs and materials have been used for recording and stimulation; however, in many applications and for invasive EMG, metallic wire electrodes are most often employed.

There are several drawbacks associated with using stiff metallic materials for invasive recordings, including the post-implant inflammatory response and degradation of the electrical properties over time caused by the foreign body reaction (FBR), the limited spatial resolution due to the trade-off between electrode size and impedance and the possible unwanted chemical reactions at the body-metal interface, especially during electrical stimulation [3].

For these reasons, many efforts have been directed toward developing advanced materials and electrode designs to overcome these limitations.

1.3 Conducting polymers

Conducting polymers are among the most promising materials for electrode modification due to their good electrochemical properties, combined with their soft/organic nature and ease of processability. These materials have been extensively used for coating neural electrodes and were shown to effectively improve the electrical and mechanical performance.

Conducting polymers are organic polymers that are capable of conducting electricity due to their conjugated structure, characterized by alternating single and double bonds. Still, to achieve high conductivities, these polymers require a chemical doping process that generates additional mobile charges inside their structure [4]. The chemical doping gives conductive polymers the ability to transduce ionic currents into electric currents, finally lowering the impedance at the electrode/tissues interface. A reduced electrode/tissue impedance is beneficial for the quality of the recorded signal and it lowers the voltage required for electrical stimulation preventing potentially harmful chemical reactions.

1.3.1 Electropolymerization

Due to the non-flat geometry and small dimensions of most of the commonly used implantable electrodes, electropolymerization is the most used technique to coat these substrates with conductive polymers as it can be applied to any kind of substrate geometry. Generally, the polymerization is performed in a three-electrode configuration, where the recording or stimulating electrode serves as the working electrode (WE) and the two remaining electrodes are the counter electrode (CE) and reference electrode (RE). The three electrodes are immersed in a solution containing the solvent, the electrolyte containing the doping ions, and the monomer. Through the application of a current or voltage at the working electrode, the monomer starts to polymerize on its surface forming an insoluble coating [4].

1.3.2 Coating stability

These materials have been widely studied, however, much is still unknown about the influence of the electropolymerization conditions on their electrical and mechanical properties, and many efforts have been spent on finding the best conditions to achieve good coating stability.

At present, the main limitation for widespread use of conducting polymers is their poor electrochemical and mechanical stability. The former is strictly related to the second, as many of the device failures reported in the literature can be related to a poor adhesion of the polymer coating to the electrodes, resulting in delamination and consequent degradation of the electrochemical properties of the device. Even though many groups have proposed useful solutions to tackle the adhesion problem, most involving electrode surface modifications or polymer functionalization, we believe that enhanced adhesion could result from carefully adjusting and selecting the polymerization conditions.

1.4 Objectives

The main objective of this work is to develop electrodes for EMG recording in small animals, able to achieve better signal quality respect to bare metal electrodes.

The following specific objectives have been set to achieve the main objective:

1. Coat an invasive EMG electrode with a layer of conductive polymer to improve its biocompatibility and electrical conductivity.

We investigated the influence of the processing solvent on the mechanical and electrochemical properties of the electropolymerized conducting polymer poly(3,4-ethylenedioxythiophene) (PEDOT) on stainless steel multi-stranded wires for invasive EMG recording. Three solvents, propylene carbonate (organic), acetonitrile (organic) and water (inorganic), were used with the electrolyte $LiClO_4$, also acting as the dopant, to electropolymerize PEDOT on the electrodes.

2. Test the electrochemical properties, the coating adhesion and the electrochemical stability of the electrodes.

The durability of the coating adhered to the metallic substrate was tested through ultrasonication, and the electrochemical stability was evaluated through accelerated ageing in a phosphate buffer solution and autoclave sterilization.

3. Test *in vivo* the electrodes for EMG recording in small animals

After extensive *in vitro* testing, the bare and coated electrodes were implanted in the acromiotrapezius muscles of mice for prolonged (6 weeks) EMG recording. The Signal to Noise Ratio (SNR) was computed to compare the performances of the electrodes with and without the PEDOT coating.

1.5 Organization

The thesis is organized as follows: Chapter 2 contains an extensive review of the relevant literature on the topics introduced in Chapter 1, Chapter 3 describes the materials and methods in detail, Chapter 4 displays the main results, Chapter 5 and 6 contain the discussion and the final conclusions and recommendations.

CHAPTER 2 STATE OF THE ART

In this chapter, section 2.1 gives an introduction to the biological phenomena involved in the generation of biopotentials, with a focus on electromyography. Section 2.2 describes the properties and limitations of current invasive electrodes, together with an overview of the principal materials employed to enhance their properties. Finally, section 2.3 and 2.4 will introduce conductive polymers, with an emphasis on the conductive polymer PEDOT, as appealing materials that can be used to overcome most of the limitations associated with the use of standard invasive electrodes.

2.1 Neural signals

Neural signal is a broad and general term that describes the electrical signals generated by specific cells, called neurons, that communicate with each other. These signals can carry the information of a particular body area neural activity, which can be used to assess the health of a patient. Common neural signals such as the Electroencephalogram (EEG) have been widely used as powerful medical tools to prevent and diagnose health complications. Moreover, neural signals can be used as input signals for body machine interfaces to help patients overcome physical impairments, such as amputations or paralyses. Finally, neural signals can also be generated by means of stimulation (electric, magnetic, optic etc.) for different purposes ranging from bladder stimulation to cochlear and retinal implants, depression and epilepsy treatment, or Deep Brain Stimulation (DBS) [1].

2.1.1 Principles of bioelectricity

The fundamental neural electrical signals are called action potentials (AP), and unlike common electronic signals that arise from electrons movement, they are generated by the movement of ions into and out of the cell's membrane.

The cells membrane contains ion-selective channels. In the case of AP, the two main ions involved are Na^+ and K^+ even if other ions such as Cl^- and Ca^{2+} are also involved. These ion concentrations vary from inside to outside of the cell membrane, with the K^+ concentration being higher inside the cell and the Na^+ concertation higher outside, which causes a gradient flow that pushes K^+ ions outside and Na^+ ions inside. At the same time, an electric potential gradient exists across the membrane, with the outside of the cell being positively charged and the inside of the cell being

negatively charged. While this potential pushes the Na^+ ions inside the cell, it also opposes to the outflow of K^+. Apart from these passive mechanisms, the cell possesses another active system which ensures that the concentration of K^+ and Na^+ remains higher inside and outside of the cell, respectively, by consuming energy to pump these ions in that direction [5].

The electric potential across the membrane can be described by the Goldman equation (1):

$$V_m = \frac{RT}{F} \ln \frac{P_K[K^+]_o + P_{Na}[Na^+]_o + P_{Cl}[Cl^-]_i}{P_K[K^+]_i + P_{Na}[Na^+]_i + P_{Cl}[Cl^-]_o} \qquad (1)$$

Where R is the gas constant (≈ 8.314 J/K·mol), T the temperature, F is the Faraday constant (96485.3 C/mol), P indicates the permeability of the ionic channels for a certain ion, and $[X]_o$ and $[X]_i$ indicate the concentration of the ionic species X outside and inside the cell, respectively. Due to the fact that the permeability of the ionic channels for K^+ is much greater than for the other ions, the resting potential of the membrane can be simplified as (2):

$$V_m = \frac{RT}{F} \ln \frac{[K^+]_o}{[K^+]_i} \qquad (2)$$

Which represents the Nernst equation applied to the K^+ ion, and usually takes the value of ≈ -70 mV [5].

Apart from the previously cited types of channels, the cell membrane contains also so-called voltage-gated ionic channels, which can vary their permeability to a specific ion depending on the value of the membrane potential. The presence of this element is key in generating AP, as it allows for positive feedback loops during which channels can be opened due to a rise of membrane potential, causing an outflow of ions that consequently contributes to a further increase of the potential [5].

Without entering too much in the details that are not the aim of this chapter, we can simply observe the typical waveform of the membrane potential during an AP displayed in Figure 2.1 [6].

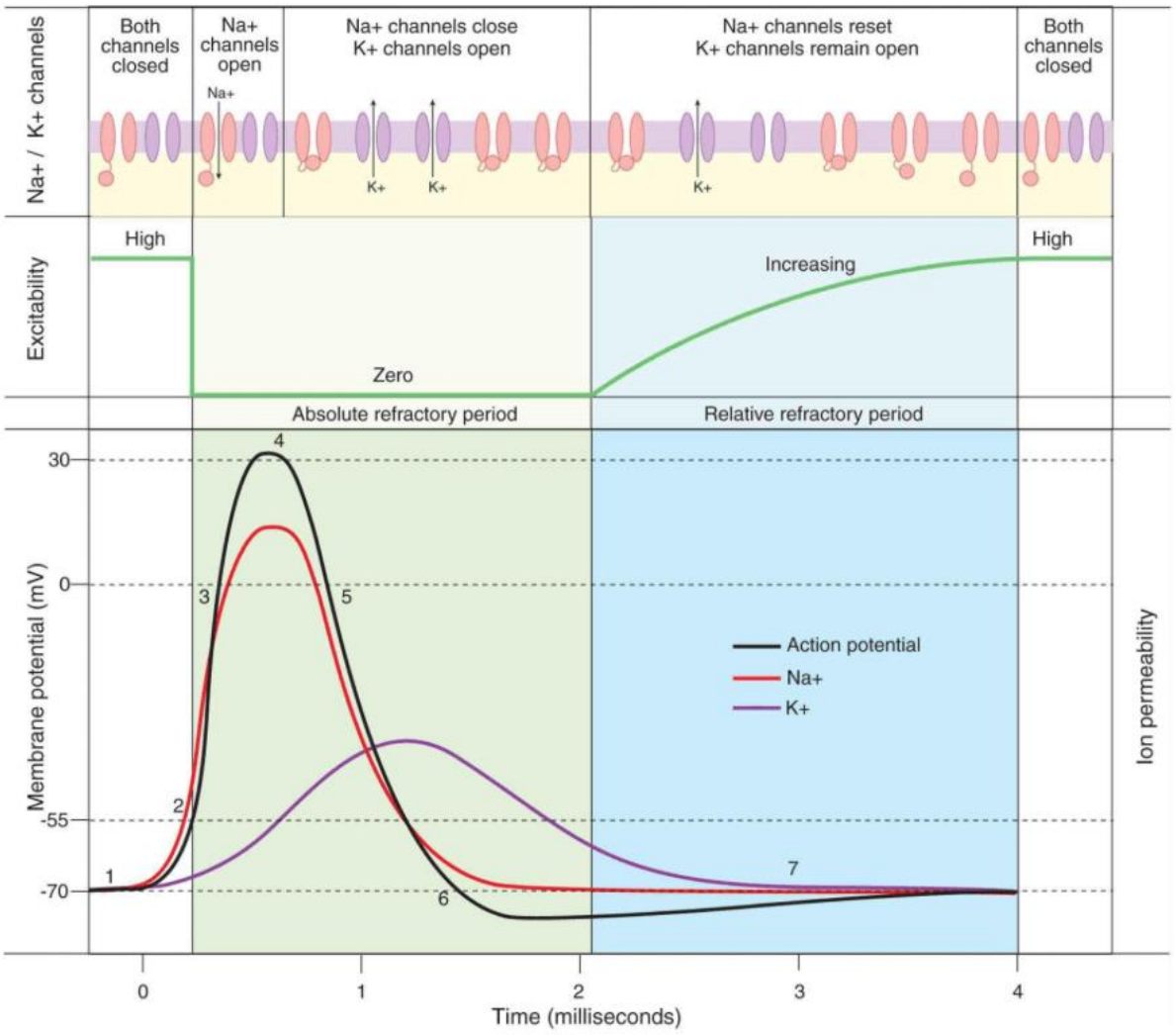

Figure 2.1 Changes in membrane potential, channel configuration and ion permeability during an action potential. Copyright McGraw-Hill Education [6].

When the cell is at rest, the voltage-gated channels for K^+ and Na^+ are both closed, and the membrane potential is around -70 mV. From this condition, the cell can be excited (AP from another neuron, external stimulation etc.) with a consequent rise in the potential (depolarization). If the depolarization is high enough to overcome a potential threshold, normally around -55 mV, the Na^+ channels open, causing an outflow of these ions and an abrupt depolarization of the membrane. At the same time the K^+ channels open, but with slower dynamics, leaving the potential to proceed towards positive values. Once the potential reaches its peak around +30 mV, the Na^+ channels close, while the K^+ channels remain open, causing a drop of the potential (repolarization).

Once the potential starts to approach the resting potential of – 70 mV, the K^+ channels start to close but, due to their slow dynamics, some remain open, causing a further drop of the potential called hyperpolarization. It is important to note that from the beginning of the AP to this point, the cell is in the absolute refractory state, meaning that the cell cannot be excited by another stimulus. After the hyperpolarization, the cell is in the relative refractory state, meaning that an incoming stimulus can excite the cell, but it needs to overcome a higher threshold compared to the threshold at rest. The potential in this phase tends to return slowly toward the resting potential as the remaining K^+ channels tend to close [5].

2.1.2 Electromyography

The Electromyography (EMG) signal measures the electrical activity of muscles during contraction, and it conveys information on neuromuscular activity [7]. The α-Motor neurons located in the spinal cord branch with their axons to several muscle fibres that interact through the motor end plates, and the combination of a single motor neuron with the innervated muscle fibres is referred to as the motor unit (MU) [8]. The number of MUs in the human muscles can vary significantly from hundreds in small muscles, to more than 1000 for large limb muscles. The motor neuron fires APs to the fibres in the MU, and the electric signal conducted through the fibres causes their contraction. The combination of all the APs conducted through the muscle fibres of a MU is called motor unit action potential (MUAP), and the force generated during a contraction results from the number of MU that are recruited and their firing rate. Finally, the type of contraction can be described as voluntary if it results from a signal sent from the brain, or involuntary if it results from a feedback system with neurons located in the spinal cord [8]. Figure 2.2 shows this general schema with a focus on the structure of the MU.

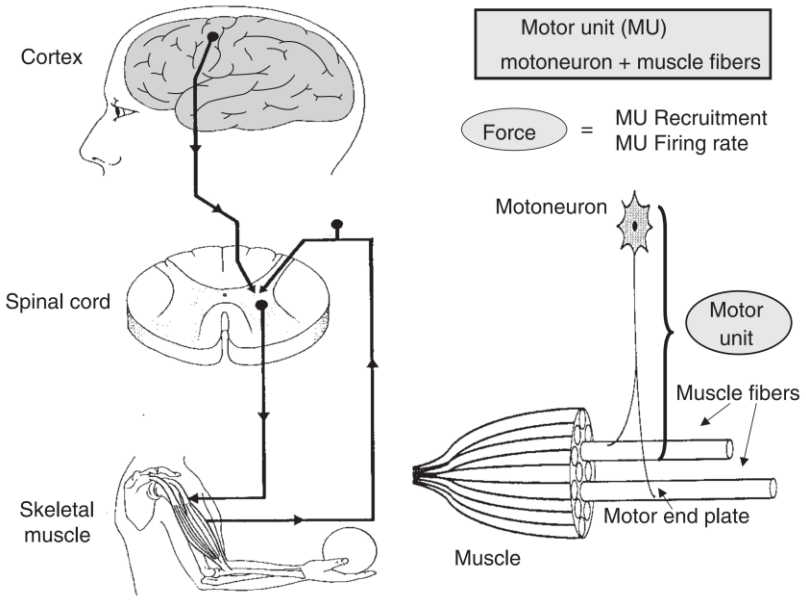

Figure 2.2 Simple schematic of the motor control system and motor units [8].

The EMG signal consists in the collection of trains of MUAPs by means of electrodes placed on the surface of the skin or in direct contact with the muscle [7]. The two main types of electrodes used for EMG detection are needle electrodes and surface electrodes. Needle electrodes generally consist of fine sharp wire electrodes that are inserted directly into the target muscle, and can collect information from specific single MUs due to their small dimensions. On the other hand, surface electrodes used for surface EMG (sEMG) are non-invasive external electrodes, often Ag/AgCl adhesive type, which convey information about several motor units due to their large pickup area. The two techniques differ in signal quality and invasiveness, with the needle electrodes providing much more localized and low noise information on single MUAPs, but with the drawback of being invasive, while sEMG electrodes are non-invasive but provide a less clean and selective signal due to the distance from the muscle, the presence of the skin which increases the electrical impedance and generates movement artefacts, and the larger dimensions. However, more than competing with each other, these two types of electrodes can be used for different applications or to obtain complementary information. Due to their ability to attain higher resolution signals, needle electrodes are often used for diagnostic applications where high quality and selective information is needed, while sEMG has been employed for biofeedbacks, prosthesis control, ergonomics and movement studies, with applications also in sport [8].

In this work, we focus on the needle electrodes as they directly interact with the biological environment and for this reason they are subject to stress and degradations that do not apply to surface electrodes. Moreover, as these electrodes are commonly used for diagnostic purposes, there is an increased interest in enhancing the quality of the acquired signal. As previously mentioned, these electrodes find several applications and can be used to study the health of MUs at the peripheral level, such as loss of nerve supply to the muscles (also called denervation), the ability for nerve regeneration (reinnervation), muscle-related diseases or problems at the neuromuscular junction level [8].

The type of electrodes used for invasive EMG have a great impact on the properties of the recorded signal, and different configurations have been studied depending on the target feature to be extracted. In particular, small-area needle electrodes are more sensitive to the electrical activity of nearby muscle fibres, with a sharp decline of the action potential amplitudes from more distant fibres, while electrodes with larger exposed conductive areas are able to pick up the signal from a higher number of fibres [8].

2.1.3 EMG electrodes

The two most common configurations of needle electrodes for clinical EMG recording are the concentric needle electrode and the monopolar needle electrode. The concentric needle electrode has an elliptic active surface area on the tip of a bevelled metallic canula, which works also as the reference [9]. On the other hand, the monopolar needle electrode consists in an insulated metallic electrode with a bare exposed conic tip with a surface area of around $0.15 – 0.20\ mm^2$. In the latter case, an additional reference electrode is needed [9].

Other EMG electrodes that have found clinical applications are the single-fibre and macro electrodes. The first generally consists in an insulated metallic wire, where a very small aperture in the insulation is created by means of electric sparks, providing a point-size recording area that allows for the recording of single fibre action potentials. The macro electrode consists in a large (tens of mm) conductive canula that records the EMG signal from a large number of MUs with respect to a surface reference electrode, and is used to obtain the information of the electrical activity of a large number of muscle fibres [9].

Another type of relevant EMG electrode which is used for EMG signal decomposition studies (i.e. the detection and separation of MUAPs) is the quadrifilar needle electrode, which consists in a cannula with four, 75 μm leads arranged in a square configuration with 200 μm sides and located in a side port 7.5 mm from the tip of the needle electrode [9].

Finally, very fine (50-100 μm diameter) stainless steel, silver or tungsten insulated wires are extensively used for EMG recording studies both in humans and animals [10-12]. The advantage of this type of electrodes is their flexibility and small diameter, which cause minimal discomfort in the subject and allow for long-term studies in animal models [13]. These electrodes are typically inserted through a fine needle and hooked at the end to avoid their removal from the target muscle [14].

2.2 Background of invasive electrodes

As previously introduced in Chapter 1, implanted electrodes have found an increasing number of applications in medicine for signal recording and stimulation [1]. In this chapter, the electrochemistry at the electrode/electrolyte interface is discussed, as it is a fundamental step to understand the behaviour of invasive electrodes once implanted in the body. The basic principles behind the recording and stimulation of biopotentials are briefly discussed, with a focus on the techniques for the characterization of the electrodes. The drawbacks associated with the use of metallic invasive electrodes and the possible solutions in terms of materials will also be explored.

2.2.1 The electrode/electrolyte interface

As both electrical stimulation and recording with common metal electrodes are associated with transduction of charge carriers from electrons in the metal to ions in the biological environment, it is necessary to understand the basic electrochemical reactions that take place at the electrode/electrolyte interface [15].

First, let’s consider a three-electrode electrochemical cell, including a working electrode (WE), a counter electrode (CE) and a reference electrode (RE), all immersed into an electrolyte. Upon application of a potential difference between the working and reference electrode, two main processes can take place: i) formation of an electrical double layer at the electrode electrolyte interface and ii) redox reaction (Faradaic charge transfer) [15].

The electrical double layer is characterized by a separation of positive and negative charges in a very narrow space at the electrode/electrolyte interface, leading to the formation of a capacitor. In this condition, capacitive charge transfer is characterized by only a redistribution of the charges forming the electrical double layer, allowing the interface to be modeled as a capacitor.

On the other hand, redox (Faradaic) processes are associated with a reduction or oxidation at the electrode/electrolyte interface, with a net electron flow through the cell. An important aspect of Faradaic charge transfer is the associated formation of products in the solution due to the redox reaction, as these products can either diffuse away from the electrode, in the case of an irreversible Faradaic reaction, or being reversed into their reactant form during a reversible Faradaic reaction [15]. Irreversible Faradaic processes are particularly dangerous in biomedical applications as they involve a modification of the biological environment potentially causing electrode and tissue damage [1, 15, 16].

Considering these two processes, it is possible to model a simple electrochemical cell with electric components mainly composed of resistors and capacitors. The Randles circuit described in Figure 2.3 is the simplest model used to describe the interactions between the electrodes and the surrounding electrolyte environment. It is composed of a resistor R_e that describes the solution resistance, the double layer capacitor C_{dl} that models the capacitive electrical double layer, and the Faradaic impedance Z_f that describes the Faradaic charge transfer [17]. The Faradaic component Z_f can be further subdivided into a charge transfer resistance R_{ct} and a Warburg element Z_w, which contains the information of the mass transfer, with high values associated to diffusion-limited processes [17]. The Warburg element generally takes the form described in (3) where σ is the Warburg coefficient, w the pulse (related to the frequency as $w = 2\pi f$), j the imaginary unit, δ the diffusion layer thickness and D the diffusion coefficient of the diffusing species [18]:

$$Z_w = \frac{\sigma}{\sqrt{w}}(1 - j)\tanh\left(\delta\sqrt{\frac{jw}{D}}\right) \qquad (3)$$

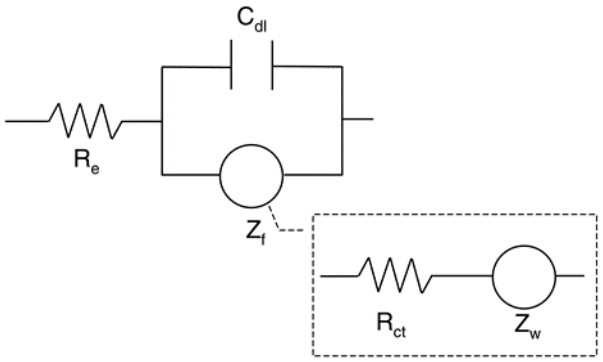

Figure 2.3 Randles electric model for a simple electrochemical cell. Reprinted from [17], Copyright (2005), with permission from Elsevier.

When an electrode comes in contact with a solution, an electron transfer at the interface may take place due to the difference in potential between the two phases, and an interfacial difference in potential $\Delta\phi$ that opposes further charge transfer is created. Whenever a new electrode is introduced in the solution, a new interfacial potential is generated, and the electrochemical cell potential can be defined as the sum of two interfacial potentials plus any potential drops occurring in the bulk solution [15]. An important cell potential is the open circuit potential, which is calculated for the working and reference electrodes when no current is flowing. If in the solution is present an oxidation/reduction (O/R), the equilibrium potential can be calculated as (4), with [O] and [R] concentrations of the oxidized and reduced chemical species, R gas constant (8.314 J/(mol K)), T absolute temperature, n number of electrons involved in the reaction, F Faraday's constant (~96,485 C/mole of electrons), and E_0 standard reduction potential (equal to the equilibrium potential when [O] = [R]) [15].

$$E_{eq} = E_0 + \frac{RT}{nF} \ln\left(\frac{[O]}{[R]}\right) \qquad (4)$$

Starting from the equilibrium, the potential can be modified by applying a voltage at the electrode and this one is said to be polarized, with polarization being expressed as (5) with E being the new potential [15].

$$\mu = E - E_{eq} \qquad (5)$$

Based on this definition, electrodes can be distinguished as polarizable and non-polarizable. An electrode is said to be polarizable if there is no electron transfer between the electrode and the

solution during stimulation or recording, and its behaviour can be modeled as a capacitor in series with the solution resistance, since only a displacement of the charges in the electrical double layer takes place. Consequently, in this situation the Faradaic element in the circuit model of Figure 2.3 has an ideally infinite impedance. Therefore, an ideally polarizable electrode can accommodate large amounts of injected charges through the electrical double layer before the appearance of Faradaic processes, and its electric potential can be easily perturbated from the equilibrium potential, thus excluding its use as a reference electrode that requires a stable potential. In a non-polarizable electrode, on the other hand, current freely passes between the electrode and the electrolyte with no polarization, and the electrode is modeled as a resistor. Consequently, this electrode has extremely low Faradaic impedance Z_f, with no potential changes upon passage of current, which is the ideal behaviour for a reference electrode such as the standard Ag/AgCl reference electrode [15].

Apart from these two opposite extremes, it is important to mention a third mechanism that can take place for some materials, among which conductive polymers, which is the pseudocapacitive behaviour. Pseudocapacitors are able to store charge by performing redox reactions (ideally reversible) with electrolyte ions, finally giving rise to a non dissipative, charge storage process that can be modeled as a capacitor [15].

2.2.2 Stimulation and recording

Electrical stimulation of biological tissues is achieved by current flow from the electrodes to the tissues. As previously described in paragraph 2.1.1., if the electrical stimulus received by the cell is strong enough to overcome the potential threshold, an action potential will be generated. Therefore, stimulating electrodes will need to deliver enough charge to elicit an electrical response in the biological tissues of interest, but at the same time, need to operate in a safe electrochemical range to avoid unwanted chemical reactions that may damage the electrodes or the surrounding tissues. A typical pulse during electrical stimulation is characterized by a cathodic (negative current) and anodic (positive current) phase, with the former being used to stimulate the target tissues, and the latter to balance the total charge to avoid electrode polarization [1]. The total delivered charge is defined as the product of the cathodic current intensity (in the case of a constant cathodic current) and the cathodic phase time.

The type of electrochemical process defines the electrical behaviour of the electrode during stimulation. Figure 2.4 shows an example of current-controlled biphasic stimulation where the electrode potential varies as a function of the type of charge injection. For an electrical double layer stimulation type (Figure 2.4.a), only a displacement of ions at the electrode/electrolyte interface takes place, and the electrode potential is described by a sawtooth curve. For a pseudocapacitor (Figure 2.4.b), the process involves charge transfer (Faradaic) during which reactants (in this case H^+ ions) are converted into products that remain close to the electrode surface and are then reconverted upon reversal of the current direction with the potential returning to zero. On the other hand, during an irreversible Faradaic reaction (Figure 2.4.c), the product isn't available for reconversion during current inversion as it diffuses away from the electrode surface. This consumption of charges that do not contribute to the charging of the capacitance causes an upward shift of the potential that becomes positive during the anodic phase [15].

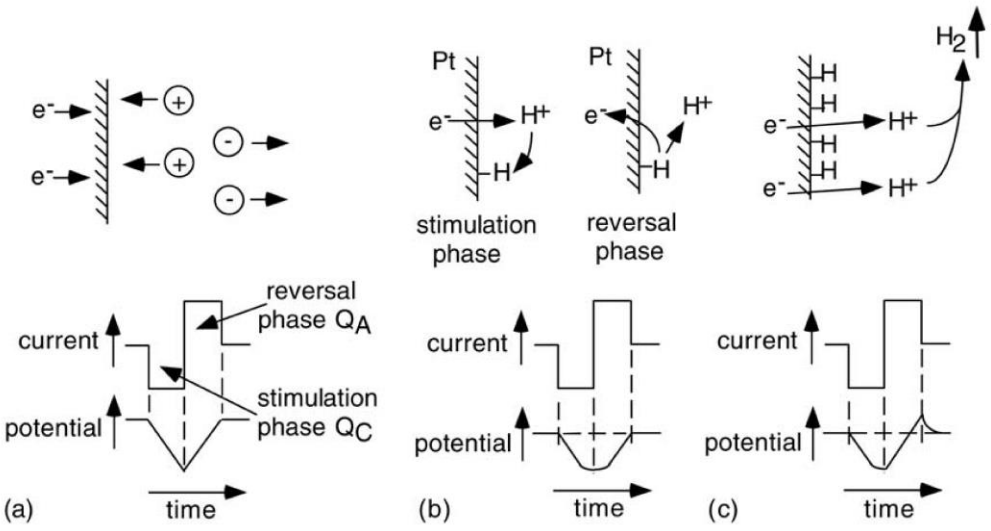

Figure 2.4 Electrode potential behaviour during current-controlled biphasic stimulation and examples of associated electrochemical reaction for a capacitive (a), pseudocapacitive (b), and irreversible Faradaic (c) electrochemical process. Reprinted from [15], Copyright (2005), with permission from Elsevier.

The area of the electrode is an important parameter as it defines the current and charge densities. It is important to distinguish it from the electrochemical surface area, which defines the electroactive surface of the electrode, and is difficult to quantify for porous and electroactive

materials [1]. Based on their geometric surface area, stimulating electrodes can be roughly distinguished in micro (less then 10 000 μm^2) and macro (more than 100 000 μm^2) electrodes [1]. Microelectrodes are obviously more selective for stimulation, but they may also lead to higher current and charge densities with a higher risk of electrode or tissue damages, while macroelectrodes are characterized by lower current and charge densities, but also higher charge per phase which may also lead to tissue damages [19].

Recording electrodes are used to collect the electrical signals generated by the biological tissue's electrical activity, and a wide range of designs and dimensions have been used for different applications. The currents involved during biopotential recording are generally negligible when considering tissues damages, but the electrode impedance is still a concern as it influences the quality of the recording. These electrodes are typically characterized by their 1 kHz impedance due to the relevance of this frequency in biological processes, with higher impedances being typically associated with higher noise and lower signal to noise ratio [1, 16, 20].

2.2.3 Electrodes characterization

Electrodes need to be fully electrochemically characterized to obtain information on their performance for both recording and stimulation.

One of the main parameters used for characterization is the impedance, commonly studied through electrochemical impedance spectroscopy (EIS). As described in Section 2.2.1, the electrode/electrolyte interface interactions can be modeled using electric components mainly consisting of resistors and capacitors and can give a physical interpretation of the generally complex impedance. The EIS aims to study this impedance by applying a current or voltage sine wave at different frequencies at the working electrode. Let's consider the general case of a three-electrode electrochemical cell composed of a WE, a CE and RE, immersed in an electrolyte solution. During EIS, a voltage sine wave at different frequencies is applied at the WE, the resulting current between the WE and CE is measured, and the impedance is obtained by computing the current/voltage transfer function. As previously stated, the measured impedance is generally complex and comprises a real and imaginary component from which the information about the impedance magnitude and phase can be obtained [1]. Typical impedance plots are the Bode plot, which displays the phase and logarithm of the absolute value of the impedance versus the

frequency, and the Nyquist plot, which displays the imaginary part of the impedance versus the real part. The two plots convey complementary useful information. The Bode plot gives immediate practical information about the magnitude of the impedance, which can be used to indicate the quality of recording or stimulation, and about the type of electrode behaviour (capacitive or resistive) derived from the value of the phase. On the other hand, the Nyquist plot is more useful to describe each component of the electric model of the electrode/electrolyte interface, and can give more detailed information about the underlying electrochemical processes [17]. If we consider the simple Randles model with a single Faradaic process depicted in Figure 2.3, it is interesting to analyse the typical Nyquist and Bode plots which are reported in Figure 2.5.

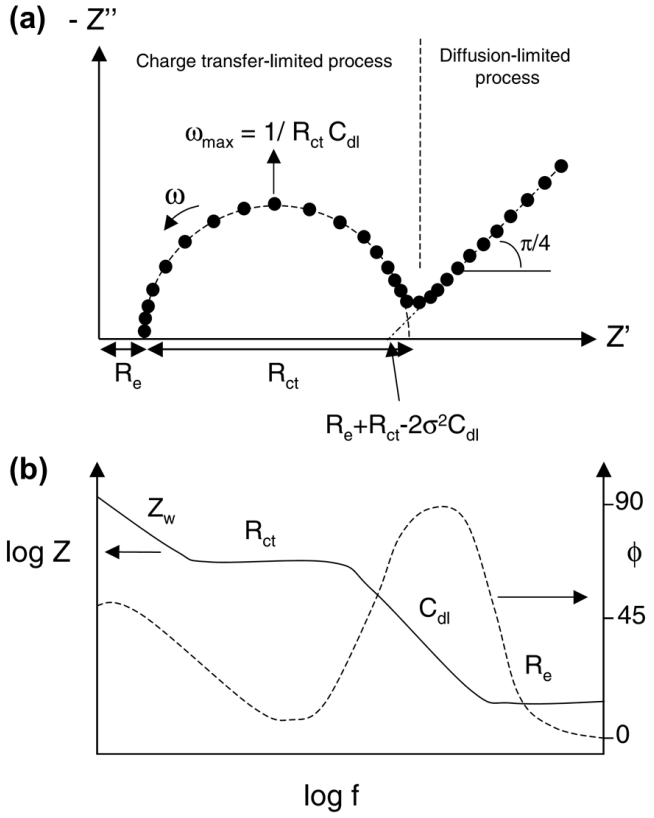

Figure 2.5 Nyquist (a) and Bode (b) plots for the single Faradaic process Randles model. Adapted from [17].

In the Nyquist plot (Figure 2.5.a), each point corresponds to a measurement at a certain frequency, with increasing frequencies moving from right to left, and the axes Z' and Z'' indicate the real and imaginary parts of the impedance, respectively. From this graph it is possible to calculate the values

for some of the elements used in the Randles model such as the electrolyte resistance R_e, the charge transfer resistance R_{ct}, the double layer capacitance C_{dl} and the Warburg coefficient σ, which is related to the diffusion. The left part of the diagram, which corresponds to the medium-high frequencies, is the charge transfer-limited process while the right part characterized by the straight line at 45° is typically identified as the Warburg impedance and contains information about ion diffusion [17].

On the other hand, the Bode plot gives information on the resistive processes, characterized by a straight horizontal line and phase values close to 0°, while the capacitive-behaviour-dominated processes have an impedance slope of -1 and phase values close to 90°, and finally, the low frequency part, related to the Warburg component, has an impedance slope close to -1/2 and phase values near 45° [17].

As discussed in the previous paragraphs, stimulating electrodes need to be capable to deliver the required amount of charge to elicit a response in the stimulated tissues, but at the same time they are limited in the amount of charge that can be delivered in order to avoid electrode polarization and the associated potentially harmful Faradaic reactions. Moreover, it is important to investigate the electrochemical reactions that take place at the electrode/electrolyte interface with particular attention to their reversibility and to the electrochemical stability of the electrode [1]. In this scenario, the cyclic voltammetry (CV) is an excellent tool to investigate aspects regarding the electrochemical interactions between an electrode and the surrounding electrolyte solution. The setup typically involves a three-electrode electrochemical cell with the electrode under investigation used as the WE, along with a RE and CE. The test involves recording the current between the WE and CE during cyclic sweep of the potential applied at the WE. Consequently, the CV appears as a sequence of curves whose shape depends on a number of factors such as the sweep rate, the potential window, the electrolyte solution, the temperature, and of course the geometry and material type of the electrode. The CV shape conveys information on the electrochemical reactions that take place at the electrode/electrolyte interface during the potential sweep, with positive and negative peaks indicating an oxidation and a reduction, respectively, following the IUPAC convention as depicted in Figure 2.6.a for a simple redox process [21].

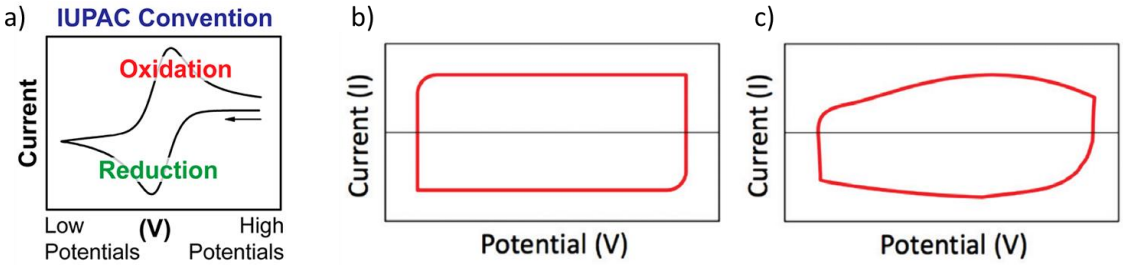

Figure 2.6 IUPAC convention for the CV (a) and examples of CV curves for an electrical double layer capacitor (b) and pseudocapacitor (c). Adapted from [21] (a) and [22] (b, c).

For example, an electrode showing purely capacitive behaviour will be characterized by a box-shape as in Figure 2.6.b, while pseudocapacitor behavior, characterized by the shape in Figure 2.6.c, may show a more squeezed box-shape caused by a slower current transition during the inversion of the potential sweep direction.

It is common in the literature to find electrodes characterizations based on what is referred to as the charge storage capacity (CSC). The CSC is computed as the time integral of the cathodic (negative) current in the CV, and it is normally obtained as an average over several cycles, performed using a potential window which is within the water electrolysis window, and at typical scan rate values of 10-1000 mV/s [1]. Finally, the CSC gives information on the amount of charge that can be delivered by an electrode during stimulation, and for this reason is one of the main parameters for electrodes characterization. However, it has been showed how CSC may be an inaccurate estimation of the charge-injection capacity of a neural electrode due to the inherent slow scan rate and associated low charge density, which are far from the experimental conditions encountered during *in vivo* stimulations [1]. In particular, it was verified that CSC *in vivo* tends to take into account not only the exposed surface area of the electrode, but also the part of the insulation where the surrounding fluids are able to penetrate, while this part does not participate in charge transfer at high sweep rates [1]. Moreover, the CSC may represent an overestimation of the charge injection capability of the electrode as not all the computed charge is available during sub-millisecond stimulations [23].

To overcome these limitations, another test consisting of the voltage transients can be performed for stimulating electrodes to obtain information on the deliverable amount of charge [1, 23]. Voltage transients measure the electrode polarization during current-controlled (typically biphasic)

stimulation, and can be used to calculate the charge injection limit, which represents the maximum charge density that polarizes the electrode at a potential for water reduction or oxidation [23]. Compared to CSC, this parameter reflects the actual capability of the electrode to operate in real conditions, and it can be used to determine if the electrode is capable to deliver the required amount of charge without reaching levels of polarization that can damage the surrounding tissues. Also in this case, attention should be put on the experimental conditions as changing parameters such as the current density can affect the charge injection limit measurement [1].

2.2.4 Current limitations

Typical invasive electrode architectures for stimulation and recording of biopotentials have been historically dominated by metals such as gold and platinum [16]. These metals have been widely studied and have demonstrated to be excellent materials for invasive electrodes, being widely used in the medical field and contributing to our current knowledge on biopotentials. However, advancements in both the medical and engineering fields require always smaller and more performant devices to be interfaced with our bodies, and these materials have shown limitations in their ability to satisfy the always stricter electrical requirements [16].

To record more localized action potentials, recording electrodes need to have a sufficiently small exposed surface area to avoid the collection of signals from surrounding undesired units (neurons, muscle fibers etc.). However, the reduction of the electrode's active area to achieve high spatial resolution reduces the amount of surface in contact with the solution, finally causing an increase in the electrode/electrolyte impedance [16]. The thermal noise (also called Johnson noise) associated with the random movement of charge carriers in a conductor due to thermal agitation can be computed for a simple resistor with the equation described in (6), where V_{rms} indicates the root mean square voltage, k_B the Boltzmann constant ($1.38064852 \times 10^{-23}$ J/K), T the temperature, R the resistance, and Δf the bandwidth [20].

$$V_{rms}{}^2 = 4k_B TR\Delta f \qquad (6)$$

Even if this expression only applies to a simple resistor, in the case of elements containing a complex impedance it can be demonstrated that the noise still depends on the real component of the impedance [24], thus confirming how a high electrode resistance can be associated with a higher

noise level that can subsequently degrade the quality of the recording. Another negative impact of a high electrode impedance on the recorded signal is due to the shunt loss. Let's consider the equivalent circuit for a neural electrode which records the electrical activity of a neuron described in Figure 2.7, where V_{sig} is the neural electric signal to be recorded, I is the generated current that flows to ground, R_s, R_e, C_e (previously seen also in the Randles model) and R_m are the solution resistance, charge transfer resistance, electrical double layer capacitance and electrode lead resistance respectively, C_s is the total shunt capacitance to ground from the tip of the electrode to the input of the amplifier composed by all the capacitive elements such as the electrode/insulation/electrolyte element and possible shielded connectors, and Z_a represents the amplifier's input impedance [3, 25].

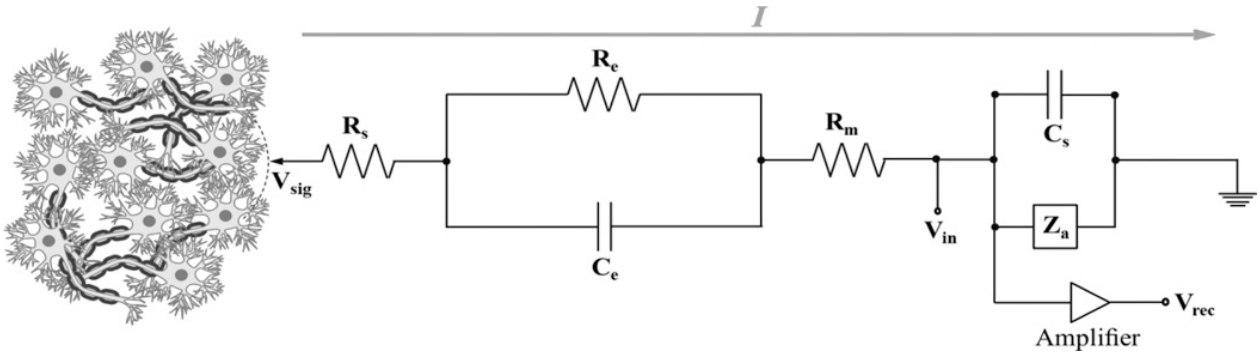

Figure 2.7 General equivalent circuit for a recording neural electrode and associated amplifier which record the electric potentials from a nearby neuron. © IOP Publishing. Reproduced with permission. All rights reserved [3].

In this situation, if we indicate Z_e as the impedance relative to the components from R_s to R_m (which therefore depends mainly on the electrode/electrolyte electrochemical interactions) and Z_{in} as the combination of C_s and Z_a (which takes into account the shunt components), the input voltage V_{in} measured at the amplifier will be given by (7) through the simple voltage divider equation:

$$V_{in} = V_{sig} \frac{Z_{in}}{Z_{in}+Z_e} \qquad (7)$$

From this expression, it is evident how, in order to avoid attenuations of the neural signal at the amplifier's input, it is necessary to have small values of Z_e compared to Z_{in}. While high values of Z_{in} can be achieved through several amplifier's input design techniques, Z_e is mainly dependent on the electrode/electrolyte impedance, whose high values can compromise the recording [16]. In this

regard, it has been observed that electrodes with impedance values higher than 5 MΩ at 1 kHz have difficulties recording the activity of single neurons due to high thermal noise and shunt loss [16].

Electrode impedance is intrinsically related to the ability of the electrodes to deliver charge through electrical stimulation, as low impedance values allow the delivery of high amount of charges without reaching high polarization levels that may damage the tissues [16]. As discussed in the previous paragraphs, stimulating electrodes need to be operated in a safe range to avoid potentially harmful electrochemical reactions at the electrode/tissue interface. Electrolysis of water with pH changes and gas formation, electrode metal dissolution or breakdown of the electrode passive layer and corrosion are just some of the detrimental electrochemical reactions that have been reported during stimulation with common metal electrodes [1]. Even if balanced charge pulses and accurate control on the stimulation waveform can be used to minimize the occurrence of such phenomena, these reactions can still take place and compromise the outcomes of the stimulation. For this reason, it is necessary to develop electrodes with high CSC and charge injection limit to avoid dangerous electrode polarization [16].

Another aspect that influences the performance of invasive electrodes, especially in long-term applications, is the degradation of the electrochemical properties due to biotic factors (i.e. issues related to the biological tissues) [16]. An implanted electrode for the body represents a foreign, non-recognised item that ruptures many biological tissues depending on the insertion site, such as blood vessels, neurons and extracellular matrix, causing an inflammatory response [26]. The inflammatory response can be separated as acute and chronic, with the former being associated with processes such as tissues rebuilding after insertion damage and macrophages recruitment to "clean" the debris surrounding the implant site [26]. As the acute inflammation decreases, the chronic inflammatory response initiates, with the formation of a connective tissue barrier (called glial scar if located in the central nervous system) around the electrode, and the activation of macrophages, that due to the impossibility of degrading the implant will fuse into multinucleated giant cells that secrete degradative agents and damage the electrode [26, 27]. The implantation of electrodes in the brain has been associated with the formation of a glial scar surrounding the implants which consequently increases the impedance at the electrode/tissues interface, finally degrading the quality of the recording or stimulation [3, 26, 27]. At the same time, the glial scar pushes neurons away from the implant creating a "kill zone" around the electrode, which

contributes to the decreased efficiency of the implant [3, 27]. One of the factors that has been identified as possibly responsible for this chronic inflammation is the mechanical mismatch between the stiff probe (e.g. the elastic modulus of silicon is around 150 GPa) and the surrounding tissues (elastic modulus around 100 kPa for the brain) [3, 27]. Typical microelectrode architectures such as the Michigan and Utah micro electrodes arrays are in fact characterized by rigid silicon probes that can cause chronic damages in the tissues due to micromotions [3]. On the other hand, it was suggested that the shape, size, texture, insertion technique and tip geometry of the electrodes only have a minor impact on the foreign body reaction and they mainly influence the acute inflammatory response in a way proportional to the electrodes size, but with no differences in the chronic response [28].

2.2.5 Advanced electrode materials

As we have seen, there are many factors contributing to the degradation of the electrode's performance for recording and stimulation, and many efforts have been put on trying to overcome such limitations, with most of the studies highlighting as a possible solution the need of new materials to interface with biological tissues [3, 26, 27]. In particular, the reduction of the impedance at the electrode/tissues interface has been a target for many studies. In fact, even if the geometry and substrates of the electrodes have been optimized over time, the active recording or stimulating sites still require metallic materials to be interfaced with the body, which as we have seen are associated with several drawbacks [29]. In the past this led to solutions such as coating metals with other materials in an attempt to improve the connection between the electrodes and the surrounding tissues. Activated iridium oxide is an example of a widely studied material that is able to reduce the impedance at the electrode/electrolyte interface because of the possibility of reversible Faradaic charge transfer, however, it was demonstrated to be mechanically and electrochemically unstable [1, 29, 30]. The electrochemical and mechanical stability of electrode coatings remains one of the main problems for their use in clinical applications, and many research groups have tried to tackle this problem by using more advanced materials.

Graphene sheets composed by a 2D layer of sp^2 hybridized and hexagonally arranged carbon atoms are an interesting alternative to bare metals due to their high electrical conductivity (1 S/m), high surface area (2630 m^2/g), transparency, mechanical stability (elastic modulus $\approx$ 1 TPa) and

biocompatibility [20, 31-34]. In particular, the combination of the peculiar optical and electrical properties inspired the researchers to employ this material for simultaneous electrocorticogram (with a SNR six times higher than similar gold electrodes) and calcium imaging *in vivo* [35]. Another interesting property of graphene is its capability to be directly formed on the substrate by modifications of the substrate itself, rather than coated on it, which reduces the risk of delamination [36]. For example, polyamide substrate pyrolysis followed by nitric acid doping led to the formation of microstructured porous graphene characterized by enhanced CSC and lower impedance compared to gold electrodes (Figure 2.8.a,b) [36]. This material is highly promising for biomedical applications and further studies must be conducted to investigate the long-term stability in terms of biocompatibility and electrochemical properties [20, 27].

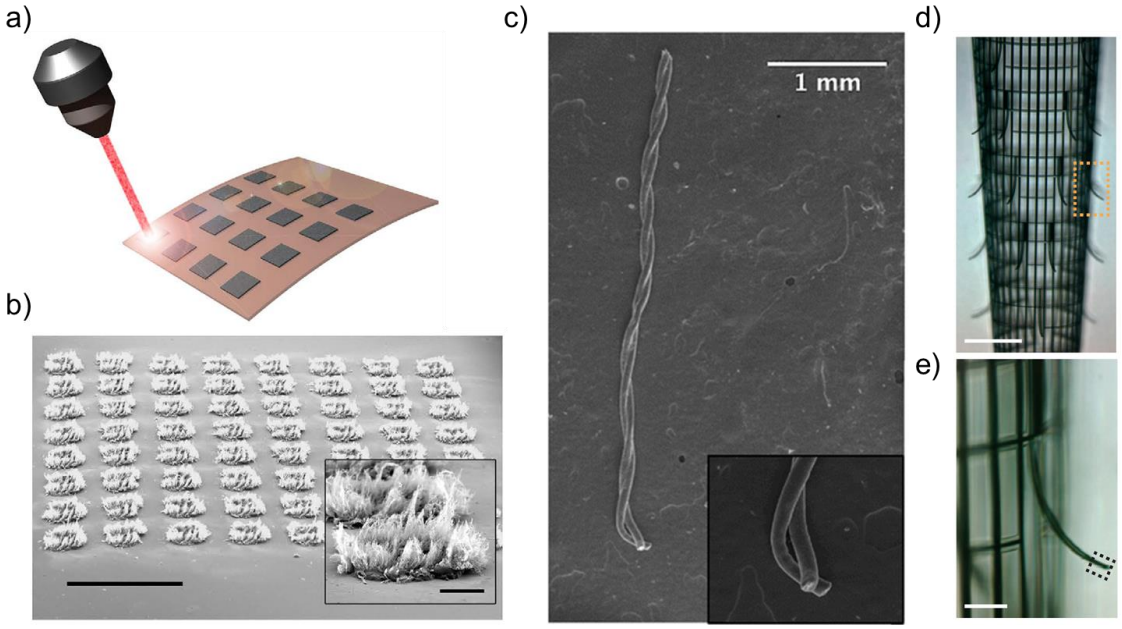

Figure 2.8 Polyamide laser pyrolysis (a), SEM picture of porous graphene sites (scale bare 1mm) and inset highlighting a single spot (scale bar 100 μm) (b) (adapted from [36]). SEM picture of twisted PS-b-PBD coated CNTs fibers with inset showing the active sites (c) (adapted with permission from [37]. Copyright (2015) American Chemical Society). Optical microscope image of the electrodes mesh (scale bar 200 μm) (d) and zoomed view of a single sensor element (50 μm) (e) (adapted from [38]).

Carbon nanotubes (CNTs) are probably one of the most investigated materials for implantable electrodes. CNTs are rolled graphite sheets, and they can be assembled in single or multi-walled

nanotubes with the latter being a concentric assembly of several single walled CNTs [39]. CNTs possess some interesting properties for *in vivo* recording such as high electroactive surface area (700 - 1000 m^2/g) [29], high conductivity and excellent mechanical stability (elastic modulus in the order of 0.64 TPa for a single nanotube [40]) [27]. CNTs can be directly electrodeposited on metallic electrodes and they are able to effectively reduce the impedance of the implant by an order of magnitude compared to bare metals [29, 41]. Another interesting approach consisted of the use of a wet spinning process to create long CNTs fibers (45 μm diameter), characterized by low specific impedance that were successfully insulated with a 3 μm layer of the copolymer polystyrene–polybutadiene (PS-b-PBD) and interfaced with the biological tissues during deep brain stimulation in animal models, demonstrating device robustness and improved biocompatibility compared to similar platinum-iridium electrodes (Figure 2.8.c) [37, 42]. The main problem associated with the use of CNTs for implantable electrodes consists of their high mechanical stiffness, which in some cases may lead to delamination from the substrate or direct mechanical damage to the surrounding tissues due to the non-compliant nature of the material [3].

A major improvement in the quality of recorded signals and stimulation can be achieved by the use of nanowire structures that extend from the electrode substrate with the aim of getting closer to the target points (e.g. neurons). This approach differs from the ones previously described as it departs from the classic plane structure of the electrode's active sites. An example of such devices is present in [38] and depicted in Figure 2.8.d,e, where a silicon based mesh was created with nanowires extending from it and containing the active sites, used to fabricate either field effect transistors (FET) or platinum electrodes (4 μm x 20 μm). In order to be inserted, the device was previously frozen under liquid nitrogen and then inserted immediately after, while it subsequently restored its flexibility once in site due to warming from the higher body temperature. As an alternative to freezing, devices able to be rolled and injected through a needle were also demonstrated [43]. The main challenge for these types of devices is the connection of the active sites leads with the external electronics, as the common I/O pins cannot pass through the needles used to implant the mesh. This requires the application of the connectors after the electrode implantation, which can make the procedure difficult by non-expert medical staff, increase the time of the surgery proportionally to the number of leads and introduces risks related to the sterilizations of the components [20, 38]. Still, this approach is extremely appealing and some groups have focused on ways to make the

connection more user-friendly [44]. Another critical aspect of this approach is the possible detachment of nanowires from the substrate which may result during or after implantation [27].

Due to the inherent mismatch between most of the previously described materials and biological tissues, the use of hydrogels has been also investigated for invasive electrodes. Hydrogels consist in water swollen, cross-linked hydrophilic polymeric networks and have gathered much attention in the biomedical field thanks to their high water content and mechanical properties which can be exploited for tissue engineering and drug delivery [27]. Hydrogels can be engineered in a variety of ways to tailor their properties for specific applications, and they are often combined with conductive polymers (CP), graphene and CNTs to form composite materials [27]. In this regard, an increasingly number of studies have pointed out how the use of composite materials could carry beneficial effects and solve some of the problem associated with the use of single electroactive materials. Other examples of such composite materials are (CPs)/CNTs, non-conductive polymers/CNTs and graphene/CPs composites [27].

2.3 Conducting polymers

From the previous paragraphs we have seen how current materials for invasive recording and stimulating electrodes fail to satisfy the requirements in terms of size, electrochemical properties and the biocompatibility necessary for new and more advanced biomedical applications.

The requirements for an optimal invasive electrode can be summarized as follows:

1) Low electrode/electrolyte impedance.
2) High deliverable charge.
3) Minimal tissues damages

Satisfying all these attributes requires the use of novel materials that can improve the interface between the electrode and the body. The functionalization of existing metal electrodes with these materials offers several advantages such as the use of existing and well-established electrode designs, but it also introduces new challenges in terms of materials stability. In this sense, electrode coatings need to possess the following features:

1) Electrochemical stability over time (i.e. low impedance and high deliverable charge).

2) Mechanical stability without delamination from the metallic substrate.

3) Resistance to sterilization (for example steam sterilization).

Conductive polymers (CPs) can offer all these advantageous features while being relatively easy to process compared to other materials. In this chapter, the principles behind their peculiar electrochemical properties are described, together with their processing and applications, with a particular focus on biomedical applications. Finally, poly(3,4-ethylenedioxythiophene) (PEDOT), one of the most promising CPs for biomedical applications, will be discussed in detail.

2.3.1 The discovery of conductive polymers

A major step in the development of conducting polymers was the report in 1973 that published that the inorganic polymer polysulfur nitride $(SN)_x$ possessed high conductivity (10^3 S/cm) and successively reported (1976-1977) that its conductivity could be enhanced by one order of magnitude by exposing the material to oxidizing agents such as bromine [45-47]. During these years Alan MacDiarmid and Alan Heeger, who were studying the properties of $(SN)_x$, came in contact with Hideki Shirakawa, who was investigating the polymerisation of acetylene using Ziegler-Natta catalyst [48]. Polyacetylene was known at the time to form a black powder, but in one occasion, a visiting researcher in Hideki Shirakawa's lab added one thousand times more catalyst, which resulted in a silver shiny polymer, suggesting that this material could have electrical properties similar to metals [48, 49]. Despite this discovery, the material was still a semiconductor, but later on the three scientists discovered that conductivity could be dramatically increased by 9 orders of magnitude by exposing the polyacetylene films to chlorine, bromine and iodine vapours which oxidised the polymer [50, 51]. This process of polymer oxidation was called doping (with an analogy to semiconductors doping) and led to the development of the first highly conductive polymer polyacetylene with a conductivity of 10^5 S/m (as a comparison, copper possess a conductivity of 10^8 S/m) [50, 51]. This discovery was ground-breaking (leading to the Nobel Prize in chemistry in 2000 for the three scientists) as polymers started to be seen not any more as just thermal and electrical insulators but also as conductors, giving rise to the field of organic electronics [49].

2.3.2 Conduction mechanism

Conducting polymers (also called conjugated polymers) are characterized by a conjugated structure which consists in alternating single and double bonds [4]. This structure arises from the sp^2 hybridization of the carbon atoms that produces 3 hybridized sp^2 orbitals and one p orbital. In a simple molecule such as ethylene (described in Figure 2.9.a) the sp^2 orbitals form in-plane σ bonds with adjacent atoms while p orbitals of adjacent carbon atoms form out-of-plane π bonds.

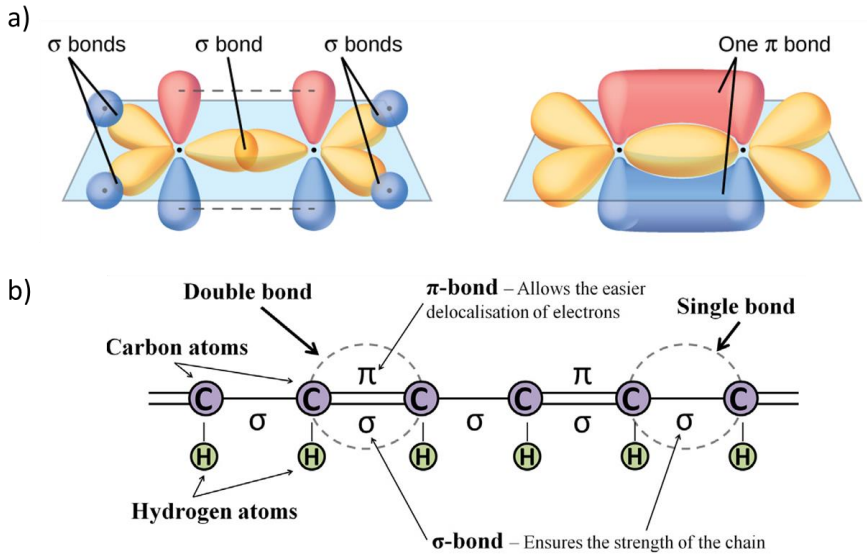

Figure 2.9 Molecular orbitals of sp^2 hybridized carbon atoms in ethylene (a) (adapted from [52]) and backbone representation of the simple conductive polymer polyacetylene (b) [4].

In CPs, single localized σ bonds give the mechanical strength while delocalized π bonds allow for the delocalization of the electrons (Figure 2.9.b). However, as we saw for polyacetylene, non-doped CPs have electrical properties similar to semiconductors with conductivities much lower than metals (i.e. polyacetylene has an intrinsic conductivity lower then 10^{-5} S/cm) [47]. Consequently, the presence of a conjugated backbone is a necessary but not sufficient condition for the high conductivities of CPs, and doping plays a key role.

The doping in CPs involves the introduction of an oxidizing (p-doping) or reducing (n-doping) chemical species that has the function of adding a positive (p-doping) or negative (n-doping) charge to the polymer backbone [4]. Typically, CPs are p-doped and the dopants are Lewis acids (i.e. oxidizing species), but also n-type CPs are possible in which case Lewis bases are used as dopants.

In the case of p-doping, the process can be expressed with the following formula where P_x and x represent the polymer units and their number, y the number of anionic dopants A^- per polymer unit and e are the electrons exchanged in the reaction (8) [53]:

$$-[P]_x- + xyA^- \rightarrow -\left[\left(P^{y+}\right)A_v^-\right]_x- + xye \qquad (8)$$

In this reaction, the polymer is oxidized (thus becoming a hole conductor), and the dopant is introduced in the polymer in order to balance the charge and ensure electrical neutrality [53].

The added charge is known as a polaron, and it consists in a localized charge carrier associated with a polymer lattice distortion [4]. Application of an electric potential to the polymer causes the movement of the aforementioned polarons allowing for electric conduction (Figure 2.10) [4].

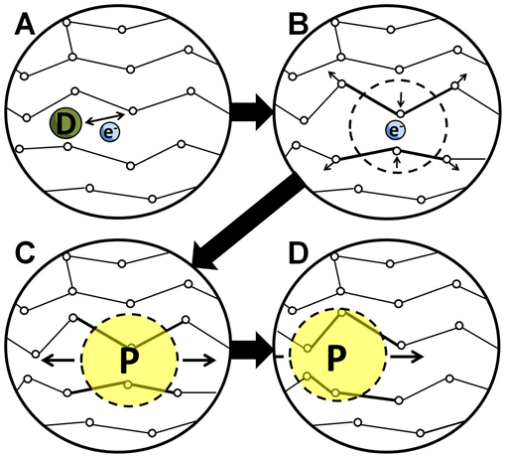

Figure 2.10 Schematics of an example of doping (n-doping) process in CPs: the introduction of the dopant D causes the addition of a delocalized charge carrier (electron e^-) in the polymer (A), the charge is localized producing a lattice distortion (B), the localized charge associated with a lattice distortion forms a polaron P (C), upon application of an electrical potential the polaron travels along the polymer (D) [4].

The doping of CPs and the polaron formation can also be conveniently described in terms of energy bands. The electronic delocalization enabled by the conjugated structure of conducting polymers as well as the pi-pi stacking result in the formation of electronic bands, where the valence band (VB) is generated by the overlap of the highest occupied molecular orbital energy levels in the single monomers, whereas the conduction band (CB) is associated with the overlap of the lowest unoccupied molecular orbital energy levels. The forbidden gap existing between the edge of the

VB and the edge of the CB is the bandgap E_g. In undoped CPs, the E_g has been determined to be larger than 1.5 eV, resulting in insulating behaviour [47]. In inorganic semiconductors, such as silicon, the doping process can either add an electron to the conduction band or add a hole to the valence band, and the charges are delocalized in an electronic cloud which results in a band-type conduction [54]. This type of band conduction poorly describe the charge carrier transport properties for conductive polymers in which the thin width of the bands results in computed mean-free path values lower than the molecule-to-molecule distance [54]. On the other hand, the doping in CPs results in the formation of intermediate energy levels that are associated to the presence of localized polarons [47]. Figure 2.11.a describes this situation in which the added dopant causes the formation of a polaron resulting in localized energy states in the energy gap due to the upward shift of the highest occupied molecular orbital (HOMO) and a downward shift of the lowest unoccupied molecular orbital (LUMO) [47].

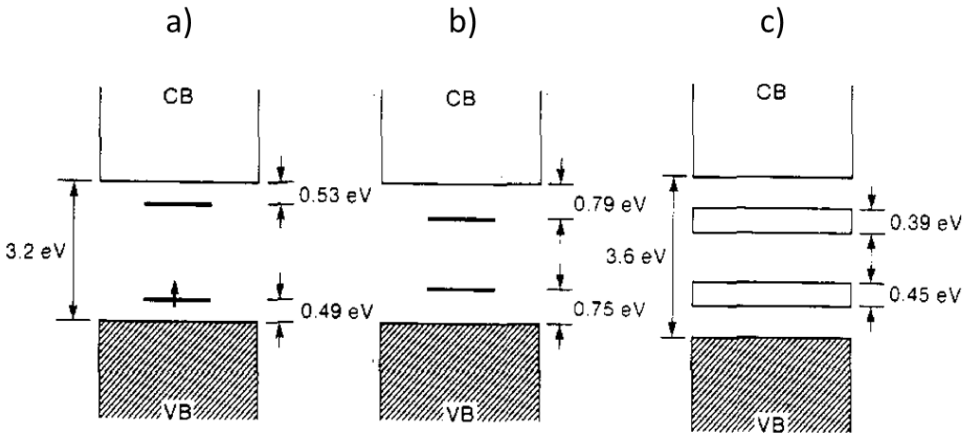

Figure 2.11 Polaron formation at low doping levels (a), bipolaron formation at moderate doping levels (b), bipolaron bands formation at high doping levels (c) in polypyrrole. Adapted with permission from [47]. Copyright (1985) American Chemical Society.

In this situation, the VB and the CB remain full and empty, respectively. As the doping level is increased, more polarons are formed and new intermediate levels are added to the energy gap. The formation of bipolarons (i.e. two polarons localized in the same molecule), as described in Figure 2.11.b, is more favorable than the formation of two separate polarons, and results in a wider displacement of the HOMO and LUMO levels. At high doping levels (Figure 2.11.c) the single

intermediate energy levels eventually merge, forming bipolaron bands and the bandgap widens due to the fact that the intermediate energy levels were moved from the VB and CB [47]. Typical models that describe the mechanism of charge carrier transport in CPs suggest the presence of thermally-activated hopping of the charge carriers between the molecules [54]. Still, there is evidence of thermally-independent behaviour in pentacene transistors, indicating a more complex conduction mechanism [54]. In this sense, Bredas and Street [47] suggested that metal-like transport behaviours observed in polythiophene could be related to the merging of the bipolaron bands with the VB and CB at high doping levels, but at the moment the true mechanism is still unknown.

2.3.3 Properties of conductive polymers

CPs possess several properties that make them appealing materials for various applications and especially for biomedical applications. These can be summarized as follows:

1. The high conductivity and the possibility to conduct both electrons and ions.

As discussed in the previous paragraph, the doping is a necessary step to increase the conductivity of conjugated polymers. Conjugated polymers can be synthetized and processed in various ways, and the range of conductivities can span from the ones of insulators to the ones of metals (Figure 2.12).

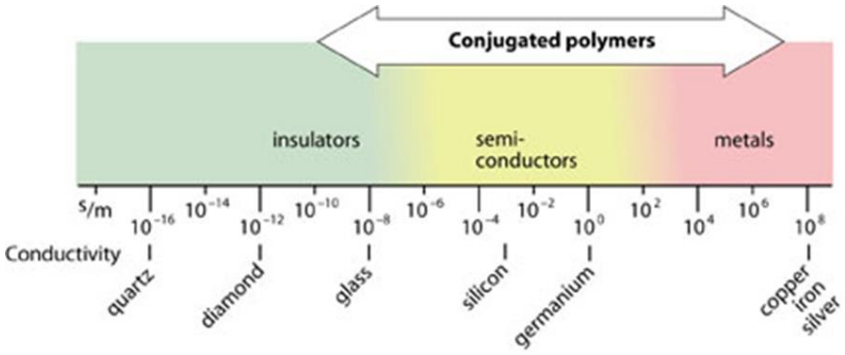

Figure 2.12 Range of conductivities ($S \cdot m^{-1}$) for conductive polymers [49].

However, what makes CPs interesting for biomedical applications is their ability to convert an ionic flow with the surrounding electrolyte into an electronic current. This property, which arises from the charge transport mechanism that involves the movement of ions in and out of the polymer,

allows them to create a suitable interface between electronics and the biological environment, with an increased efficacy in biological signal recording and current delivery [3, 4, 16, 55]. In particular, recalling the Randles model, CPs have the property of reducing the charge transfer resistance associated with Faradaic charge transfer. As discussed in the precious paragraphs, typical metal electrodes only show a capacitive behaviour once in contact with the biological environment, while CPs also allow for reversible non-harmful Faradaic reactions to take place at the interface, which finally causes a lowering of the electrode/electrolyte interface impedance [56]. This property is also extremely interesting for drug delivery applications in which the drug itself can be used as the dopant and consequently released in a controlled way once the electrode is implanted [4].

2. The mechanical and optical properties.

Besides their high conductivity, CPs gained interest because of their peculiar mechanical properties. Due to the weak van der Waals interactions between adjacent molecules, conductive polymers are soft and can offer a more compliant interface with the tissues compared to the stiffer metals and silicon interfaces, thus reducing the inflammatory response in the body [57]. These materials can be also processed to obtain flexible and stretchable devices that compensate for tissue movements, absorbing the mechanical stress that arises from skin deformation, for example, consequently improving the quality of recording/stimulation when used as part of wearable and on-skin sensors [57-60]. Some CPs possess interesting optical properties such as electrochromism, arising from the doping/de-doping process, and they can yield transparent films [59, 61, 62]. The latter property is extremely important for biomedical applications as the possibility of transparent devices allows to better control their positioning e.g. during surgery procedure and makes further medical analysis such as medical imaging feasible without removing the device [35, 57].

3. The improved biocompatibility.

The chemical structure of CPs, together with their mechanical and thermal stability, gives them the ability to be implanted for long periods without harming the patient's body [4, 63-68]. CPs can offer a soft and rough surface to interface with biological tissues compared to the stiff and smooth surface of most metal-based electrodes, and have been shown to possess good in-vitro and in-vivo biocompatibility, with better cells proliferation compared to bare metals [4].

2.3.4 Processing techniques

Several techniques can be used to process CPs, and among them electropolymerization, spin coating, vapor phase polymerization (VPP) and electrospinning are the most popular [55].

Electropolymerization allows the deposition of CPs on conductive substrates, such as the exposed tip of a metal electrode, through the application of an electric potential or current in a solution containing the monomer of the CP and the dopant dissolved in a solution. This allows for fine control of the electrochemical properties of the CP compared to other techniques because of the possibility to choose among different electrodeposition techniques as well as among a wide range of dopants and solvents [4, 55]. Electropolymerization has found several uses for biomedical applications since it is possible to create CP coatings on very small and non-flat conductive surfaces, but it is limited for other applications as it requires a conductive substrate for the CP deposition.

Spin coating is probably the simplest among all the processing techniques as it can be applied to commercially available CPs formulations. It is able to easily cover large areas and several additives such as conductivity enhancers, plasticizers and cross-linkers can be added to the solution to tailor the mechanical and electrical properties of the films [55, 58-60, 69].

In VPP, a film of the oxidant is exposed to the vapours of monomer that polymerizes when in contact with the surface, allowing for the creation of thin and uniform films [70].

Finally, electrospinning process generally involves the use of a syringe filled with the polymer solution and a charged metallic needle directed toward a grounded or oppositely charged surface. A high-voltage power supply causes the formation of microfibers and nanofibers starting from the syringe tip and depositing on the opposite surface. This technique is particularly appealing as it allows for the creation of fibers with high conductivity and peculiar mechanical properties that can be employed as scaffolds and stretchable mats [4, 55].

2.3.5 Principal conductive polymers

A wide range of conductive polymers have been developed over time (Figure 2.13), with the first studies being focused on polyacetylene, that ultimately demonstrated the material to be difficult to process and unstable when exposed to air and therefore not suitable for applications [4].

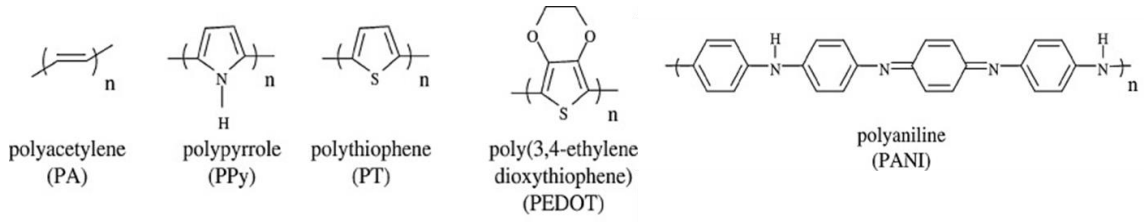

Figure 2.13 Examples of some of the most studied CPs. Note the conjugated structure that is present in each of them. Reprinted from [71], Copyright (2007), with permission from Elsevier.

Most of the past research on CPs has been concentrated on polyaniline (PANI) and polypyrrole (PPY) [4]. While most CPs only have two electrochemical states (reduced and oxidized), PANI possesses three states: leucoemeraldine (fully reduced), pernigraniline (fully oxidized) and emeraldine (half oxidized), with the latter being the most stable and conductive form, and has been observed to possess conductivities in the order of 100-200 S/cm [72]. However, its low processability, non-biodegradability, and loss of conductivity at physiological pH values [73] have limited its use in biomedical applications. In addition, some studies have observed that the polymer caused chronic inflammation upon implantation [4].

The second most investigated CP is polypyrrole, which possesses higher conductivity (10^2 – 7.5 x 10^3 S/cm) compared to PANI, and is also more biocompatible and easy to process [4, 74]. The major drawback in the use of PPY for biomedical applications is its poor electrochemical stability which causes a deterioration of the electrochemical impedance and charge storage capacity over time [75-79]. The main reason for this degradation are structural pulverization and counterion drain effect [80]. The former arises from the doping/de-doping process which causes repeated expansions and contractions of the polymer lattice that eventually causes either a delamination from the substrate or cracks in the polymer, while the latter is due to the fact that expelled ions during reduction cannot re-enter in the polymer due to the simultaneous collapse of the ion channels, leading to a reduction of the number of polarons and to the decay of the electrochemical properties [80].

Finally, an important CP consists in the polythiophene and its derivatives such as poly(3,4-ethylenedioxythiophene) (PEDOT). This one in particular has found many applications in different fields and is one of the most promising CPs for biomedical applications (this CP will be described in detail in the next paragraph).

2.4 PEDOT

Poly(3,4-ethylenedioxythiophene) (PEDOT) consists in a polythiophene containing a dioxyalkylene bridging group across the 3- and 4- positions of its heterocyclic ring. The presence of this group is the reason for the enhanced electrochemical properties of PEDOT since it lowers its bandgap and reduction and oxidation potentials [4]. Moreover, this group blocks the 3- and 4-positions preventing α-β coupling, considered to be one of the main reasons for the deterioration of the conjugated structure in PPY, giving PEDOT excellent electrochemical stability [81].

One of the most successful formulations of PEDOT is the one that uses polystyrene sulfonate (PSS) as the dopant (Figure 2.14), and several solutions are commercially available for specific applications [82]. PEDOT:PSS commercial formulations can achieve conductivities up to 1000 S/cm but polymer films can be further treated to achieve conductivities up to 4600 S/cm [82, 83]. Other available formulations can achieve high transparency and flexibility, which led to the use of PEDOT in organic light emitting diodes (OLEDs) to fabricate flexible, and transparent displays [82].

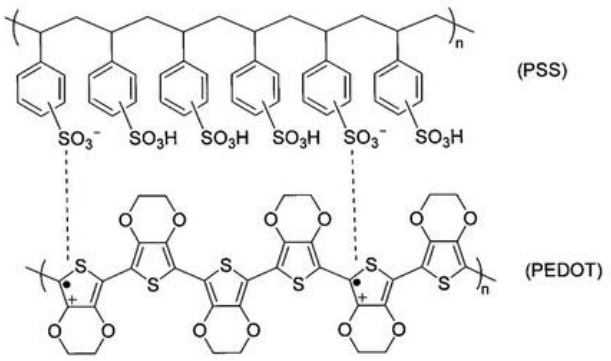

Figure 2.14 Structure of PEDOT:PSS [82].

PEDOT is also currently as channel material for organic electrochemical transistors (OECTs). The structure of an OECT is similar to that of an ion sensitive field effect transistor (ISFET) but with the difference that in this one the dielectric layer is removed, and the electrolyte put in direct contact with the channel, which is commonly made of an organic CP (see Figure 2.15). A gate electrode is then immersed in the electrolyte and the application of a gate potential causes a redistribution of the ions inside the solution. In this way, ions in the electrolyte can penetrate inside the channel material, modulating its doping level and consequently the drain current.

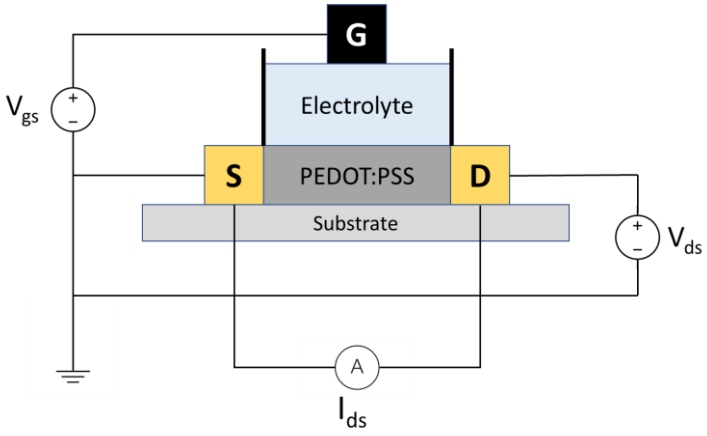

Figure 2.15 General structure of an OECT employing PEDOT:PSS as the channel material with G,D and S being the gate, drain and source electrodes respectively. A change in the gate voltage V_{gs} modifies the distribution of the ions in the electrolyte, causing the doping/de-doping of the PEDOT:PSS films, finally modulating the channel current I_{ds}.

OECTs typically work in depletion mode (i.e. the application of a gate voltage causes the de-doping of the channel, reducing the final channel current), which allows for low gate voltage operation in the saturation region. The electrolyte gating and absence of dielectric material results in higher transconductances of OECTs compared to field effect transistors, and OECTs are also more stable with respect to ISFETs due to the lower gate voltages. Finally, they can be fabricated on a variety of substrates such as stretchable and flexible materials, paving the way for new lab-on-skin and wearable applications [58-60, 69, 84].

Finally, our group recently discovered that PEDOT:PSS films with thickness over 1 μm possess self-healing properties in aqueous environments with very fast response (150 ms) when a drop of water is applied on a 40 μm cut in the film. When healed films are then baked (140 °C for 1h) to let the water evaporate, the current remains stable indicating that the presence of water after healing is not necessary for the healing of the film. The group was also able to achieve the healing of the films through water vapour exposure (relative humidity above 80%) and verified that wet films do not show a drop in current when cut. PEDOT:PSS films treated with conductivity enhancers (glycerol) and plasticizers (Capstone FS-30) deposited on flexible substrates (PET and polyamide) also showed self-healing properties, indicating that this property is intrinsic of PEDOT:PSS. The authors suggested that this behaviour could be due to the swelling of PSS shells which could move

the PEDOT:PSS grains in the damaged area, finally causing the bridging of the two sides through hydrogen bonds between PSS shells. The fact that PEDOT:PSS shows self-healing properties is extremely powerful and the authors proposed it could be exploited for water-erasable read-only memory, water-controlled switches for inflatable life jackets, wireless transmitters for maritime search and rescue, and disposable water detectors for food packaging [55, 85].

2.4.1 PEDOT-based electrodes for biomedical applications

Most of the previous works in the medical field focused on the use of PEDOT as a coating for electrodes for neural recording and stimulation, with only a few examples of EMG recording.

Mandal et al. polymerized PEDOT doped with tetrafluoroborate (TFB) on microelectrode arrays (MEAs) for neural signal recording and in vivo impedance spectroscopy. The comparison with the bare electrodes showed that once implanted PEDOT-coated electrodes were able to maintain the impedance at least one order of magnitude lower respect to the uncoated electrodes, with both showing a similar increase in impedance over time, probably due to the biological reaction. The reduced impedance helped achieve lower noise signal levels and a higher signal quality [86].

Abidian et al. used Poly (L-lactide) (PLLA) electrospun nanofiber templates to create PEDOT doped with $LiClO_4$ nanotubes on Michigan neural microelectrodes for chronic neural recordings and in vivo EIS in the barrel cortex of rats [87]. Data displayed an increase of the 1 kHz impedance for both coated and uncoated electrodes during the first days after surgery probably due to protein absorption, also showing an increase in impedance over the whole frequency spectrum at day 8 and 49, which can be associated with acute and chronic inflammatory response. Over the whole testing period, PEDOT coated electrodes achieved lower impedance levels compared to the controls and could detect in a larger number of electrodes (65% of total PEDOT coated electrodes) high quality (SNR > 4) units compared to 35% of control sites. Thanks to the reduction in the noise, PEDOT-coated electrodes were able to achieve higher SNR, and low frequency artefacts (< 0.1 Hz, most likely due to motion related artefact or low frequency perturbations of the open circuit potential at the recording sites) that were on the other hand present in the local field potentials (LFP) recordings from the uncoated sites. The authors suggested that further improvements could be made on the PEDOT-based implants by incorporating drugs into the polymer matrix for controlled drug delivery.

Ludwig et al. also explored the electrodeposition of PEDOT:PSS on Michigan neural microelectrodes for neural recordings [88]. Bare electrodes were selected to have very small dimensions (15 μm and 177 μm^2 geometric surface area) and an impedance at 1 kHz of 9.1 ± 1.4 MΩ, which was previously reported to be problematic for single neurons recording [25]. After PEDOT electrodeposition, the impedance dropped to 0.37 ± 0.05 MΩ. Also, in this case, impedance increased over the days after surgery with the final 1 kHz impedance being 11.4 ± 2.2 MΩ for the uncoated electrodes and 2.21 ± 0.7 MΩ for the PEDOT coated ones at day 8. The noise level always remained lower for the PEDOT-coated electrodes throughout the recording period, with an increase over time which corresponded to a decrease of the total number of detected units (0.8 ± 0.1 average units per site post-surgery, compared to 0.4 ± 0.2 average units per site between days 6 and 8). On the other hand, the noise levels in the uncoated sites completely obscured any neural activity and thus neural activity was not detected during this study. In this case the authors suggested that the PEDOT-based electrode performance could be further enhanced by reducing the dimensions of the electrodes even more to cause minimal trauma during insertion and avoid the inflammatory response which was attributed as the cause for the decrease in total number of active sites over time.

Khodagholy et al. departed from the electrodeposition of PEDOT by instead fabricating planar and conformable electrode arrays based on PEDOT:PSS patterned on gold electrodes on a Parylene C substrate [89]. The $GABA_A$ receptor antagonist bicuculline was used to trigger sharp-wave events which mimic epileptic spikes in rats, and the electrode array was used for electrocorticography (ECoG). The performance of the PEDOT-based electrodes was compared to bare gold sites, which allowed them to determine that electrodes coated with PEDOT were able to achieve higher power in the range 1-10 Hz and 30 Hz, which are the main components during bicuculline-triggered sharp-wave events.

Tian et al. explored the use of PEDOT for acute EMG recordings. PEDOT doped with pTS was electrodeposited from an aqueous solution on gold wire electrodes insulated with Parylene C [56]. The wire electrodes were embedded together with flexible microtube channels for drug delivery inside a teflon casing. The coated electrodes were subjected to 5 min of ultrasonication (50 W power ultrasonic bath) which led only to a partial peeling off of PEDOT clusters from the surface, and to repeated (1000 cycles) CV which decreased the CSC from 58.83 ± 4.23 C/cm^2 to 45.40 ±

6.89 C/cm^2. Both coated and uncoated electrodes were implanted in the rat's gastrocnemius and used for acute EMG recording during nerve stimulation. PEDOT coated electrodes showed enhanced signal amplitude and lower 50 Hz noise, which resulted in better single motor unit action potentials recording. The same group later improved this device using a single structure obtained by wrapping a Parylene C substrate containing the gold electrodes on a flexible polymer-based microtubular structure for parallel drug delivery [90]. PEDOT:PSS was then electropolymerized on the gold electrodes, which caused a dramatic reduction of the impedance over the whole frequency range (10^{-1} – 10^5 Hz) and an increase in CSC compared to bare gold. Rat pheochromocytoma PC-12 cells were also cultured on the PEDOT covered electrodes. The cells became neural cells forming neurite-like interconnections with each other with the addition of neural growth factor, highlighting the good biocompatibility of PEDOT:PSS. Electrodes were also implanted in the gastrocnemius and tibialis anterior of rats and EMG signals were recorded during sciatic nerve stimulation and drug delivery. SNR of PEDOT-based electrodes was improved mainly thanks to a reduction of the noise especially at 50 Hz.

Mandal et al. also demonstrated the capabilities of PEDOT to provide neural stimulation [91]. The group implanted in rats NeuroNexus probes containing Pt/Ir active sites that were then separately treated to obtain Au-coated, PEDOT:PSS, PEDOT:TFB, and CNT:PEDOT:PSS-coated electrodes. In vivo stimulation was performed using current-controlled biphasic pulses on anesthetized animals, while neural signal recording was carried out in free-moving conditions. Results demonstrated how PEDOT doped with TFB was able to achieve lower voltages during stimulation and higher signal to noise ratio during neural recordings compared to the other PEDOT formulations over a 50-day period, also demonstrating better stability, capable of maintaining a higher number of recorded units over time.

Recently, we demonstrated PEDOT-based electrodes for deep brain stimulation (DBS) [92]. PEDOT doped with tetrafluoroborate ($TEABF_4$) was electrodeposited on Pt/Ir single wire electrodes using three different solvents (acetonitrile, propylene carbonate and deionized water) and was subjected to various harsh treatments to test the stability, such as steam sterilization, prolonged PBS soaking, ultrasonication and in vitro current-controlled biphasic stimulation. PEDOT coatings demonstrated excellent stability in organic solvents and were used for in vivo DBS and EIS. Results demonstrated an increase in impedance over time for both uncoated and

coated electrodes, which was tentatively attributed to the inflammatory response, with the coated electrodes maintaining lower impedance with respect to the bare electrodes before the stimulation session. Interestingly, neural stimulation caused a decrease in impedance after the DBS session, which could be explained by the cleaning of the electrodes surface through the electric pulses, removing adhered cells and adsorbed proteins.

2.4.2 Electropolymerized PEDOT coatings

When dealing with small, sharp, and non-flat surfaces, such as the ones of some implantable electrodes, electropolymerization is one of the best (and sometimes the only) method to deposit CP films. As mentioned in the previous paragraphs, the electropolymerization setup consists of a solution containing the monomer of the CP, the dopant (which works also as the supporting electrolyte) and the solvent (Figure 2.16). The common method for polymerization is performed in a three-electrode electrochemical cell, where the working electrode (WE) is the one to be coated, the counter electrode (CE) is used to close the electrical circuit, and the reference electrode (RE) is used to obtain a stable reference potential.

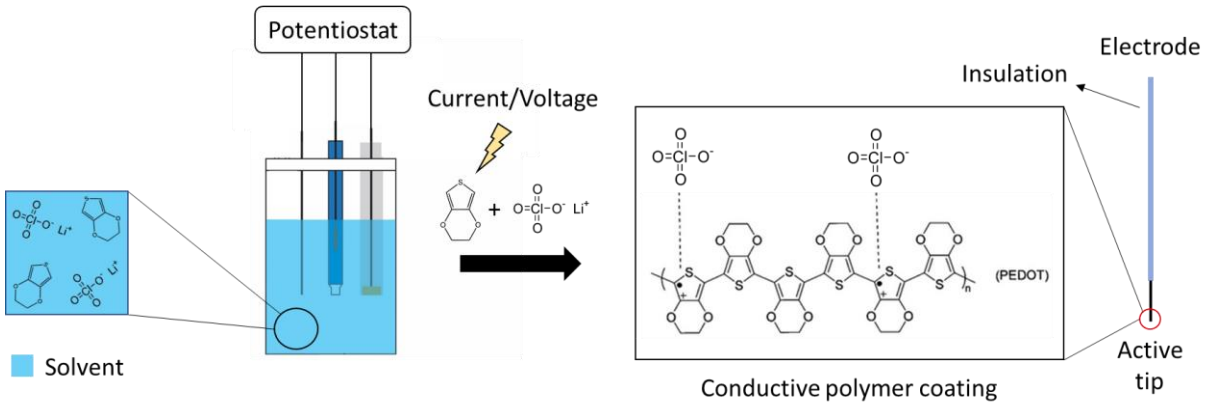

Figure 2.16 Schema for the electropolymerization of PEDOT doped with $LiClO_4$ on the surface of the metallic active tip of an electrode. Adapted from [93].

By applying a potential or current at the WE, the monomers polymerize to form an insoluble CP coating on its surface. Initially the application of a current or potential oxidizes the monomers causing the formation of radical cations that react together to form oligomers [94, 95]. The nucleation phase then involves the oligomers precipitation on the WE surface to form the initial nuclei. Due to the fact that new nuclei will continue to form during the electropolymerization (i.e.

they do not necessarily grow from previous nuclei) there will be nuclei with different dimensions. Finally, different nuclei will continue to grow until they merge to form polymer globules and cover the whole electrode surface. Typically the electropolymerization causes the formation of a positively charged (oxidized) polymer on the surface of the electrode, and the dopants from the solution are embedded in the polymer lattice during the process to balance the charge and ensure the electroneutrality of the polymer.

2.4.3 Influence of the electropolymerization conditions

The properties of the resulting polymer coating depend on a number of factors such the deposition technique, the choice of the solvent and dopant, the type of substrate, and the amount of deposited material.

Three main techniques are available for CPs electropolymerization: constant current (galvanostatic), constant potential (potentiostatic) and cyclic voltammetry (potentiodynamic). Among all the techniques, galvanostatic polymerization is the one that offers better control of the polymerization conditions since the rate of the radical formation (i.e. the current) is controlled, and it has been demonstrated to produce more uniform coatings compared to potentiostatic [96]. On the other hand, both potentiostatic and potentiodynamic polymerization only control the voltage, letting the current evolve in an uncontrolled way. In particular for potentiodynamic, the deposition rate changes continuously as the potential is swept from low to high potentials, resulting also in a layer-by-layer deposition. However, this technique is particularly useful to understand the electrochemical reactions that take place during the polymerization and to reveal some additional information such as the onset of the polymerization (i.e. the oxidation potential of the CP).

The choice of the type of dopant has a dramatic effect on the conduction of CPs. In fact, as an electric potential is applied to the material (in contact with an electrolyte), it causes the movement of ions inside and outside the polymer with a consequent change of its dimensions. The types of dopants can be separated into two main classes depending on their size: large and small dopants [4]. One of the most common large dopants used in combination with PEDOT is the polyanion polystyrene sulfonate (PSS), which acts as a doping anion when embedded in the PEDOT matrix. In the case of PEDOT:PSS, the dopant is not mobile due to its polymeric nature, which implies the incorporation and expulsion of ionic species present in the electrolyte to perform the doping/de-

doping process. In its oxidized (conductive) state, only the PSS^- is present inside the polymer matrix, which causes the polymer to have the smallest volume. During reduction, due to the impossibility of PSS^- expulsion, cations from the electrolyte penetrate in the polymer lattice to de-dope the polymer, causing at the same time an increase of its volume (swelling). In this scenario, the volume of the polymer increases during reduction. The process for non polymeric small dopants (i.e. ionic species that can move in and out of the polymer) is different and it depends on the nature of the dopant (anion or cation) and on the type of ions that are present in the electrolyte. Since CPs are generally p-type doped, and the dopant is an anion such as perchlorate (ClO_4^-) or tetrafluoroborate (BF_4^-), the dopant is expelled during reduction (de-doping) causing the polymer to contract, while it penetrates back into the polymer during the oxidation (re-doping), resulting in an expansion of the material volume. This process is not general, as it implies only anionic species in the surrounding electrolyte. In the presence of cations in the solution a process similar to PEDOT:PSS can take place, specifically, an incorporation of positive charges during reduction (with an increase in polymer volume) and their expulsion during the oxidation [97].

Moreover, the choice of the dopant has a direct impact on the morphology, biocompatibility, electrochemical properties and stability of PEDOT. Baek et al. systematically studied the influence of the dopant on the mechanical, electrochemical and biocompatibility properties of electrodeposited PEDOT [98]. Lithium perchlorate ($LiClO_4$), sodium benzenesulfonate (BS), sodium p-toluenesulfonate (pTS), sodium dodecylbenzene sulfonate (DBS) and PSS (dopants are ordered in increasing molecular size) were used as dopants for PEDOT galvanostatic electropolymerization (total passed charge = 0.1 C/cm^2) on a Pt substrate in a mixture of 50/50 water/acetonitrile (0.1 M monomer concentration). They observed that film roughness decreases with increasing dopant size, with $LiClO_4$ giving the roughest and most nodular films. At the same time, a nanoindentation mechanical test showed that film stiffness increased with increasing dopant size with PSS giving films with highest elastic moduli. Nonetheless, all coated substrates possessed an elastic modulus 2 orders of magnitude lower compared to bare Platinum. In addition, the choice of the dopant had a major influence on the electrochemical properties of the PEDOT films, with small dopants having higher CSC and lower impedance compared to large dopants. After repeated cyclic voltammetry, the PEDOT films processed with small dopants showed a larger loss in CSC but still possessed higher values compared to large dopants. The lower conductivities of

PEDOT:PSS could be due to the increased spacing between PEDOT chains due to the excess of PSS in the films, which consumes more space than required, thus making charge carriers hopping more difficult. This can be understood by looking back at Figure 2.14, where due to the fact that PSS contains a doping group for every repeating unit, it ends up occupying more space than required for PEDOT doping (CPs doping levels are around 20/30 %). On the other hand, small monomeric dopants are present per three to five CP monomer units, finally optimizing the doping. Finally, the study revealed a better growth of PC12 cells on PEDOT doped with $LiClO_4$ compared to all the other films. In this case, it was expected that dopants with higher toxicity should lead to worse biocompatibility of the films. However, this was not the case as the lower toxicity dopant BS had similar low levels of cell density as DBS, the most toxic, highlighting the influence of other parameters such as the film stiffness and surface morphology [98].

The same research group investigated the influence of the thickness of the deposited layers on the biocompatibility of PEDOT coatings [99]. PEDOT films were electrodeposited on Pt substrates using pTS, $LiClO_4$ and PSS as dopants with deposition charges ranging from 0.05 to 1 C/cm^2. As the total passed charge increased, the thickness, the nodularity and the amount of dopant increased too, with a corresponding enhancement of the electrochemical properties (lower impedance and higher CSC). Again, films doped with the large dopant PSS were smoother respect to PEDOT films doped with $LiClO_4$ and pTS, showing also lower CSC and higher impedance at similar deposition charge. An interesting finding in this study was that the PC12 cell viability decreased with increasing film thickness, which was explained as the influence of higher amounts of potentially cytotoxic dopants (but also solvent traces and other chemicals introduced during the polymerization process) embedded in the films and that can be released in the cell culture, finally decreasing cell attachment and growth. All films deposited with charge densities lower than 0.1 C/cm^2 (except for PEDOT films doped with $LiClO_4$) enhanced cell proliferation compared to bare Pt, but showed a steep decrease in cell viability with increasing charge density, with $LiClO_4$ showing the smallest changes and having better performances than the other dopants at high (>0.5 C/cm^2) charge densities. Among all the dopants, pTS showed better performance at low charge densities (0.05 C/cm^2) during the in vitro biocompatibility study, which is in contrast with what observed by the same group in a previous work where $LiClO_4$ showed better performance [98]. This may be due to the high deposition charge (1 C/cm^2) used in that previous study, which is supported by the

observation in the new study that with increasing deposited charge, the smaller dopant ClO_4 outperforms pTS and PSS in the in vitro cells study. It should be noted that films deposited at lower charge densities offered a more modest improvement in the electrochemical properties compared to bare Pt [99]. This highlights several aspects such as, the trade-off between the mechanical, electrical and biological properties of CPs for biomedical applications, but also the dependence of the results on the type of substrate. In fact, even if not highlighted by the authors, the choice of a large Pt disk as a substrate offered a low starting impedance (< 1kΩ at 1kHz), which of course requires a large amount of CP to be deposited in order to cause an appreciable drop of the impedance at the biologically relevant frequency of 1kHz. This is not the case of most implantable neural electrodes where the 1 kHz impedance can easily be close to 10^6 Ω, in which case even a thin CP coating can cause a major improvement of the electrochemical properties, also allowing for enhanced biocompatibility [88].

Mandal et al. electrodeposited PEDOT doped with PSS, tetrafluoroborate (TFB) and PEDOT:PSS with CNT incorporated on Pt/Ir electrodes electroplated with Au to offer a more porous surface to help polymer adhesion [86]. The group tested the electrodes under prolonged accelerated ageing at 60 °C for 80 days and reported an increase in impedance for all the electrodes. The impedance increase was suggested to result from a change in the coating morphology from porous to smooth. This observation was supported by the increase of the charge transfer resistance and simultaneous drop of the double layer capacitance, which can be due to the collapse of the porous structure. However, PEDOT:TFB was able to achieve a lower initial and final impedance compared to both PEDOT:PSS and PEDOT:CNT:PSS, and also no differences were found between the two PSS doped formulations. The group suggested that the improved performance of TFB compared to PSS as a dopant could be due to the higher crystallinity of PEDOT when doped with the former, leading to a better structural stability of the polymer coating [86].

2.4.4 PEDOT biocompatibility

Several studies have reported the good biocompatibility of PEDOT in both in vitro and in vivo studies, many of them involving $LiClO_4$ as the dopant.

Del Valle et al. studied the cellular adhesion and proliferation of epithelial cells (Hep-2) derived from a human laryngeal carcinoma on PEDOT doped with $LiClO_4$ films electrodeposited on

stainless steel substrates in the organic solvent acetonitrile [65]. It was found that not only PEDOT promoted cells adhesion and proliferation better then bare stainless steel, but also that PEDOT films covered with cells had higher charge storage capacities compared to uncovered PEDOT films, which suggest also the electrocompatibility of this material [65].

Luo et al. also reported the good biocompatibility of PEDOT both in vitro and in vivo [100]. Various PEDOT derivatives were electropolymerized on ITO substrates in presence of the dopant $LiClO_4$. Cells from NIH3T3 fibroblast cell line and HepG2 human heptocarcinoma cell line were used to evaluate the in vitro biocompatibility of PEDOT films and displayed better proliferation on the CP-covered substrates compared to bare ITO. The covered substrates were also implanted in vivo subcutaneously for a maximum of 28 days and only thin layers of tissue capsule and no vascularization were observed after explant, with also no immune reaction or cell invasion on the implant even after 1 week [100].

In an interesting study, David Martin's group studied the feasibility of in vivo electropolymerization to bypass the glial scar resulting from neural implants [101]. First, the cytotoxicity of PEDOT:PSS directly polymerized on cultured cells was evaluated. It was found that cells could be exposed for as long as 72 h to commonly used concentrations (0.01M) of EDOT and PSS (0.02M) maintaining at least 75% viability. This demonstrated the feasibility of direct on-cell PEDOT polymerization as the process typically requires only 30 s – 10 min. Then, SH-SY5Y neuroblastoma-derived cells and mouse primary dissociated cortical cultures (MCC) were cultured on custom-made Au/Pd electrodes and Applied BioPhysics (Troy, NY) ECIS electrodes, and PEDOT:PSS was electrochemically deposited on them using a solution containing the EDOT monomer (0.01 M), PSS (0.02 M) and phosphate buffer solution (PBS). PEDOT was able to cover the substrate and the cells without disrupting them, but it couldn't access areas in which cells were strongly bound to the substrate. The influence of the PEDOT coating on the cell viability was also assessed and it was verified that neurons partially embedded in the PEDOT matrix could survive for at least 1 week after polymerization. However, cells eventually started to die by apoptosis between 24 and 72 h. The group was also able to create cell-templated PEDOT films by removing the cells from the substrate in order to create a biomimetic topology. This novel structure was demonstrated to promote new cells adhesion and proliferation compared to non-shaped PEDOT zones [101]. The same group also managed to electropolymerize in vivo PEDOT:PSS following

the infusion of a EDOT/PSS/PBS solution into the brain close to the electrode by using a canula [102]. The polymer formed a ≈ 500 μm cloud around the electrode, much larger than the size of typical glial scars (150 μm). The in vivo polymerization helped to dramatically decrease the electrode-tissue impedance, even though the results depended on the timing of the electropolymerization, with late (7-8 weeks) and immediate polymerization showing worse results compared to early (4-4 weeks) polymerization. Astrocytes and other cell arrangements, suggesting activated microglia and macrophages, were found around the implant during histology, and second-scarring was observed [102]. Still, this study demonstrated the potential of PEDOT for biomedical applications and better results in terms of biocompatibility could be achieved optimizing the technique and using other PEDOT-functionalized variants.

2.4.5 Coating stability

A major concern for biomedical applications of CP-based implantable electrodes is represented by their poor adhesion to the metallic substrates. Cui and Zhou observed that PEDOT:PSS coatings tended to form cracks and delaminate from the metallic substrates during prolonged (2 weeks) charge-balanced biphasic electrical stimulation and that thicker films were more prone to this phenomenon [103]. Green et al. reported PEDOT doped with PSS, pTS and $LiClO_4$ delamination from the smooth Pt electrodes during biphasic stimulation regardless of the used dopant [104]. The same group reported also the formation of fine cracks on PEDOT:pTS coatings on Pt electrodes following ethylene oxide sterilization [105]. For this reason, several groups have tried to solve this problem using different techniques such as electrodes surface modifications or by studying new PEDOT formulations.

Green et al. demonstrated that roughening of the metallic substrate can offer more anchoring points for the polymer to attach, resulting in better adhesion to the substrate [104]. The same principle was applied by Pranti et al. who used a iodine etching to improve PEDOT adhesion by creating a rough morphology on Au electrodes [106]. Using another approach, Wei et al. used a carboxylic acid-modified version of EDOT to promote adhesion to the substrate [107]. ITO substrates were immersed in a solution containing the EDOT-acid and ethanol to create a first anchoring layer, followed by the electrodeposition of PEDOT doped with tetrabutyl ammonium perchlorate (TBAP). This technique allowed the coatings to withstand 2 min of harsh ultrasonication compared

to only 5 s for common PEDOT coatings. The same group developed also another EDOT formulation modified with the amine moiety -NH_2 which formed a covalent bond with the ITO substrate, and followed by PEDOT electropolymerization was able to survive the impressive time of 1 h of harsh ultrasonication [108]. Finally, using a similar approach, Chhin et al. modified Pt and Pt/Ir surfaces with a diazonium salt to create an anchoring layer for PEDOT, allowing the coating to remain intact for over 10 min of ultrasonication compared to only 10 s for unmodified substrates [109].

CHAPTER 3 MATERIALS AND METHODS

3.1 Chemicals and substrates

Multi-stranded Perfluoroalkoxy (PFA)-coated SST 316 medical grade wires with a total bare electrode diameter of 76.2 μm were purchased from A-M systems.

Isopropanol (IPA, C_3H_8O, 70%) and acetone (C_3H_6O, 90%) were purchased from Honeywell Research Chemicals. ACN and PC (anhydrous, 99.7%) were purchased from Caledon Laboratories and Millipore Sigma, respectively. 3,4-ethylenedioxythiophene (C_6H_6OS, 97%), and lithium perchlorate ($LiClO_4$, ≥95) were purchased from Millipore Sigma. Phosphate buffer solution (PBS) of pH 7.4 was prepared using PBS tablets purchased from Millipore Sigma, and the pH levels were adjusted using hydrochloric acid. All chemicals were used as received [92].

3.2 PEDOT Electropolymerization

Electrochemical experiments were performed in a three-electrode configuration using a Bio-Logic VSP-300 Potentiostat equipped with the EC-Lab software. Reference electrode and counter electrode consisted in a silver/silver chloride (Ag/AgCl) electrode and Pt coil respectively. Multi-stranded SST wires were used as the working electrodes. The insulating layer of (SST) microwires was removed in order to have an exposed metallic tip of about 1 mm (total surface exposed ≈ 0.240 mm^2). All working electrodes were rinsed in IPA and deionized water (DIW) and gently dried with nitrogen prior to electrodeposition. The polymerization solution consisted in the solvents ACN, PC or DIW, the EDOT monomer and the dopant $LiClO_4$ [120 mM]. The EDOT concentration was 30 mM in the organic solvents and 10 mM in DIW, due to the lower aqueous solubility of the monomer [92].

PEDOT coatings were electropolymerized using the galvanostatic (constant current) technique. Electropolymerization parameters are summarized in Table I and were adjusted to avoid PEDOT overoxidation. Prior to electropolymerization, all solutions were degassed for 10 minutes using nitrogen and a nitrogen blanket was kept during the electropolymerization to avoid unwanted monomer oxidations. After electrodeposition, the electrodes were soaked in deionized water, gently dried with nitrogen, and stored in ambient conditions [92].

Table I Parameters for galvanostatic deposition of PEDOT.

Substrate	[Dopant]	[EDOT]	Solvent	Current applied	Deposition time	Electropolymerization charge density
SST wires	$[LiClO_4]$ 120 mM	30 mM	PC	8 μA	600 s	≈ 2 C/cm^2 (regular film)
			ACN	50 μA	100 s	
		10 mM	DIW	2 μA	2400 s	
		30 mM	PC	8 μA	400 s	≈ 1.3 C/cm^2 (thinner film)
			ACN	50 μA	64 s	

3.3 Electrode characterization

Electrochemical characterizations were carried out in PBS pH 7.4. Cyclic voltammetry (CV) was conducted within the range -0.8V – 0.6V (50 mV/s). This window was selected to prevent PEDOT overoxidation and water electrolysis [92]. Electrochemical impedance spectroscopy (EIS) was performed using a sine wave of 10 mV amplitude within the frequency range of 0.1 Hz – 100 kHz. Each EIS spectrum was fitted with equivalent circuit models using Zsimpwin software to extract parameters.

3.4 Stability tests

3.4.1 Adhesion Test

During the adhesion test, PEDOT-coated electrodes were placed inside a beaker filled with DIW and immersed in an ultrasonic bath (Eumax ud100sh-4l) at 100 W ultrasonic power.

3.4.2 Accelerated ageing

For accelerated ageing tests, the coated electrodes were placed in PBS solution stored at 60°C for 21 days (which simulates 103 days at the body temperature of 37°C) to monitor the evolution of the electrochemical properties of PEDOT coatings in a physiological solution. EIS and CV were performed before and after soaking.

3.4.3 Sterilization

Sterilization tests were performed by subjecting PEDOT-coated electrodes to steam sterilization in autoclave (Steris/AMSCO Century Sterilizer V136) at 121 °C for 30 minutes.

All experiments were repeated at least three times (n=3).

3.5 Imaging

Optical microscope images were obtained using an Olympus SZX7 stereo microscope. Scanning Electron Microscopy was carried out using a Scanning Electron Microscope equipped with a Field Emission Gun (SEM-FEG) (JEOL JSM7600F) [92]. The acceleration voltage was adjusted depending on the electrode under study to obtain the best image quality and it is specified for each SEM picture.

3.6 In vivo testing

3.6.1 Surgery

EMG implantation surgeries were performed on C57BL/6 mice (Jackson Laboratory, n=5, 5 months age) under isoflurane anaesthesia. After carefully exposing the skull, a stainless-steel grounding screw was placed over the cerebellum together with two stainless-steel anchor screws (Figure 3.1.a). Each mouse was implanted with 2 coated and 2 uncoated EMG electrodes for bipolar measurement (each bipolar pair consisting in 1 mm of exposed wire positioned 2 mm apart, see Figure 3.1.b). EMG electrodes were inserted approximately 5 mm deep in the acromiotrapezius muscle using a 22-gauge needle. The remaining external insulated part of the electrodes was attached to the skull using dental cement to prevent the electrodes from exiting from the

implantation site. All EMG wires and the grounding wire were connected to a custom-made connector (Axona) fixed to the skull using dental cement (Figure 3.1.c). The animals were left to recover for one week after the surgery before any measurement.

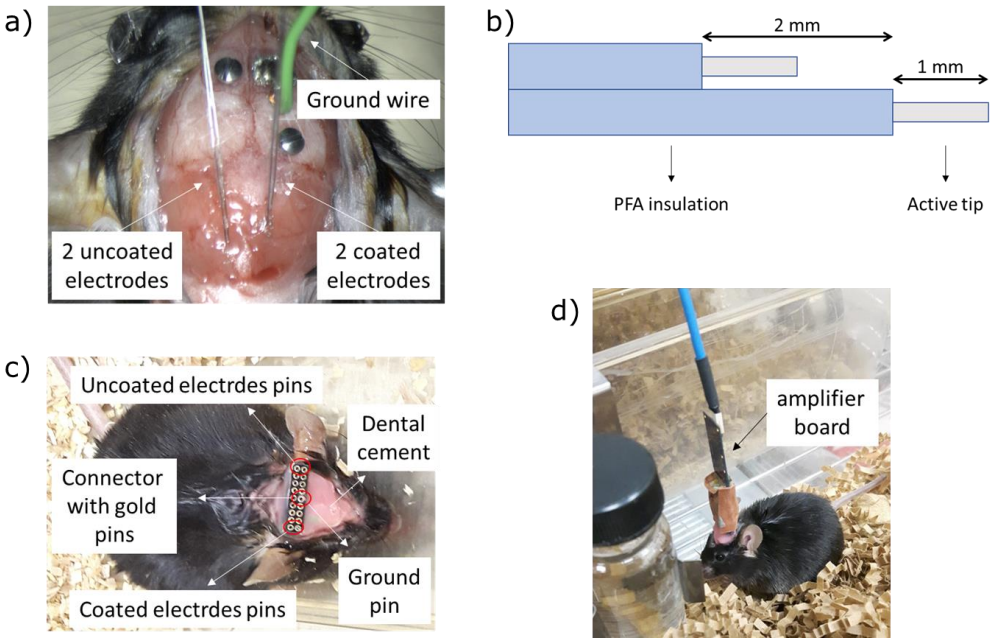

Figure 3.1 Bipolar measurement electrodes arrangement for in vivo EMG recording.

3.6.2 EMG recording

EMG signal were acquired on the 5 mice once per week for 6 consecutive weeks during 1h of free-moving condition inside the mice home cages. The open source open-ephys [110] system for signal recording was interfaced to a RHD2164 (Intan Technologies) amplifier board that performed signal acquisition (Figure 3.1.d). EMG signals were bandpass filtered between 10 Hz and 1000 Hz using a second order Butterworth filter and sampled at 10 kHz. The signals were analysed offline for signal to noise ratio (SNR) computation. A 3-axis accelerometer on the acquisition board carried information on the movements of the animals during the recording, which allowed to identify periods of quiet and activity. The baseline noise was obtained as the rms value of the signal during a quiet phase, as during this period no muscle activity could be detected in the EMG signal. The maximum and minimum values of the noise were used as a double threshold to separate the useful signal from the baseline noise, and the SNR was obtained as the ratio of the rms value of the signal and the rms value of the noise in decibel. The Fourier Transform of the signal was used to identify

the amplitude of the 60 Hz noise associated with the power line, which typically affects most recordings.

3.6.3 In vivo impedance spectroscopy

In vivo EIS was performed to evaluate the impedance of the electrodes. This test was performed only at the end of the 6 weeks of recording to avoid potential tissues or electrodes damage resulting from the currents passed during EIS. The parameters for EIS were the same as the in vitro EIS but the frequency range was reduced to 1 Hz – 100 kHz to avoid electrode polarization at very low frequencies, which could damage the tissues.

3.6.4 Data analysis

Statistical differences between the coated and uncoated electrodes were evaluated using a two tailed paired t-test at 0.05 significance level. Data analysis was performed in MATLAB (MathWorks).

CHAPTER 4 RESULTS

4.1 PEDOT electropolymerization

Electropolymerization was carried out galvanostatically, as this technique has been demonstrated to yield more uniform coatings compared to potentiostatic [96]. Upon the application of a constant current, the potential initially peaks, then stabilizes and the current starts to decrease due to the formation of the electroactive coating with a reduction of the impedance [96] (Figure 4.1).

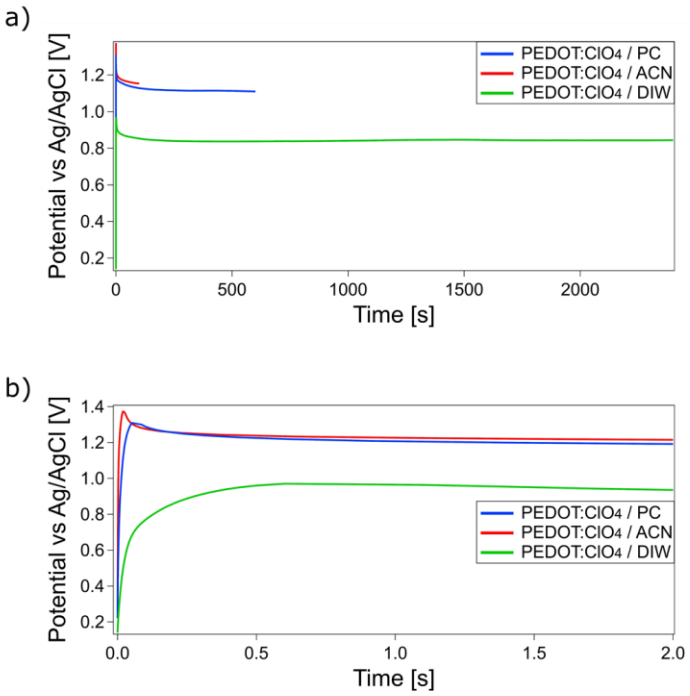

Figure 4.1 Galvanostatic deposition of PEDOT:ClO_4 on SST microwires in water, PC and ACN a), with a zoom on the initial potential overshoot b).

The electropolymerization currents were adjusted for each solvent to avoid PEDOT overoxidation, which is associated with a rise in the potential. Higher currents could be used for organic solvents than for water, which led to a faster electropolymerization. With the same monomer concentration in the two organic solvents, a higher current (50 µA) could be achieved in ACN respect to PC (8 µA). As for the dopant, we selected ClO_4^- since small dopants typically lead to significantly better electrochemical properties (lower impedance and higher deliverable charge) and better adhesion of

the coating to the substrate with respect to larger dopants, which may generate large non-conductive volumes inside the polymer matrix [99, 104].

All the electropolymerization conditions explored here produced PEDOT layers on the metal tips that could be visually detected as dark coatings (Figure 4.2).

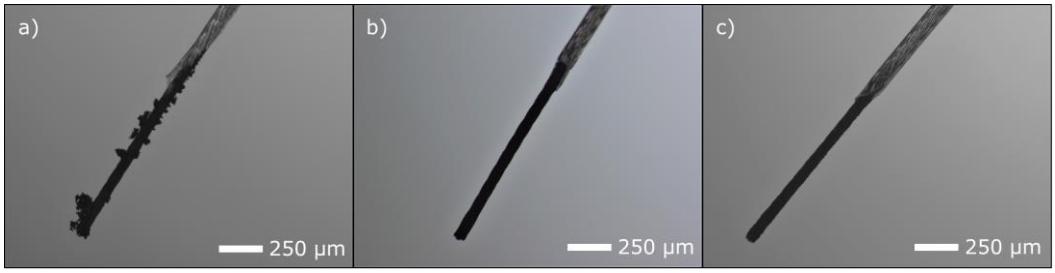

Figure 4.2 PEDOT:ClO_4 coatings galvanostatically deposited on SST microwires in a) PC, b) ACN and c) water.

PEDOT coatings obtained in ACN (Figure 4.2.b) and water (Figure 4.2.c) appear macroscopically homogeneous, while those obtained on PC (Figure 4.2.a) display additional overgrowing clusters whose growth was difficult to control and avoid, even when polymerization time was reduced (Figure 4.3).

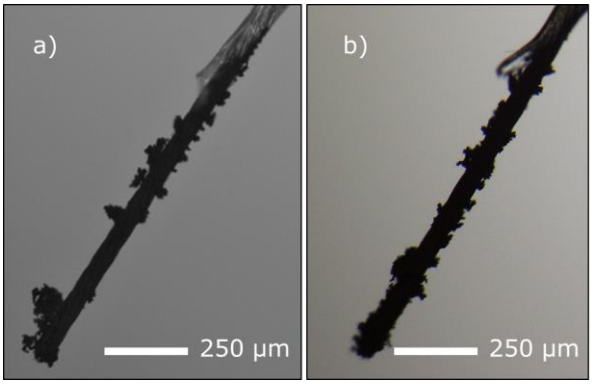

Figure 4.3 Overgrown PEDOT clusters in standard PEDOT:ClO_4 coating a) and thinner layer b).

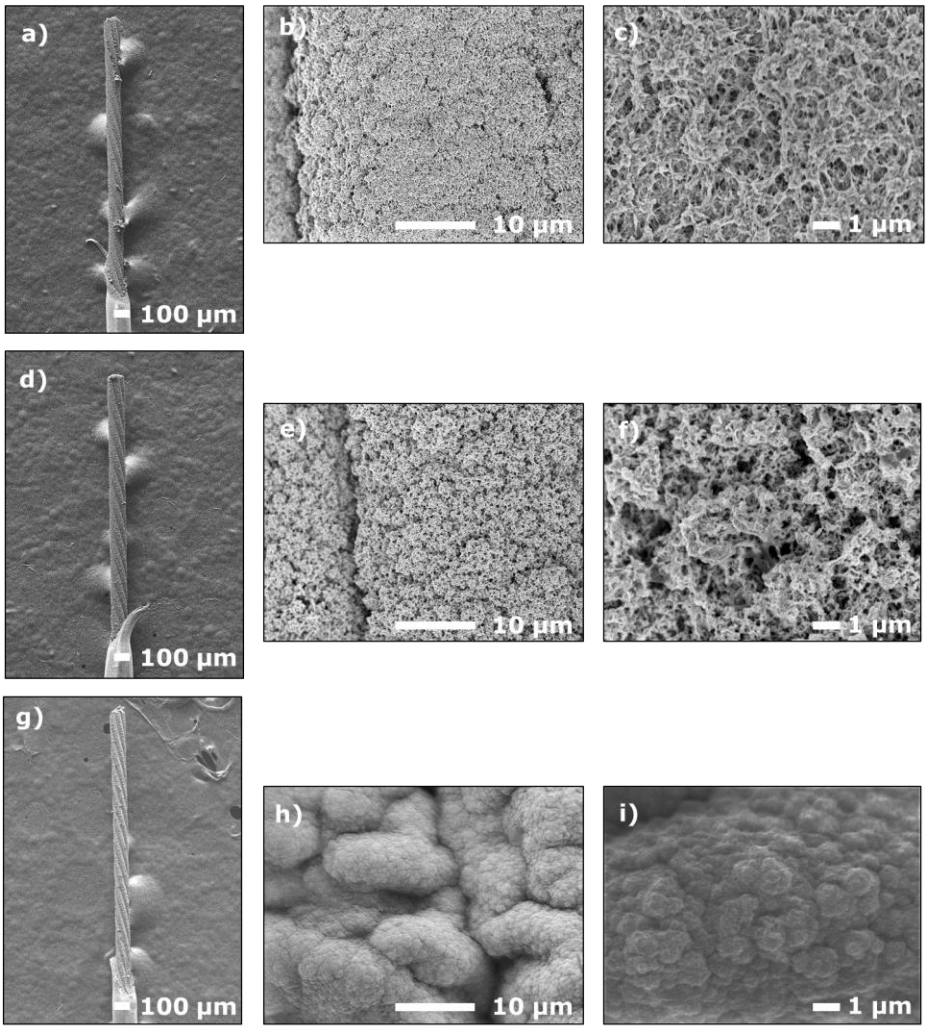

Figure 4.4 SEM pictures of PEDOT:ClO_4 galvanostatically deposited on SST microwires in a), b) and c): PC (8 µA, 600 s), in d), e) and f): ACN (50 µA, 100 s) and in g), h) and i): water (2 µA, 2400 s). SEM voltage: 2 kV for a-g and 0.5 kV for h, i.

SEM images at higher magnification revealed that coatings processed in organic solvents showed a clear porous structure, with ACN providing larger pores than PC (Figure 4.4). On the other hand, PEDOT processed in DIW showed a compact, cauliflower-like structure.

4.2 Electrochemical characterization

CV and EIS measurements were performed to evaluate the electrochemical properties of the electrodes. Charge storage capacity (CSC) extracted from the CV represents the total amount of charge available from an electrode. This parameter is of paramount importance for stimulation

purposes, as it defines the amount of charge that can be delivered by the electrode. The CSC can be evaluated calculating the time integral of the voltammetric cathodic current [1].

Table II contains all the values for the CSC and 1 kHz impedance for the bare and PEDOT-coated electrodes processed in the three solvents.

Table II CSC and 1 kHz impedance results for the bare and PEDOT-coated electrodes. All data are reported as mean ± standard deviation (n=3).

	PC	ACN	DIW	SST
CSC [mC]	0.53 ± 0.008	0.54 ± 0.005	0.34 ± 0.01	0.01 ± 0.0003
1 kHz Impedance [kΩ]	0.21 ± 0.017	0.28 ± 0.022	1.12 ± 0.27	2.65 ± 0.52

All the PEDOT-coated electrodes show an enhanced CSC with respect to the bare electrodes (Figure 4.5.a,d). The CSC is 0.01 ± 0.0003 mC for SST electrodes, and increased to 0.34 ± 0.01 mC for PEDOT processed in DIW, 0.54 ± 0.005 mC in ACN and 0.53 ± 0.008 mC in PC. Coatings prepared in ACN and PC showed the typical box shape of PEDOT and larger CSC with respect to those prepared in water, which were also characterized by an unbalanced cathodic/anodic charge. The CV profiles of coatings processed in water indicate a low doping/de-doping efficiency, expressed as the ratio between the anodic current and cathodic current.

Low impedance values are required to achieve high signal to noise ratios for recording electrodes [111]. As shown in Figure 4.5.b, the presence of the PEDOT coatings on the SST electrodes led to a significant decrease of the impedance modulus within the investigated frequency range, regardless of the processing solvent. Remarkably, at a frequency of 1 kHz which is commonly used as a benchmark value due to the importance of this frequency in the biological processes, a decrease of one order of magnitude is observed. Starting from an impedance of 2.65 ± 0.52 kΩ for bare SST, the PEDOT coating led to a reduction of the impedance of about one order of magnitude when processed in PC and ACN, and 1.52 ± 0.25 kΩ when processed in water. Interestingly, it can be observed that the impedance is lower for PEDOT prepared in organic solvents with respect to water and that differences between PEDOT coatings prepared with PC and ACN are not significant.

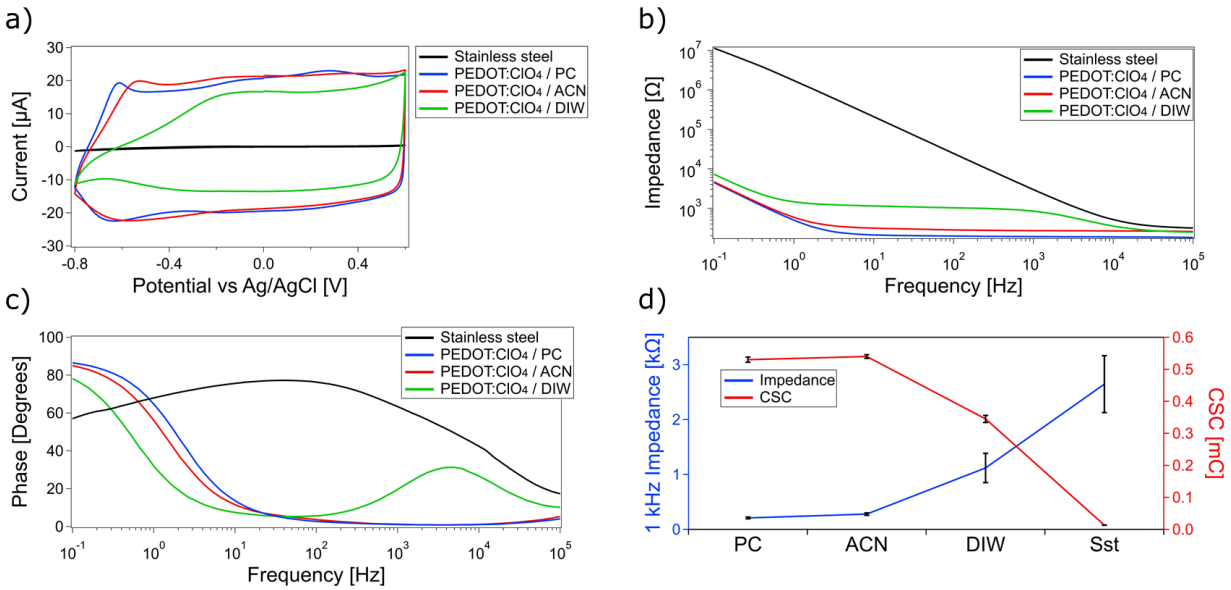

Figure 4.5 Cyclic voltammetry a), impedance modulus b), phase c), and 1kHz impedance and charge storage capacity CSC d) measurements for bare metal and PEDOT-coated electrodes, with PEDOT:ClO_4 galvanostatically deposited in different solvents (propylene carbonate PC, acetonitrile ACN and water DIW). Data for d) are reported as mean ± standard deviation (n=3).

The phase graph of the impedance modulus (Figure 4.5.c) displays additional differences between bare and coated electrodes. Phase values close to 0° suggest a Faradaic charge transfer while phase values near 90° suggest a capacitive behaviour [23]. From Figure 4.5.c, it is clear how at biologically relevant frequencies (1 - 10 kHz) the bare metal shows a strong capacitive component while PEDOT-coated electrodes show lower phase values associated with a resistive charge transfer due to the doping/de-doping process. Again, water-processed coatings differ from the ones prepared in organic solvents, with higher phase values in the range 0.1 - 100 kHz which approach the phase values obtained for stainless steel.

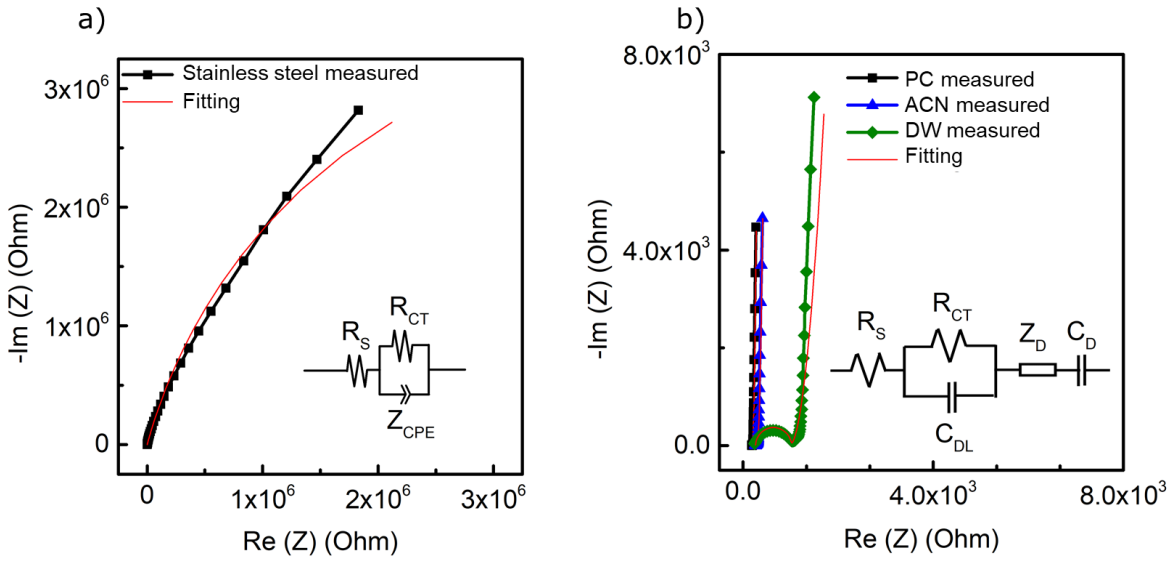

Figure 4.6 Nyquist plot and data fitting for the impedance of bare a) and coated b) electrodes. The inset in each image displays the equivalent circuit model used for the fitting.

The fittings of the Nyquist plots in Figure 4.6 give more insights on the differences in electrochemical properties between coated and bare electrodes. The equivalent circuit models used to fit the experimental data, according to [56], are shown in the insets of Figure 4.6.a (bare metal electrode) and Figure 4.6.b (coated electrodes) while the model's parameters extracted from EIS data fittings are listed in Table III. The equivalent circuit model of the bare metal electrode contains a solution resistance R_s, a charge transfer resistance R_{ct} and a constant phase element (CPE). The impedance of CPE can be expressed as follows (9):

$$Z(CPE) = \frac{1}{Y_0(jw)^n} \qquad (9)$$

With w angular frequency (rad^{-1}), j imaginary unit, n constant parameter comprised between 0 and 1 indicating a pure resistive (n = 0) or a pure capacitive CPE element (n = 1), and Y_0 representing the capacitance value when n = 1.

For the PEDOT-coated electrodes, the model consisted of solution resistance R_s, double layer capacitance C_{dl}, charge transfer resistance R_{ct}, bounded Warburg element Z_d and bulk capacitance C_d (which depends by the electroactive surface area and thickness of the coating [56]).

Table III Equivalent model's parameters obtained by EIS data fitting.

Electrode	R_s (Ω)	$Y_0(S \cdot s^n)$	n	R_{ct} (Ω)	C_{dl} (F)	Z_d	C_d (F)	χ^2
Bare metal	264.9	3.5×10^{-7}	0.8	8.7×10^{6}				8×10^{-3}
PEDOT:ClO_4 (PC)	172.5			19.3	1.2×10^{-7}	0.01	0.00037	3×10^{-4}
PEDOT:ClO_4 (ACN)	266.5			26.7	7.3×10^{-5}	0.007	0.00035	7×10^{-4}
PEDOT:ClO_4 (DIW)	262.1			739.2	1×10^{-7}	0.001	0.00026	5×10^{-3}

Overall, the model used for the EIS data fitting seems to describe well the system under study, with χ^2 values equal or below to 10^{-3}.

From this analysis it is clear how the bare metal electrode is characterized by a strong capacitive component as the charge transfer resistance that represents the faradaic process at the electrode-electrolyte interface is extremely high and the value n value of the CPE is close to 1, indicating a capacitive behaviour.

On the other hand, the PEDOT-coated electrodes present a much lower charge transfer resistance due to the ionic transfer between the PEDOT matrix and the electrolyte, and this contributes to the decrease of the total impedance. Moreover, among all the films, the ones prepared in ACN possess also the higher C_{dl}. It should be noted that the parallel between R_{ct} and C_{dl} is dominated by the lowest of the two impedances, which finally causes R_{ct} to determine the main impedance due to the very small values of C_{dl}, which leads to a high impedance for the capacitor at almost all frequencies. It is also interesting to note that the water-processed PEDOT coatings present a higher charge transfer resistance and also lower Z_d and C_d values than the respective coatings processed in organic solvents.

4.3 Adhesion test

To be used for recording and stimulation, the PEDOT coatings need to have a strong adhesion to the substrate and a good electrochemical stability to resist sterilization, implantation and in vivo operation. For this reason, we performed a series of adhesion and stability tests on PEDOT electrodes, including ultrasonication, prolonged immersion in a physiological solution and autoclave sterilization.

PEDOT:ClO_4 coatings prepared in ACN and PC showed good adhesion during the ultrasonication test. In particular, both were able to sustain 2 minutes of ultrasonication without any damage, with minor detachment occurring after 5 minutes (Figure 4.7).

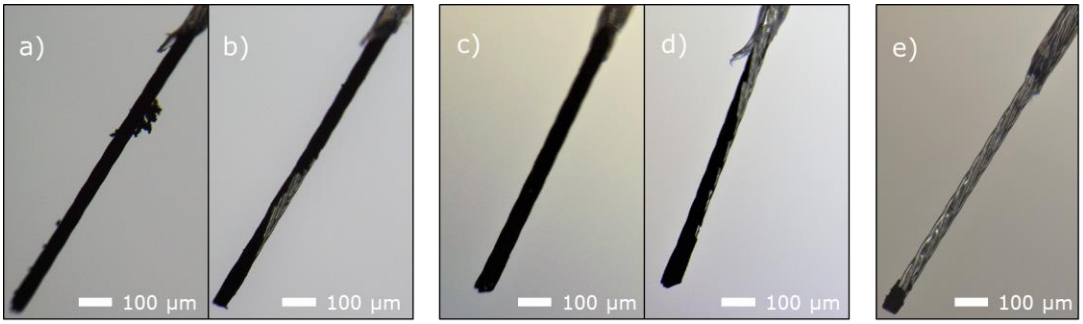

Figure 4.7 Optical images of PEDOT-coated electrodes in PC a,b), ACN c,d) during 2 min and 5 min of ultrasonication test and DIW processed electrodes after 5 s of ultrasonication e).

Interestingly, even after detachment of part of the coating, the electrodes showed lower impedance and higher charge storage capacity with respect to uncoated ones (Figure 4.8).

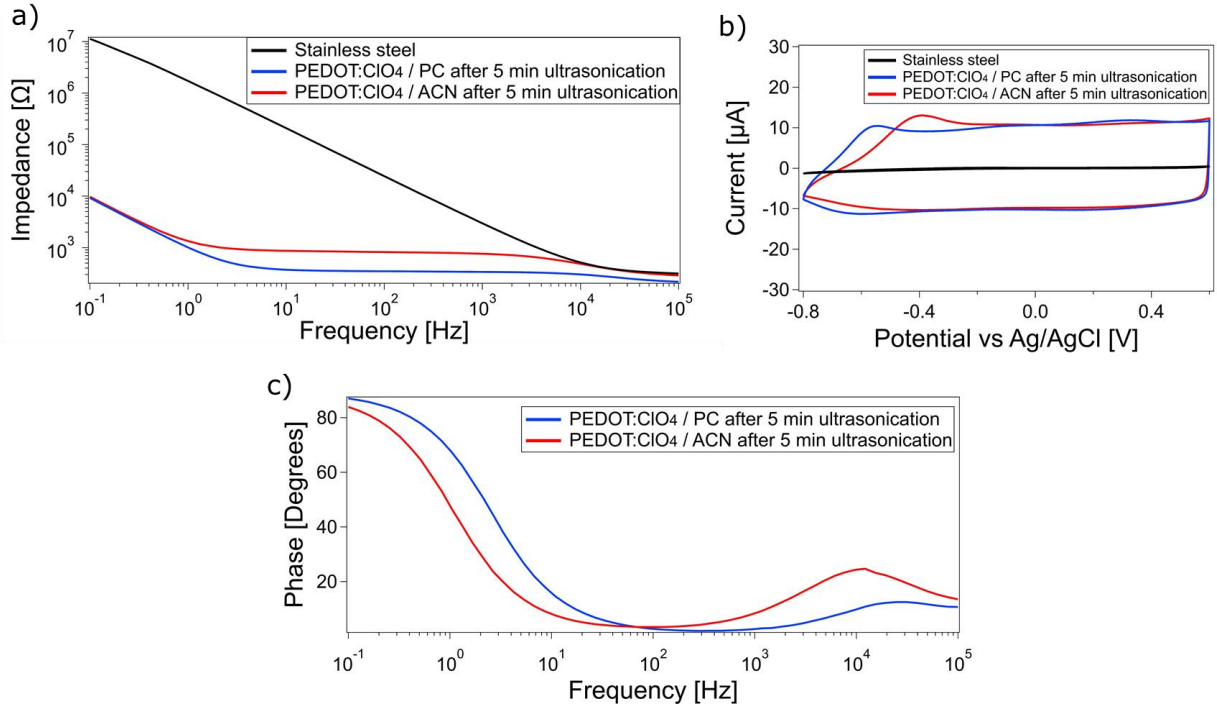

Figure 4.8 Impedance modulus a), CV b) and phase c) of PEDOT:ClO_4 coatings on SST microwires processed in ACN and PC after 5 minutes of ultrasonication.

The CV curves obtained after PEDOT delamination indicate a shift in the cathodic peak towards less negative potentials and also a decrease in the amplitude of the anodic peak. Thinner coatings, obtained with a lower total passed charge (i.e. ≈1.3 mC/cm^2 respect to ≈2 mC/cm^2), tended to detach after a few seconds (Figure 4.9).

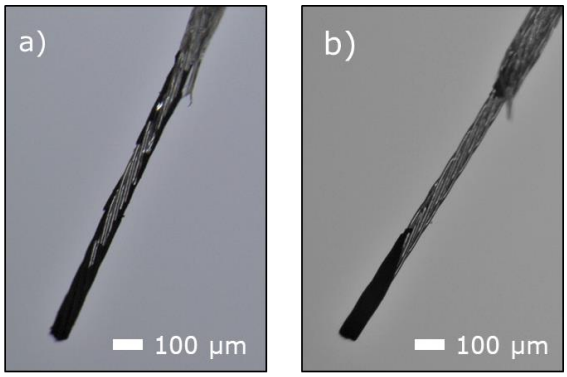

Figure 4.9 Thin layers of PEDOT:ClO_4 galvanostatically deposited in PC a) and ACN b) on SST microwires after 30 seconds of sonication.

PEDOT coatings prepared in DIW showed a weaker adhesion as they completely detached in less than 5 s of ultrasonication. It can be observed from Figure 4.8.c that PEDOT delamination in organic solvents is associated with a rise in the phase during EIS similarly to the water-processed PEDOT coatings after polymerization.

4.4 Accelerated ageing and steam sterilization

It is necessary that recording and stimulating electrodes possess good electrochemical stability to remain functional over time inside the body. For this reason, an accelerated ageing aimed to simulate the long-term stability of the PEDOT-coated electrodes was performed. The guidelines presented in [112] establish that equation (10) can be used to determine the simulated age in a solution at the body temperature of 37 °C:

$$t_{37} = t_T \times Q10^{(T-37)/10} \qquad (10)$$

Where t_{37} is the simulated time at 37 °C, t_T the actual time for which samples are exposed to the elevated temperature T, and $Q10$ is a constant value that was set to 2 to remain conservative [112].

To test their long-term stability, PEDOT-coated electrodes were immersed in a PBS (pH 7.4) solution at 60 °C for three weeks, which correspond to almost 103 days at the body temperature of 37 °C. The electrochemical cyclic voltammetry and impedance were measured before and after the test Figure 4.10.a,b.

It is possible to observe that all the coated electrodes experienced an increase in the impedance after the 3 weeks of soaking, with the water-processed coatings displaying the largest change. It can be observed from the Bode plot that the rise in impedance was mainly due to an increased charge transfer resistance, which is associated to the impedance plateau in the mid-frequencies range.

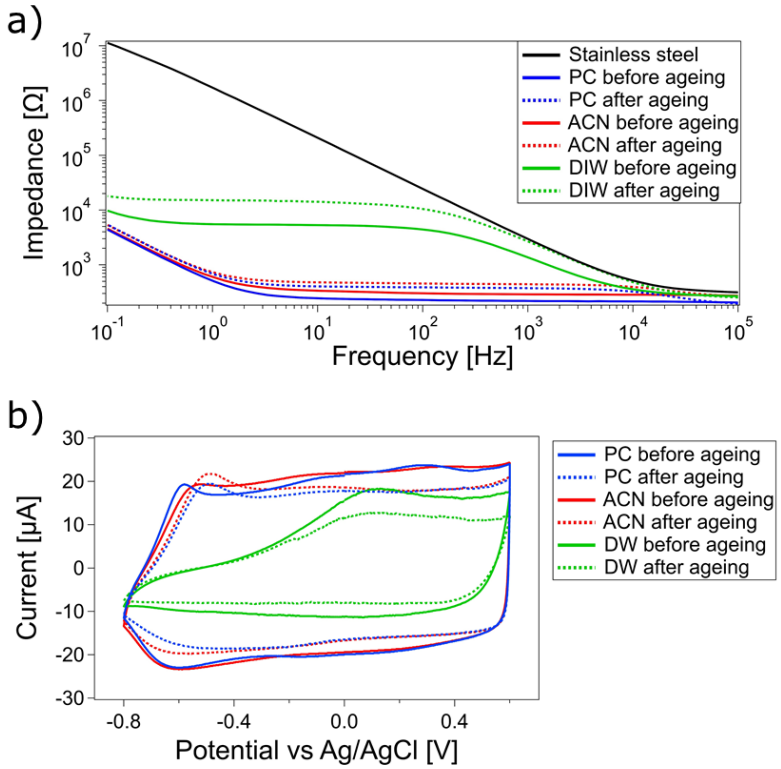

Figure 4.10 EIS a) and CV b) of PEDOT-coated electrodes processed in the different solvents before and after accelerated ageing at 60 °C for 21 days.

For electrodes prepared in PC and ACN the impedance remained much lower with respect to bare SST over the testing period (Figure 4.11.a).

These results indicate that PEDOT:ClO_4-coated SST microwires prepared in these two organic solvents are capable of retaining their electrochemical properties over time. The changes in the 1kHz impedance were 136 ± 25 Ω for PEDOT in PC and 119 ± 29 Ω for PEDOT in ACN, with the final impedance much lower compared to the bare metal impedance of up to about 2.25 kΩ, corresponding to one order of magnitude difference. The results of CV revealed a similar trend (Figure 4.11.b). In this case, a shift in the oxidation peak was observed towards less negative potentials (Figure 4.10.b), coupled with a decrease of the charge storage capacity (0.09 ± 0.016 mC in PC and 0.06 ± 0.002 mC in ACN) and a smaller negative current peak, but with the final CSC five orders of magnitude larger than bare SST.

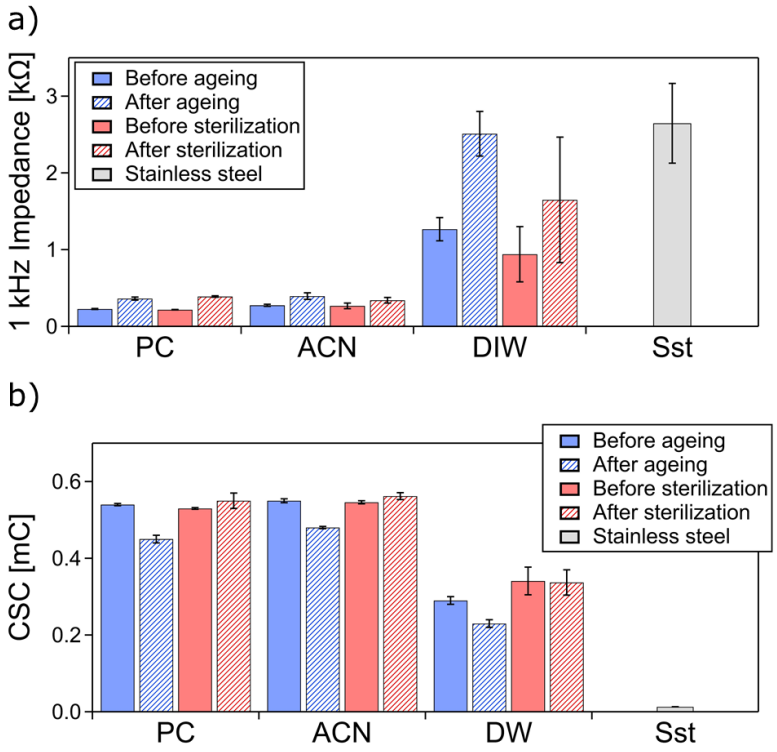

Figure 4.11 Evolution of the impedance a) and charge storage capacity (CSC) b) of PEDOT coatings on SST microwires during 3 weeks of accelerated ageing at 60 °C in PBS pH 7.4 and steam sterilization. All data are reported as mean ± standard deviation (n=3).

On the other hand, electrodes processed in water experienced larger impedance changes during the testing period (1.25 ± 0.15 kΩ), with the final impedance at 1 kHz after 3 weeks being approximately the same as the bare SST electrode (Figure 4.11.a). Changes in the CSC (0.06 ± 0.006 mC) were comparable to the ones observed for coatings processed in organic solvents, with the final CSC much larger than for the bare SST electrodes, probably due to the higher surface area of the PEDOT-coated electrode.

All the coatings experienced a rise in the phase values after the 3 weeks of testing (Figure 4.12).

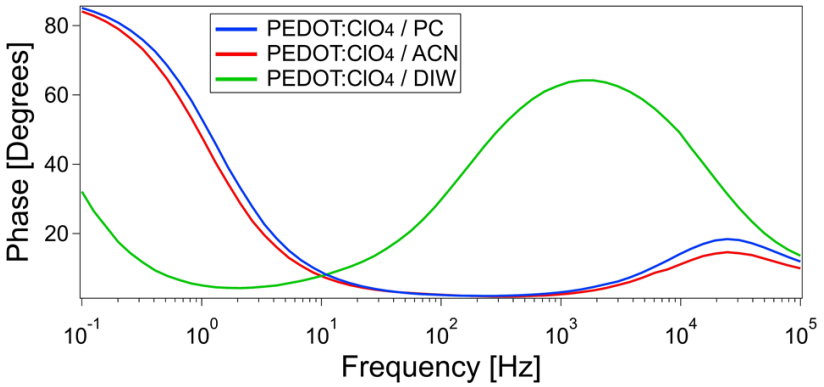

Figure 4.12 Phase values obtained during EIS after the 3 weeks of accelerated ageing for the coated electrodes in the three solvents.

In the case of PEDOT coatings processed in water the increase in phase values was larger and it clearly followed the phase trend observed for bare stainless steel, indicating possible coating delamination. On the other hand, the PEDOT coatings processed in organic solvents presented a much smaller increase in phase values, which could indicate only partial stainless steel exposure.

It has been previously observed that one of the reasons for the change in the electrochemical properties of PEDOT coatings over prolonged soaking is the change in the PEDOT morphology, whose porous structure tends to collapse into a compact structure after about 10 days of accelerated ageing [86]. For this reason, we acquired SEM picture after the accelerated ageing period.

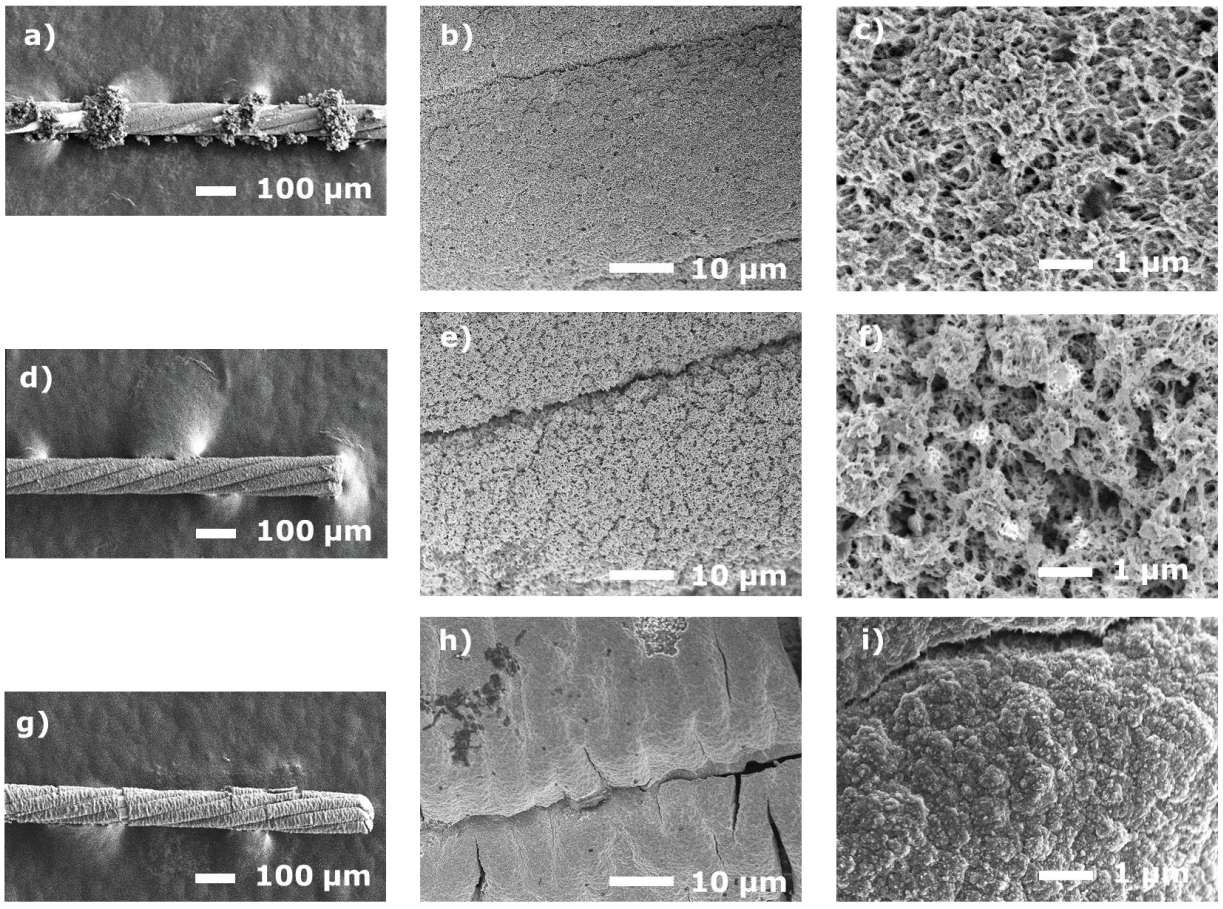

Figure 4.13 SEM pictures of PEDOT coatings processed in PC a), b), c), ACN d), e), f) and water g), h), i) after the 3 weeks of accelerated ageing. SEM voltage: 2 kV.

Figure 4.13 displays the morphology of the PEDOT coatings at the same magnification used for the images of Figure 4.4. From these pictures it is clear how the porous morphology of PEDOT coatings processed in organic solvents is preserved, and the same can be assessed for the films processed in water, whose morphology remains compact and globular. However, clear film cracks are visible in the coating processed in water, leaving the bare stainless steel exposed. On the other hand, the PEDOT coatings processed in organic solvents do not show evident cracks or delamination from the substrate.

Implantable electrodes need to be sterilized before use. One of the most common techniques for sterilization is autoclaving due to its simplicity and low cost of the equipment [113]. PEDOT-coated electrodes were sterilized by autoclaving at 121 °C for 30 minutes. Electrochemical characterizations before and after the treatment were conducted (Figure 4.14.a,b).

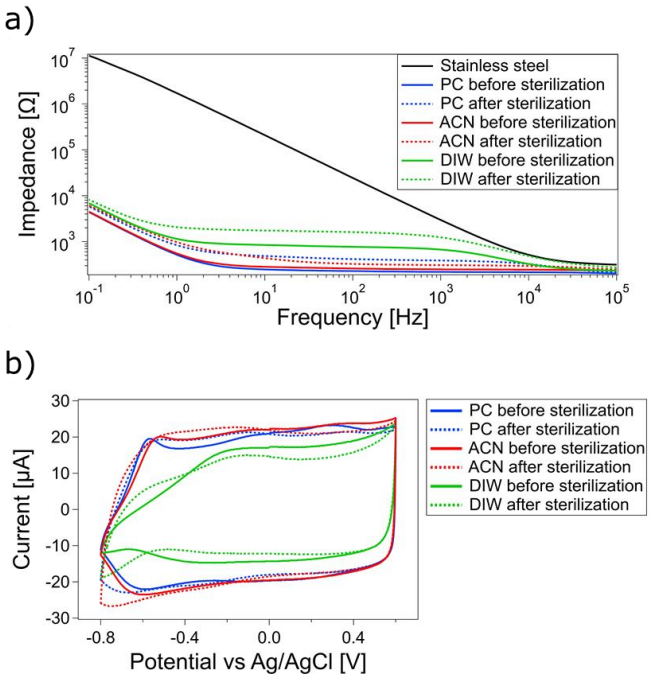

Figure 4.14 EIS a) and CV b) of PEDOT-coated electrodes processed in the different solvents before and after steam sterilization.

Results are similar to the ones obtained during the accelerated ageing, with water-processed films showing again the larger changes in impedance.

Our measurements revealed a slight increase in the impedance for both PEDOT:ClO_4 coatings prepared in ACN and PC, with a change of only 169 ± 13.3 Ω for PC and 66 ± 4.3 Ω for ACN and the final impedance one order of magnitude lower than the impedance of bare SST (Figure 4.11.a).

On the other hand, as for the accelerated ageing, water processed electrodes experienced larger impedance changes of approximately 707 ± 478 Ω and with the final impedance much closer to the one of the bare SST compared to coatings processed in organic solvents. CV results reveal excellent stability of the CSC (Figure 4.11.b). Before sterilization, the electrodes possessed CSC values of 0.53 ± 0.002 mC, 0.54 ± 0.004 mC and 0.34 ± 0.036 mC in PC, ACN and DIW respectively, while after the test these values passed to 0.55 ± 0.02 mC, 0.56 ± 0.009 mC and 0.34 ± 0.033 mC.

The steam sterilization results indicate that PEDOT coatings processed in organic solvents retained superior electrochemical properties compared to bare metals.

4.5 In vivo EMG recording

Due to the more regular coating morphology compared to PC, PEDOT:ClO_4 films prepared in ACN were used for in vivo signal recording in 5 mice. Figure 4.15.a shows a schematic of the electrode implantation in vivo. Due to the lower impedance, PEDOT-coated electrodes are expected to reduce the noise level and enhance the quality of the recording by achieving a higher SNR compared to bare electrodes.

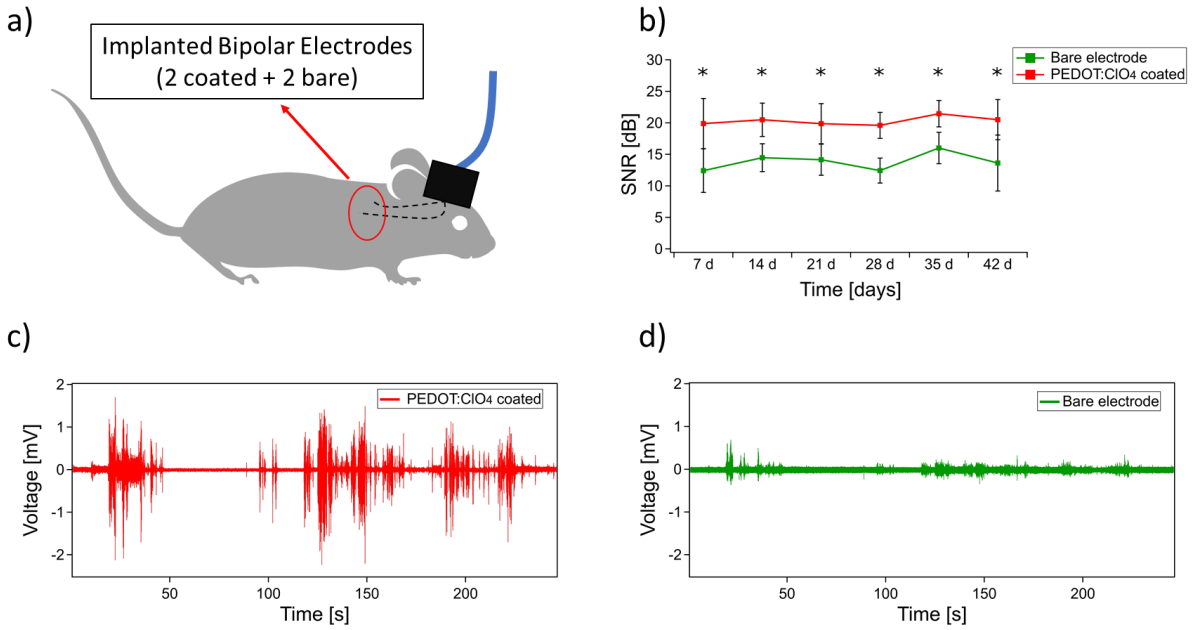

Figure 4.15 Schematic showing the electrodes implantation in vivo a), computed SNR values over the 6 weeks recording period for coated and uncoated electrodes b), exemplificative EMG traces showing the differences in the recorded signals for coated c) and uncoated d) electrodes. Data for b) are reported as mean ± standard deviation (n=5) and * indicates a significant difference ($p < 0.05$).

Figure 4.15.b shows the results for the SNR computations. The PEDOT-coated electrodes achieved statistically significant higher SNR compared to bare electrodes throughout the whole recording period of six weeks. Figure 4.15.c,d show two exemplificative EMG traces recorded by coated and uncoated electrodes, from which it is evident that the PEDOT-coated electrodes achieve a better signal quality characterized by higher signal amplitude and lower baseline noise (Figure 4.16 offers a zoomed view of the two overlapped baseline noises for coated and uncoated electrodes).

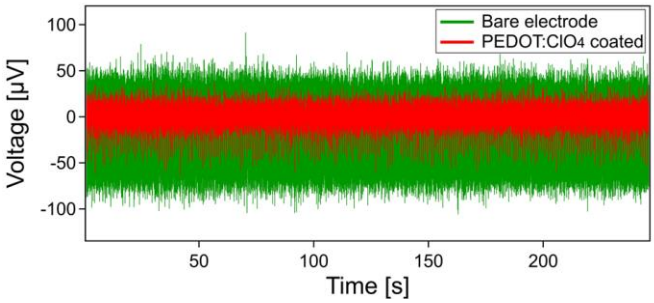

Figure 4.16 Zoomed view of the baseline noise for bare and coated electrodes during EMG recording.

Figure 4.17 displays the method for the selection of the baseline noise in the signals starting from the signal from the accelerometer as described in the methods chapter.

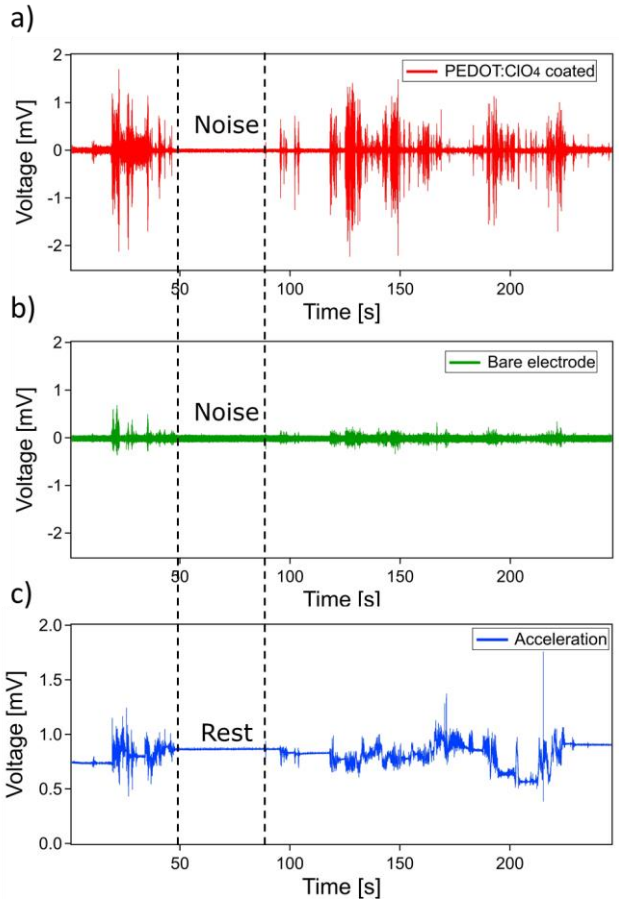

Figure 4.17 Noise selection using the data from the accelerometer. Examples of EMG traces for coated a) and uncoated b) electrodes and corresponding acceleration profile c). The accelerometer

data are used to identify periods of rest characterized by a flat profile. The dotted lines indicate the selected time frame corresponding to a period of rest with no evident EMG activity in the traces a) and b), which is used for noise computation.

From the literature, it is known that the mechanisms through which PEDOT-coated electrodes are capable to achieve better signal qualities are mainly two: reduced thermal noise and reduced shunt loss [16]. In both cases, the lower impedance of PEDOT-coated electrodes can decrease the baseline noise and avoid important signal loss.

Still, other groups have also reported that the 50 Hz (or 60 Hz) noise, which normally affects all the signal measurements due to the electronic noise from all the electronic components in the recording room, is reduced by using PEDOT as an electrode coating [56, 90]. This was also the case in this study (Figure 4.18) as the 60 Hz noise amplitude was consistently higher for uncoated electrodes (except for the last week during which in one of the animals the bare electrodes experienced an anomalous drop of the noise).

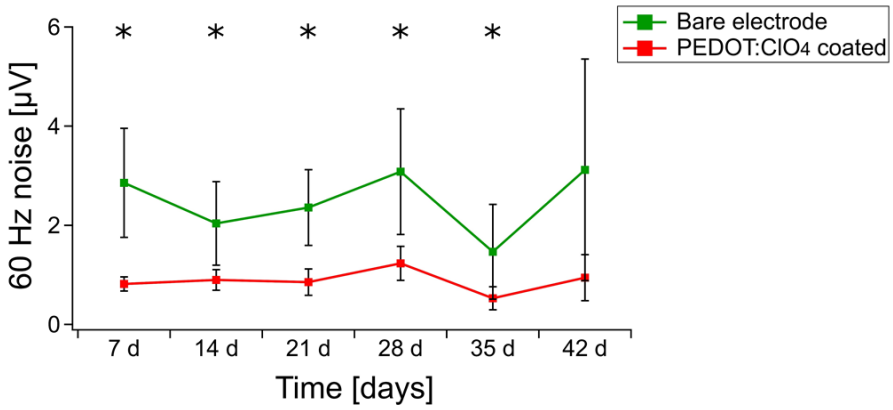

Figure 4.18 Diagram of the 60 Hz noise amplitude from coated and uncoated electrodes over time. All data re reported as mean ± standard deviation (n=5), * indicates a significant difference ($p < 0.05$).

In order to obtain more information about the mechanism behind the enhanced signal quality obtained with PEDOT-coated electrodes, an in vivo EIS was conducted. Figure 4.19 shows the bode plot together with the 1 kHz and 60 Hz impedance for coated and uncoated electrodes acquired at the end of the 6 weeks of recording.

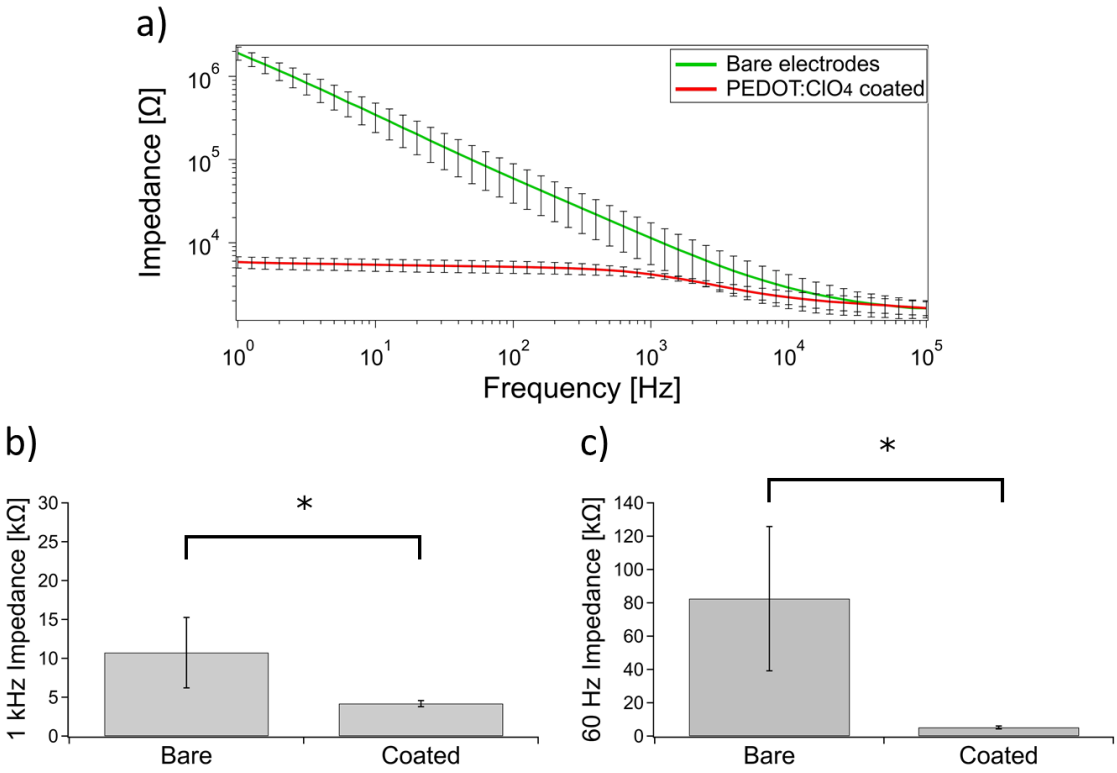

Figure 4.19 Impedance modulus a), 1 kHz impedance b) and 60 Hz impedance c) of PEDOT-coated and bare electrodes obtained during in vivo EIS. All data are reported as mean ± standard deviation (n=5), * indicates a significant difference ($p < 0.05$).

As for to the in vitro characterization, coated electrodes are characterized by a lower impedance over the whole frequency range (except very high frequencies) respect to uncoated electrodes, with the impedance values at 1 kHz and 60 Hz showing a significative reduction. In particular, after the 6 weeks of recording, the 1 kHz impedance value for coated electrodes was 4.17 ± 0.39 kΩ compared to 10.73 ± 4.53 kΩ for bare electrodes, and the difference was even higher at 60 Hz with the impedance of coated electrodes being 5.1 ± 0.87 kΩ and the one of bare electrodes being 82.5 ± 43.3 kΩ.

CHAPTER 5 GENERAL DISCUSSION

5.1 Electropolymerization and coating morphology

Higher currents could be used for organic solvents than for water, which led to a faster electropolymerization. This is consistent with our observations on PEDOT doped with $TEABF_4$ electropolymerized on Pt/Ir electrodes in the same solvents [92], and it could be partially due to the higher concentration of the monomer in organic solvents. Moreover, a higher current could be used in ACN compared to PC. Singh et al suggested that the higher viscosity of PC with respect to ACN (2.51 mPa vs 0.34 mPa at 25°C) leads a slower deposition rate and thus to a lower current [114].

Films prepared in organic solvents possessed an open and porous morphology compared to the compact and globular structure obtained in water. It has been previously reported that PEDOT:ClO_4 films electropolymerized in acetonitrile possessed a porous structure compared to the compact and granular (or "cauliflower") morphology obtained in water [94, 115, 116].

PEDOT coatings processed in PC were characterized by PEDOT agglomerates on the surface, while films prepared in ACN did not present this feature. This observation is consistent with what we previously observed on PEDOT:tetrafluoroborate electropolymerized on Pt/Ir micro electrodes in organic and inorganic solvents [92]. It was previously proposed that an enhanced EDOT solubility could allow for oligomeric radical cations to first diffuse away from the electrode and later precipitate as flocculent powder [117]. Poverenov et al. also suggested that the difference between coatings processed in ACN and PC can be explained by the differences in solubility of PEDOT oligomers, which is about three times lower in ACN [62]. This information explains why PEDOT coatings obtained in PC are characterized by the presence of polymer clusters, as more oligomers are able to diffuse away from the electrode and then precipitate back. The lower solubility in ACN would also lead to a higher number of nucleation sites at the electrode surface and to the growth of short oligomers at the electrodes while the higher solubility of PEDOT oligomers in PC leads to the growth of a higher quantity of long polymeric chains at the electrode [62].

It is possible that the low solubility of EDOT in water would not allow for the diffusion and successive precipitation of oligomers, finally giving rise to smoother coatings compared to organic

solvents. However, it is important to note that the EDOT concentration was higher in organic solvents compared to water, and that higher currents were used in organic solvents. These elements could also have an impact in the final PEDOT morphology.

5.2 Electrochemical characterization

All the PEDOT-coated electrodes possessed lower impedance and higher CSC compared to bare electrodes independently from the choice of the solvent. This is an expected result, as the presence of PEDOT not only greatly expands the active surface area, but it also allows for ionic exchange between the solution and the electrode, thus reducing the impedance and increasing the CSC [20].

The CV of the PEDOT-coated electrodes processed in DIW displayed unbalanced anodic and cathodic phase, with the former presenting a lower total charge. It is possible, due to the less accessible structure of the PEDOT films processed in water, that once the dopants are expelled during the cathodic phase, they cannot be fully reinserted in the polymer matrix upon reversion of the potential, which leads to a higher cathodic charge compared to the anodic one. It is also interesting to note that the shape of the CV was very similar to the one obtained by Cui and Zhou for PEDOT:PSS films after delamination from the metallic substrate [103]. This might indicate the formation of cracks or possible delamination from the stainless steel, even if SEM analysis showed films with no defects.

The impedance profile of PEDOT-coated electrodes presented lower values over the whole frequency range compared to bare electrodes, with similar values only at very high frequencies (> 10 kHz). This is due to the fact that at these frequencies the applied potential varied too fast for ions to move in and out of the polymer matrix, thus reducing the impact of PEDOT's presence.

Coatings obtained in organic solvents were characterized by a lower impedance and higher CSC compared to films processed in water. The superior electrochemical properties of coatings processed in organic solvents could be explained by their porous structure, with respect to the globular and compact structure of those processed in water. In fact, a porous structure not only increases the total exposed surface are of the electrode, but it also facilitates the flux of ions in and out of the polymer lattice.

The phase profiles of PEDOT-coated electrodes indicate that a faradaic process associated with the doping and de-doping of the polymer takes place, while a strong capacitive component is present for the bare electrode. Films processed in water differ from the ones prepared in organic solvents as the phase values tend to approach the ones of the bare electrode, suggesting a possible exposure of the bare metal.

The Nyquist plot fittings seem to confirm this hypothesis, as the charge transfer resistance of films prepared in water is considerably higher than the one obtained for organic solvents. However, this could be also associated with a bad connection with the underlying metallic substrate. It is also likely that, as discussed for the CV results, the compact structure of the PEDOT films processed in water is less accessible to the ions in the solution, which causes a rise in the charge transfer resistance.

The C_{dl} value was higher for films prepared in ACN respect to the other two solvents, which may result from the more porous nature of the film. At the same time, the C_d values were higher for films obtained in organic solvents compared to coating polymerized in water, which may suggest a thicker layer in the formers [90]. This would be confirmed also by the lower bounded Warburg element value obtained for coatings prepared in water, which in the literature has been associated with thinner PEDOT coatings due to the lower diffusion time constant values [90].

5.3 Adhesion test

PEDOT coatings processed in organic solvents possessed good adhesion to the substrate as demonstrated by the ultrasonication test, while water-processed PEDOT coatings were delaminated after a few seconds. It should be noted that the resistance of the PEDOT coatings processed in organic solvents is remarkable considering the fact that no substrate treatments of polymer modifications were used. After partial delamination of the coatings prepared in organic solvents, the CV displayed a shift in the anodic and cathodic peak potentials toward more positive potentials. These results are consistent with the observation of Cui and Zhou, who reported a shift of the redox peaks towards more positive potentials and a reduction in the peak currents after PEDOT:PSS delamination [103]. Moreover, the phase profile obtained by EIS displayed a rise in the phase which is similar to the one observed for coatings polymerized in water. This might confirm that the rise in phase observed in the water-processed PEDOT coatings after polymerization could be due

to the poor adhesion of the coating to the substrate, or even to partial crack formation or delamination even if SEM analysis showed intact coatings. In this case, it is possible that the PEDOT delamination could be localized in correspondence of the single strand junctions, which would explain why SEM inspection did not reveal any damage.

Green et al hypothesized that their PEDOT:PSS films suffered from more delamination than PEDOT:ClO_4 and PEDOT:pTS films due to the higher rigidity induced by the stiffness of PSS [104]. In their study, the solvent was not varied (1:1 ACN/water), thus it was not a factor in delamination. However, their explanation that the flexibility of the polymeric backbone allows it to anchor better to the imperfections of the electrodes could apply to our work. As we have shown, water leads to compact coatings when compared to PEDOT coatings processed in organic solvents. A compact structure could induce high rigidity that drastically decreases the adhesion quality during stability tests. The poor adhesion of water-processed PEDOT coatings could also explain the differences in electrochemical properties observed for the coatings obtained in organic solvents, and especially the higher charge transfer resistance of the former which may be due to a poor adhesion of the film to the metallic substrate.

Our tests showed that reducing the amount of PEDOT on SST microwires led to poorer adhesion. We believe the decrease in adhesion observed in films with less PEDOT might be due to the peculiar geometry of the SST microwires. The geometry of SST microwires consists of several twisted wires, requiring a larger amount of polymer to pack around the structure of the wire and create a cohesive structure.

5.4 Stability tests

PEDOT coatings processed in organic solvents possessed good electrochemical stability during accelerated ageing and steam sterilization. SEM picture obtained after the 3 weeks of ageing showed that PEDOT coatings processed in water had cracks and that bare stainless steel was exposed. This result is in agreement with the observation of the change in phase and can be due to both the prolonged soaking but also to the characterization (CV and EIS) that was performed on the electrodes to monitor the electrochemical properties. In fact, the ions movement during the doping/de-doping process in the CV causes the polymer lattice to expand and shrink, which in the case of the compact structure of the water processed films could lead to the formation of cracks

with a consequent increase in the impedance, as it was observed during the accelerated ageing. A rise in the phase values was observed also for films prepared in organic solvents, even if the change was less dramatic respect to films prepared in water and SEM pictures showed coatings with no defects. In this case, it is possible that during the 3 weeks of soaking the PBS solution could have penetrated under the insulation, exposing the bare metal to the solution and causing the rise in phase, but possible crack formation in correspondence of the single strand junctions cannot be excluded.

Due to the low cost of the equipment and simplicity of the technique, autoclaving is one of the most common sterilization techniques. However, steam sterilization can cause the degradation of moisture-sensitive materials such as organic materials due to intrinsic materials degradation, morphological/structural changes, or mechanical damage due to thermal expansion [113].

In this study, films prepared in organic solvents demonstrated to be stable respect to steam sterilization, with 1 kHz impedance and CSC values showing only minor changes. Again, water-processed coatings experienced larger increase in the impedance, even if the CSC values were less affected by this type of treatment.

Green et al observed a relative decrease of more than 30% in CSC for PEDOT:pTS, PEDOT:ClO_4 and PEDOT:PSS electrodeposited on smooth Pt and the best result (20%) was achieved by pTS deposited on roughened Pt [104]. In this work, the changes in CSC were negligible, showing good stability to sterilization for the coatings prepared in organic solvents, and only partial resistance to sterilization for coatings polymerized in water due to the still larger increase in impedance.

5.5 In vivo testing

PEDOT-coated electrodes were capable to achieve higher SNR values compared to bare electrodes during the whole recording period of 6 weeks. As discussed in the introduction, the two main mechanisms that allow PEDOT-coated electrodes to achieve a better signal quality are the reduced thermal noise and the reduced shunt loss. However, another interesting finding has been previously reported, which involves the reduction of the 50 Hz (or 60 Hz) noise which results from the electronic recording setup, but the authors did not provide an explanation of the phenomenon [56,

90]. In this study, we observed the same phenomenon as the 60 Hz noise was constantly lower for PEDOT-coated electrodes.

While the reduction in the thermal noise and shunt loss are a direct consequence of the reduced electrode impedance, the reduction of the common mode voltage caused by the power line noise can be due to a reduced mismatch of the impedances between the single electrodes and the reference stainless steel ground screw, and also the two monopolar electrodes themselves. It is known that the common mode voltage effect can be enhanced by a mismatch in the electrodes impedances that are connected to a differential amplifier. Instead of being cancelled by taking the voltage difference at the two nodes, the impedance mismatch causes the common mode voltage to produce a differential voltage at the amplifier's input, which will finally cause this signal to be amplified [118].

Let's consider Figure 5.1, which represents a basic schematic of a differential amplifier. V_1 and V_2 represent the two input signals, while $R_{1,2,3,4}$ are the amplifier's resistances that are chosen to achieve a certain gain.

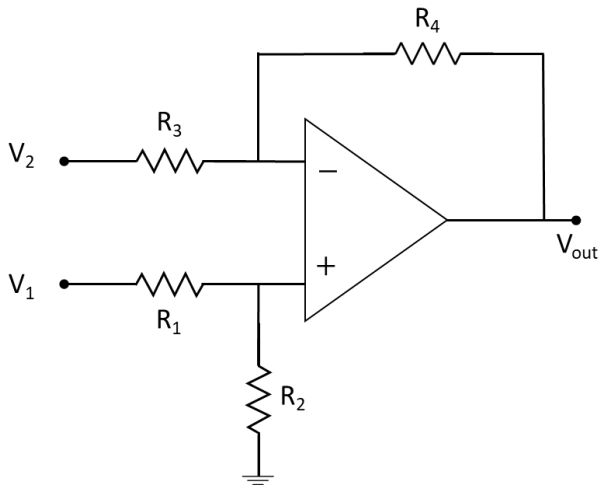

Figure 5.1 Schematic of a simple differential amplifier for bipolar measurement.

It is convenient to calculate the output voltage V_{out} in function of the differential voltage V_d and the common mode component V_{cm} which are defined as follows (11):

$$Vd = V1 - V2 \qquad Vcm = \frac{V1 + V2}{2} \qquad (11)$$

It can be demonstrated that the output voltage V_{out} is finally given by equation (12):

$$\frac{Vd}{2}\left[\frac{R2}{R1}\cdot\frac{1+\frac{R4}{R3}}{1+\frac{R2}{R1}}+\frac{R4}{R3}\right]+Vcm\left[\frac{R2}{R1}\cdot\frac{1+\frac{R4}{R3}}{1+\frac{R2}{R1}}-\frac{R4}{R3}\right] \quad (12)$$

From this expression, it can be seen that one way to eliminate the effect of the common mode voltage on the output signal is to choose $R_2 / R_1 = R_4 / R_3$. This in reality cannot be achieved due to the tolerances of the resistances, but also a mismatch in the electrodes impedances can enhance the effect of the common mode voltage. In fact, the impedances R_1 and R_2 will be also connected to the impedances of the single electrodes, whose mismatch will cause a larger difference between the impedances connected to V_1 and V_2, finally causing the common mode signal to generate a differential signal that will be amplified.

One way to avoid this problem is to reduce the mismatch between the electrodes impedances. The in vivo EIS showed that PEDOT-coated electrodes still possess lower impedance compared to bare electrodes after the 6 weeks of recording. This on one side confirms that the PEDOT coatings are still present on the bare metallic substrates, but it also suggests that thanks to the lower impedance, it is most likely that PEDOT-coated electrodes are characterized by a reduced mismatch between them and between the ground screw that was fixed on the skull, finally reducing the effect of the common mode voltage.

CHAPTER 6 CONCLUSION AND RECCOMANDATIONS

In this work, the conductive polymer PEDOT was successfully electropolymerized on SST electrodes for EMG recording in small animals. Two organic solvents (PC and ACN) and water were employed. The results showed that organic solvents gave coatings with better electrochemical properties and good adhesion to the metallic substrate. Electrodes processed in organic solvents are electrochemically stable over accelerated ageing and steam sterilization, and show lower impedance and larger charge storage capacitance with respect to bare metal electrodes. This makes them attractive for chronic EMG recording.

When implanted in mice, PEDOT:ClO_4 coated electrodes processed in ACN displayed better SNR values with respect to bare electrodes. This is explained by the higher signal amplitudes and the lower noise levels resulting from the lower electrodes impedances. Thanks to their good mechanical and electrochemical stability, PEDOT-coated electrodes allowed for stable high-quality recordings over a 6-week period, demonstrating their potential for high quality EMG recordings. These electrodes can find applications to study neuromuscular diseases and movement disorders, in body movement studies (kinesiology) and in the research for prolonged and stable EMG recording in animals.

This study demonstrated that the mechanical and electrochemical properties of PEDOT coatings can be dramatically improved by carefully selecting and optimizing the electropolymerization conditions. Many studies have used PEDOT coatings to enhance the electrical properties of implantable electrodes, but the deposition methods were often very different in terms of used solvents, dopants, and electropolymerization technique. This variability in the processing technique is also present in the methods used for electrodes characterization. For example, adhesion tests have been conducted using ultrasonication machines having different powers, which of course can change the time the polymer coating stays attached to the metallic substrate. This variety of results has been somewhat misleading in establishing the real capabilities of PEDOT coatings to sustain harsh treatments, and more efforts should be directed towards more systematic studies on the influence of the processing and characterization techniques.

Many challenges still remain for the design of implantable electrodes based on PEDOT. In this work we have demonstrated how adding a conductive polymer coating to metal electrodes can

improve the quality of the recording, but the stability of these electrodes still needs to be tested especially for applications involving electrical stimulation. In our previous work we showed the importance of impedance characterization not only before, but also after electrical stimulation [92]. Many studies involving PEDOT coatings on implantable microelectrodes only studied the impedance before stimulation, which also in our case demonstrated that PEDOT-coated electrodes have lower impedance compared to bare electrodes. However, impedance data after stimulation displayed a reduction in the electrode impedance, with bare electrodes experiencing the biggest impedance improvements. Our preliminary results pointed out the need for further investigation in the interactions between implantable electrodes and surrounding neural tissues during deep brain stimulation.

Future work in this field must also consider the still problematic mechanical mismatch between implantable electrodes and surrounding soft tissues. Even if adding a layer of conducting polymer can offer a softer interface respect to the stiff bare electrode, the electrode core is still made up of a stiff metal, which will cause damages to the surrounding tissues due to electrode micromovements. Some group have started to tackle these problems by using thermoplastic polymer substrates that are rigid at room temperature (allowing for insertion) and then soften at body temperature causing minimal damage to the tissues [119], or by exploring hydrogel-based solutions [120]. These works are very promising, but more studies will need to investigate the possible degradation of these materials inside the body and the problem of their connection to other rigid electronic components.

REFERENCES

[1] S. F. Cogan, "Neural Stimulation and Recording Electrodes," *Annual Review of Biomedical Engineering*, vol. 10, no. 1, pp. 275-309, 2008.

[2] P. P. R. Merletti, "Frontmatter," in *Electromyography*, 2005.

[3] M. Jorfi, J. L. Skousen, C. Weder, and J. R. Capadona, "Progress Towards Biocompatible Intracortical Microelectrodes for Neural Interfacing Applications," *Journal of neural engineering*, vol. 12, no. 1, pp. 011001-011001, 2015.

[4] R. Balint, N. J. Cassidy, and S. H. Cartmell, "Conductive polymers: Towards a smart biomaterial for tissue engineering," *Acta Biomaterialia*, vol. 10, no. 6, pp. 2341-2353, 2014.

[5] L. Mainardi and P. Ravazzani, *Principi di bioelettricità e bioelettromagnetismo*. Pàtron, 2011.

[6] K. E. Barrett, S. M. Barman, S. Boitano, and H. Brooks, "Excitable Tissue: Nerve," in *Ganong's Review of Medical Physiology, 24th Edition*24 ed.: Mcgraw-hill, 2012, pp. 79-92.

[7] M. B I Raez, M. S Hussain, and F. Mohd-Yasin, *Techniques of EMG signal analysis: Detection, processing, classification and applications*. 2006, pp. 11-35.

[8] T. Moritani, D. Stegeman, and R. Merletti, "Basic Physiology and Biophysics of EMG Signal Generation," in *Electromyography*, 2005.

[9] J. J. J. V. Trontelj, M. Mihelin, "Needle and Wire Detection Techniques," in *Electromyography*, 2004.

[10] P. Maria, K. Lydia, J. C. Jia-Jin, and H.-P. Irena, "Assessment of Human Motoneuron Afterhyperpolarization Duration in Health and Disease," *Biocybernetics and Biomedical Engineering*, vol. 32, no. 3, pp. 43-61, 2012.

[11] O. Prasartwuth, E. Binboğa, and K. Türker, *A study of synaptic connection between low threshold afferent fibres in common peroneal nerve and motoneurones in human tibialis anterior*. 2008, pp. 465-72.

[12] C. W. MacDonell, T. D. Ivanova, and S. J. Garland, "Afterhyperpolarization time-course and minimal discharge rate in low threshold motor units in humans," *Experimental Brain Research*, vol. 189, no. 1, p. 23, 2008.

[13] V. Srikanth, P. Kunal, and W. Cristin, "Rodent model for assessing the long term safety and performance of peripheral nerve recording electrodes," *Journal of Neural Engineering*, vol. 14, no. 1, p. 016008, 2017.

[14] J. V. Basmajian and G. Stecko, "A new bipolar electrode for electromyography," *Journal of Applied Physiology*, vol. 17, no. 5, pp. 849-849, 1962.

[15] D. R. Merrill, M. Bikson, and J. G. R. Jefferys, "Electrical stimulation of excitable tissue: design of efficacious and safe protocols," *Journal of Neuroscience Methods*, vol. 141, no. 2, pp. 171-198, 2005.

[16] Z. Aqrawe, J. Montgomery, J. Travas-Sejdic, and D. Svirskis, "Conducting polymers for neuronal microelectrode array recording and stimulation," *Sensors and Actuators B: Chemical,* vol. 257, pp. 753-765, 2018.

[17] C. Fernández-Sánchez, C. J. McNeil, and K. Rawson, "Electrochemical impedance spectroscopy studies of polymer degradation: application to biosensor development," *TrAC Trends in Analytical Chemistry,* vol. 24, no. 1, pp. 37-48, 2005.

[18] Q. Wang, J.-E. Moser, and M. Grätzel, "Electrochemical Impedance Spectroscopic Analysis of Dye-Sensitized Solar Cells," *The Journal of Physical Chemistry B,* vol. 109, no. 31, pp. 14945-14953, 2005.

[19] D. B. McCreery, W. F. Agnew, T. G. H. Yuen, and L. Bullara, "Charge density and charge per phase as cofactors in neural injury induced by electrical stimulation," *IEEE Transactions on Biomedical Engineering,* vol. 37, no. 10, pp. 996-1001, 1990.

[20] M. D. Ferro and N. A. Melosh, "Electronic and Ionic Materials for Neurointerfaces," *Advanced Functional Materials,* vol. 28, no. 12, 2018.

[21] N. Elgrishi, K. J. Rountree, B. D. McCarthy, E. S. Rountree, T. T. Eisenhart, and J. L. Dempsey, "A Practical Beginner's Guide to Cyclic Voltammetry," *Journal of Chemical Education,* vol. 95, no. 2, pp. 197-206, 2018.

[22] E. A Zhao, W. A Gu, and G. A Yushin, "Electrical Energy Storage: Supercapacitors," in *Handbook of Solid State Chemistry*.

[23] S. Venkatraman *et al.*, "In Vitro and In Vivo Evaluation of PEDOT Microelectrodes for Neural Stimulation and Recording," *IEEE Transactions on Neural Systems and Rehabilitation Engineering,* vol. 19, no. 3, pp. 307-316, 2011.

[24] H. Nyquist, "Thermal Agitation of Electric Charge in Conductors," *Physical Review,* vol. 32, no. 1, pp. 110-113, 1928.

[25] D. A. Robinson, "The electrical properties of metal microelectrodes," *Proceedings of the IEEE,* vol. 56, no. 6, pp. 1065-1071, 1968.

[26] V. S. Polikov, P. A. Tresco, and W. M. Reichert, "Response of brain tissue to chronically implanted neural electrodes," *Journal of Neuroscience Methods,* vol. 148, no. 1, pp. 1-18, 2005.

[27] P. Fattahi, G. Yang, G. Kim, and M. R. Abidian, "A Review of Organic and Inorganic Biomaterials for Neural Interfaces," *Advanced Materials,* vol. 26, no. 12, pp. 1846-1885, 2014.

[28] D. H. Szarowski *et al.*, "Brain responses to micro-machined silicon devices," *Brain Research,* vol. 983, no. 1, pp. 23-35, 2003.

[29] E. W. Keefer, B. R. Botterman, M. I. Romero, A. F. Rossi, and G. W. Gross, "Carbon nanotube coating improves neuronal recordings," *Nature Nanotechnology,* Article vol. 3, p. 434, 2008.

[30] S. F. Cogan, A. A. Guzelian, W. F. Agnew, T. G. H. Yuen, and D. B. McCreery, "Over-pulsing degrades activated iridium oxide films used for intracortical neural stimulation," *Journal of Neuroscience Methods,* vol. 137, no. 2, pp. 141-150, 2004.

[31] A. K. Geim, "Graphene: Status and Prospects," *Science,* vol. 324, no. 5934, p. 1530, 2009.

[32] C. Lee, X. Wei, J. W. Kysar, and J. Hone, "Measurement of the Elastic Properties and Intrinsic Strength of Monolayer Graphene," *Science,* vol. 321, no. 5887, p. 385, 2008.

[33] S. Stankovich *et al.*, "Graphene-based composite materials," *Nature,* vol. 442, p. 282, 2006.

[34] H. Y. Mao *et al.*, "Graphene: Promises, Facts, Opportunities, and Challenges in Nanomedicine," *Chemical Reviews,* vol. 113, no. 5, pp. 3407-3424, 2013.

[35] D. Kuzum *et al.*, "Transparent and flexible low noise graphene electrodes for simultaneous electrophysiology and neuroimaging," *Nature Communications,* Article vol. 5, p. 5259, 2014.

[36] Y. Lu, H. Lyu, A. G. Richardson, T. H. Lucas, and D. Kuzum, "Flexible Neural Electrode Array Based-on Porous Graphene for Cortical Microstimulation and Sensing," *Scientific Reports,* Article vol. 6, p. 33526, 2016.

[37] F. Vitale, S. R. Summerson, B. Aazhang, C. Kemere, and M. Pasquali, "Neural Stimulation and Recording with Bidirectional, Soft Carbon Nanotube Fiber Microelectrodes," *ACS Nano,* vol. 9, no. 4, pp. 4465-4474, 2015.

[38] C. Xie, J. Liu, T.-M. Fu, X. Dai, W. Zhou, and C. M. Lieber, "Three-dimensional macroporous nanoelectronic networks as minimally invasive brain probes," *Nature Materials,* Article vol. 14, p. 1286, 2015.

[39] S. Iijima, "Helical microtubules of graphitic carbon," *Nature,* vol. 354, no. 6348, pp. 56-58, 1991.

[40] G. Gao, T. Cagin, and W. Goddard, *Energetics, Structure, Mechanical and Vibrational Properties of Single-Walled Carbon Nanotubes*. 1998.

[41] J. H. Shin *et al.*, "Carbon-Nanotube-Modified Electrodes for Highly Efficient Acute Neural Recording," *Advanced Healthcare Materials,* vol. 3, no. 2, pp. 245-252, 2014.

[42] N. Behabtu *et al.*, "Strong, Light, Multifunctional Fibers of Carbon Nanotubes with Ultrahigh Conductivity," *Science,* vol. 339, no. 6116, p. 182, 2013.

[43] J. Liu, C. Xie, X. Dai, L. Jin, W. Zhou, and C. M. Lieber, "Multifunctional three-dimensional macroporous nanoelectronic networks for smart materials," *Proceedings of the National Academy of Sciences of the United States of America,* vol. 110, no. 17, pp. 6694-6699, 2013.

[44] T. G. Schuhmann, J. Yao, G. Hong, T.-M. Fu, and C. M. Lieber, "Syringe-Injectable Electronics with a Plug-and-Play Input/Output Interface," *Nano Letters,* vol. 17, no. 9, pp. 5836-5842, 2017.

[45] W. D. Gill *et al.*, "Structure and Electronic Properties of Polymeric Sulfur Nitride Modified by Bromine," *Physical Review Letters,* vol. 38, no. 22, pp. 1305-1308, 1977.

[46] V. V. Walatka, M. M. Labes, and J. H. Perlstein, "Polysulfur Nitride---a One-Dimensional Chain with a Metallic Ground State," *Physical Review Letters,* vol. 31, no. 18, pp. 1139-1142, 1973.

[47] J. L. Bredas and G. B. Street, "Polarons, bipolarons, and solitons in conducting polymers," *Accounts of Chemical Research,* vol. 18, no. 10, pp. 309-315, 1985.

[48] S. H. Institute. *Alan G. MacDiarmid, Alan J. Heeger, and Hideki Shirakawa*. Available: https://www.sciencehistory.org/historical-profile/alan-g-macdiarmid-alan-j-heeger-and-hideki-shirakawa

[49] NobelPrize.org. *Popular information*. Available: https://www.nobelprize.org/prizes/chemistry/2000/press-release/

[50] H. Shirakawa, E. J. Louis, A. G. MacDiarmid, C. K. Chiang, and A. J. Heeger, "Synthesis of electrically conducting organic polymers: halogen derivatives of polyacetylene, (CH)," *Journal of the Chemical Society, Chemical Communications,* 10.1039/C39770000578 no. 16, pp. 578-580, 1977.

[51] C. K. Chiang *et al.*, "Electrical Conductivity in Doped Polyacetylene," *Physical Review Letters,* vol. 39, no. 17, pp. 1098-1101, 1977.

[52] Chemistry. *ALKANES AND ALKENES*. Available: https://chemistryclinic.co.uk/alkanes-and-alkenes/

[53] A. G. MacDiarmid *et al.*, *The Concept of `Doping' of Conducting Polymers: The Role of Reduction Potentials [and Discussion]*. 1985.

[54] S. F. Nelson, Y. Y. Lin, D. J. Gundlach, and T. N. Jackson, "Temperature-independent transport in high-mobility pentacene transistors," *Applied Physics Letters,* vol. 72, no. 15, pp. 1854-1856, 1998.

[55] T. Kitto, C. Bodart-Le Guen, N. Rossetti, and F. Cicoira, "25 - Processing and patterning of conducting polymers for flexible, stretchable, and biomedical electronics," in *Handbook of Organic Materials for Electronic and Photonic Devices (Second Edition)*, O. Ostroverkhova, Ed.: Woodhead Publishing, 2019, pp. 817-842.

[56] H.-C. Tian *et al.*, "Flexible multi-channel microelectrode with fluidic paths for intramuscular stimulation and recording," *Sensors and Actuators A: Physical,* vol. 228, pp. 28-39, 2015.

[57] J. Rivnay, R. Owens, and G. G. Malliaras, *The Rise of Organic Bioelectronics*. 2013.

[58] S. Zhang, E. Hubis, C. Girard, P. Kumar, J. DeFranco, and F. Cicoira, "Water stability and orthogonal patterning of flexible micro-electrochemical transistors on plastic," *Journal of Materials Chemistry C,* 10.1039/C5TC03664J vol. 4, no. 7, pp. 1382-1385, 2016.

[59] S. Zhang *et al.*, "Tuning the Electromechanical Properties of PEDOT:PSS Films for Stretchable Transistors And Pressure Sensors," *Advanced Electronic Materials,* vol. 0, no. 0, p. 1900191, 2019.

[60] S. Zhang, E. Hubis, G. Tomasello, G. Soliveri, P. Kumar, and F. Cicoira, "Patterning of Stretchable Organic Electrochemical Transistors," *Chemistry of Materials,* vol. 29, no. 7, pp. 3126-3132, 2017.

[61] E. Nasybulin, S. Wei, I. Kymissis, and K. Levon, "Effect of solubilizing agent on properties of poly(3,4-ethylenedioxythiophene) (PEDOT) electrodeposited from aqueous solution," *Electrochimica Acta,* vol. 78, pp. 638-643, 2012.

[62] E. Poverenov, M. Li, A. Bitler, and M. Bendikov, "Major Effect of Electropolymerization Solvent on Morphology and Electrochromic Properties of PEDOT Films," *Chemistry of Materials,* vol. 22, no. 13, pp. 4019-4025, 2010.

[63] A. Ramanaviciene, A. Kausaite, S. Tautkus, and A. Ramanavicius, "Biocompatibility of polypyrrole particles: an in-vivo study in mice," *Journal of Pharmacy and Pharmacology,* vol. 59, no. 2, pp. 311-315, 2007.

[64] D. D. Ateh, H. A. Navsaria, and P. Vadgama, "Polypyrrole-based conducting polymers and interactions with biological tissues," *Journal of the Royal Society Interface,* vol. 3, no. 11, pp. 741-752, 2006.

[65] L. J. del Valle *et al.*, "Cellular adhesion and proliferation on poly(3,4-ethylenedioxythiophene): Benefits in the electroactivity of the conducting polymer," *European Polymer Journal,* vol. 43, no. 6, pp. 2342-2349, 2007.

[66] R. M. Miriani, M. R. Abidian, and D. R. Kipke, "Cytotoxic analysis of the conducting polymer PEDOT using myocytes," in *2008 30th Annual International Conference of the IEEE Engineering in Medicine and Biology Society*, 2008, pp. 1841-1844.

[67] A. F. Quigley *et al.*, "In vitro growth and differentiation of primary myoblasts on thiophene based conducting polymers," *Biomaterials Science,* 10.1039/C3BM60059A vol. 1, no. 9, pp. 983-995, 2013.

[68] Z. Baghmanli *et al.*, "Biological and Electrophysiologic Effects of Poly(3,4-ethylenedioxythiophene) on Regenerating Peripheral Nerve Fibers," *Plastic and reconstructive surgery,* vol. 132, no. 2, pp. 374-385, 2013.

[69] S. Zhang, P. Kumar, A. S. Nouas, L. Fontaine, H. Tang, and F. Cicoira, "Solvent-induced changes in PEDOT:PSS films for organic electrochemical transistors," *APL Materials,* vol. 3, no. 1, p. 014911, 2014.

[70] A. T. Lawal and G. G. Wallace, "Vapour phase polymerisation of conducting and non-conducting polymers: A review," *Talanta,* vol. 119, pp. 133-143, 2014.

[71] N. K. Guimard, N. Gomez, and C. E. Schmidt, "Conducting polymers in biomedical engineering," *Progress in Polymer Science,* vol. 32, no. 8, pp. 876-921, 2007.

[72] L. Ghasemi-Mobarakeh *et al.*, "Application of conductive polymers, scaffolds and electrical stimulation for nerve tissue engineering," *Journal of Tissue Engineering and Regenerative Medicine,* vol. 5, no. 4, pp. e17-e35, 2011.

[73] N. V. Blinova, J. Stejskal, M. Trchová, and J. Prokeš, "Control of polyaniline conductivity and contact angles by partial protonation," *Polymer International,* vol. 57, no. 1, pp. 66-69, 2008.

[74] S.-Z. Yow, T. H. Lim, E. K. F. Yim, C. T. Lim, and K. W. Leong, "A 3D Electroactive Polypyrrole-Collagen Fibrous Scaffold for Tissue Engineering," *Polymers,* vol. 3, no. 1, p. 527, 2011.

[75] J. B. Schlenoff, *Evolution of Physical and Electrochemical Properties of Polypyrrole during Extended Oxidation*. 1992.

[76] C. Debiemme-Chouvy and T. T. M. Tran, "An insight into the overoxidation of polypyrrole materials," *Electrochemistry Communications,* vol. 10, no. 6, pp. 947-950, 2008.

[77] T. W. Lewis, G. G. Wallace, C. Y. Kim, and D. Y. Kim, "Studies of the overoxidation of polypyrrole," *Synthetic Metals,* vol. 84, no. 1, pp. 403-404, 1997.

[78] Y.-C. Liu and B.-J. Hwang, "Mechanism of conductivity decay of polypyrrole exposed to water and enhancement of conductivity stability of copper(I)-modified polypyrrole," *Journal of Electroanalytical Chemistry,* vol. 501, no. 1, pp. 100-106, 2001.

[79] K. G. Neoh, T. T. Young, E. T. Kang, and K. L. Tan, "Structural and mechanical degradation of polypyrrole films due to aqueous media and heat treatment and the subsequent redoping characteristics," *Journal of Applied Polymer Science,* vol. 64, no. 3, pp. 519-526, 1998.

[80] Y. Song, T. Y. Liu, X. X. Xu, D. Y. Feng, Y. Li, and X. X. Liu, "Pushing the Cycling Stability Limit of Polypyrrole for Supercapacitors," *Advanced Functional Materials,* vol. 25, no. 29, pp. 4626-4632, 2015.

[81] C. A. Thomas, K. Zong, P. Schottland, and J. R. Reynolds, "Poly(3,4‐alkylenedioxypyrrole)s as Highly Stable Aqueous‐Compatible Conducting Polymers with Biomedical Implications," *Advanced Materials,* vol. 12, no. 3, pp. 222-225, 2000.

[82] *Clevios™ - PEDOT:PSS*. Available: https://www.heraeus.com/en/hep/products_hep/clevios/clevios_prod/clevios_1.aspx

[83] B. J. Worfolk *et al.*, "Ultrahigh electrical conductivity in solution-sheared polymeric transparent films," *Proceedings of the National Academy of Sciences,* vol. 112, no. 46, p. 14138, 2015.

[84] G. Scheiblin, R. Coppard, R. M. Owens, P. Mailley, and G. G. Malliaras, "Referenceless pH Sensor using Organic Electrochemical Transistors," *Advanced Materials Technologies,* vol. 2, no. 2, p. 1600141, 2016.

[85] S. Zhang and F. Cicoira, "Water-Enabled Healing of Conducting Polymer Films," *Advanced Materials,* vol. 29, no. 40, p. 1703098, 2017.

[86] H. S. Mandal *et al.*, "Improving the performance of poly(3,4-ethylenedioxythiophene) for brain–machine interface applications," *Acta Biomaterialia,* vol. 10, no. 6, pp. 2446-2454, 2014.

[87] M. R. Abidian, K. A. Ludwig, T. C. Marzullo, D. C. Martin, and D. R. Kipke, "Interfacing Conducting Polymer Nanotubes with the Central Nervous System: Chronic Neural Recording using Poly(3,4‐ethylenedioxythiophene) Nanotubes," *Advanced Materials,* vol. 21, no. 37, pp. 3764-3770, 2009.

[88] A. L. Kip, B. L. Nicholas, D. J. Mike, M. R.-B. Sarah, L. H. Jeffrey, and R. K. Daryl, "Poly(3,4-ethylenedioxythiophene) (PEDOT) polymer coatings facilitate smaller neural recording electrodes," *Journal of Neural Engineering,* vol. 8, no. 1, p. 014001, 2011.

[89] D. Khodagholy *et al.*, "Highly Conformable Conducting Polymer Electrodes for In Vivo Recordings," *Advanced Materials,* vol. 23, no. 36, pp. H268-H272, 2011.

[90] H.-C. Tian *et al.*, "Enhanced Flexible Tubular Microelectrode with Conducting Polymer for Multi-Functional Implantable Tissue-Machine Interface," *Scientific Reports,* Article vol. 6, p. 26910, 2016.

[91] H. S. Mandal, J. S. Kastee, D. G. McHail, J. F. Rubinson, J. J. Pancrazio, and T. C. Dumas, "Improved Poly(3,4 - Ethylenedioxythiophene) (PEDOT) for Neural Stimulation," *Neuromodulation: Technology at the Neural Interface,* vol. 18, no. 8, pp. 657-663, 2015.

[92] C. Bodart *et al.*, "Electropolymerized Poly(3,4-ethylenedioxythiophene) (PEDOT) Coatings for Implantable Deep-Brain-Stimulating Microelectrodes," *ACS Applied Materials & Interfaces,* vol. 11, no. 19, pp. 17226-17233, 2019.

[93] D. Harvey. (2009). *Analytical Chemistry 2.0*. Available: http://dpuadweb.depauw.edu/harvey_web/eTextProject/version_2.0.html

[94] V. Castagnola, C. Bayon, E. Descamps, and C. Bergaud, "Morphology and conductivity of PEDOT layers produced by different electrochemical routes," *Synthetic Metals,* vol. 189, pp. 7-16, 2014.

[95] A. H. Ismail, M. N. Mustafa, A. H. Abdullah, R. M. Zawawi, and Y. Sulaiman, "Effect of Electropolymerization Potential on the Properties of PEDOT/ZnO Thin Film Composites," *Journal of The Electrochemical Society,* vol. 163, no. 2, pp. G7-G14, 2016.

[96] X. Cui and D. C. Martin, "Electrochemical deposition and characterization of poly(3,4-ethylenedioxythiophene) on neural microelectrode arrays," *Sensors and Actuators B: Chemical,* vol. 89, no. 1, pp. 92-102, 2003.

[97] C. Weidlich, K. M. Mangold, and K. Jüttner, "EQCM study of the ion exchange behaviour of polypyrrole with different counterions in different electrolytes," *Electrochimica Acta,* vol. 50, no. 7, pp. 1547-1552, 2005.

[98] S. Baek, R. A. Green, and L. A. Poole - Warren, "Effects of dopants on the biomechanical properties of conducting polymer films on platinum electrodes," *Journal of Biomedical Materials Research Part A,* vol. 102, no. 8, pp. 2743-2754, 2014.

[99] S. Baek, R. A. Green, and L. A. Poole-Warren, "The biological and electrical trade-offs related to the thickness of conducting polymers for neural applications," *Acta Biomaterialia,* vol. 10, no. 7, pp. 3048-3058, 2014.

[100] S.-C. Luo *et al.*, "Poly(3,4-ethylenedioxythiophene) (PEDOT) Nanobiointerfaces: Thin, Ultrasmooth, and Functionalized PEDOT Films with in Vitro and in Vivo Biocompatibility," *Langmuir,* vol. 24, no. 15, pp. 8071-8077, 2008.

[101] S. M. Richardson-Burns, J. L. Hendricks, B. Foster, L. K. Povlich, D.-H. Kim, and D. C. Martin, "Polymerization of the conducting polymer poly(3,4-ethylenedioxythiophene) (PEDOT) around living neural cells," *Biomaterials,* vol. 28, no. 8, pp. 1539-1552, 2007.

[102] O. Liangqi, L. S. Crystal, K. Chin-chen, L. G. Amy, and C. M. David, "In vivo polymerization of poly(3,4-ethylenedioxythiophene) in the living rat hippocampus does not cause a significant loss of performance in a delayed alternation task," *Journal of Neural Engineering,* vol. 11, no. 2, p. 026005, 2014.

[103] X. T. Cui and D. D. Zhou, "Poly (3,4-Ethylenedioxythiophene) for Chronic Neural Stimulation," *IEEE Transactions on Neural Systems and Rehabilitation Engineering,* vol. 15, no. 4, pp. 502-508, 2007.

[104] R. A. Green *et al.*, "Substrate dependent stability of conducting polymer coatings on medical electrodes," *Biomaterials,* vol. 33, no. 25, pp. 5875-5886, 2012.

[105] R. A. Green *et al.*, "Performance of conducting polymer electrodes for stimulating neuroprosthetics," *Journal of Neural Engineering*, vol. 10, no. 1, p. 016009, 2013.

[106] A. S. Pranti, A. Schander, A. Bödecker, and W. Lang, "PEDOT: PSS coating on gold microelectrodes with excellent stability and high charge injection capacity for chronic neural interfaces," *Sensors and Actuators B: Chemical*, vol. 275, pp. 382-393, 2018.

[107] B. Wei, J. Liu, L. Ouyang, C.-C. Kuo, and D. C. Martin, "Significant Enhancement of PEDOT Thin Film Adhesion to Inorganic Solid Substrates with EDOT-Acid," *ACS Applied Materials & Interfaces*, vol. 7, no. 28, pp. 15388-15394, 2015.

[108] L. Ouyang, B. Wei, C.-c. Kuo, S. Pathak, B. Farrell, and D. C. Martin, "Enhanced PEDOT adhesion on solid substrates with electrografted P(EDOT-NH2)," *Science Advances*, vol. 3, no. 3, 2017.

[109] D. Chhin, D. Polcari, C. B.-L. Guen, G. Tomasello, F. Cicoira, and S. B. Schougaard, "Diazonium-Based Anchoring of PEDOT on Pt/Ir Electrodes via Diazonium Chemistry," *Journal of The Electrochemical Society*, vol. 165, no. 12, pp. G3066-G3070, 2018.

[110] J. H. Siegle, A. C. López, Y. A. Patel, K. Abramov, S. Ohayon, and J. Voigts, "Open Ephys: an open-source, plugin-based platform for multichannel electrophysiology," *Journal of Neural Engineering*, vol. 14, no. 4, p. 045003, 2017.

[111] A. L. Kip, D. U. Jeffrey, Y. Junyan, C. M. David, and R. K. Daryl, "Chronic neural recordings using silicon microelectrode arrays electrochemically deposited with a poly(3,4-ethylenedioxythiophene) (PEDOT) film," *Journal of Neural Engineering*, vol. 3, no. 1, p. 59, 2006.

[112] *Standard Guide for Accelerated Aging of Sterile Barrier Systems for Medical Devices*, 2011.

[113] I. Uguz *et al.*, "Autoclave Sterilization of PEDOT:PSS Electrophysiology Devices," *Advanced Healthcare Materials*, vol. 5, no. 24, pp. 3094-3098, 2016.

[114] R. Singh and A. Kumar, "Effect of electrode surface on the electrochromic properties of electropolymerized poly(3,4-ethylenedioxythiophene) thin films," *Organic Electronics*, vol. 30, pp. 67-75, 2016.

[115] L. Groenendaal, G. Zotti, P. H. Aubert, S. M. Waybright, and J. R. Reynolds, "Electrochemistry of Poly(3,4 - alkylenedioxythiophene) Derivatives," *Advanced Materials*, vol. 15, no. 11, pp. 855-879, 2003.

[116] N. Sakmeche, S. Aeiyach, J.-J. Aaron, M. Jouini, J. C. Lacroix, and P.-C. Lacaze, "Improvement of the Electrosynthesis and Physicochemical Properties of Poly(3,4-ethylenedioxythiophene) Using a Sodium Dodecyl Sulfate Micellar Aqueous Medium," *Langmuir*, vol. 15, no. 7, pp. 2566-2574, 1999.

[117] B. Bergman and T. W. Hanks, "Spectroscopic, Microscopic, and Surface Analysis of Alkanethiol- and Fluoroalkanethiol-Modified Conducting Polymer Thin Films," *Macromolecules*, vol. 33, no. 21, pp. 8035-8042, 2000.

[118] J. Webster, *22. Webster, J. G. (ed.), Medical instrumentation: application and design, Fourth edition, John Wiley & Sons, Hoboken, NJ, 2010*. 2010.

[119] S. Yoshimoto *et al.*, "Implantable wireless 64-channel system with flexible ECoG electrode and optogenetics probe," in *2016 IEEE Biomedical Circuits and Systems Conference (BioCAS)*, 2016, pp. 476-479.

[120] B. Lu *et al.*, "Pure PEDOT:PSS hydrogels," *Nature Communications*, vol. 10, no. 1, p. 1043, 2019.